To design and develop Brewster Angle Microscope coupled with LB trough for observing and analyzing monolayers formed at air water interface

THESIS SUBMITTED TO

THE UNIVERSITY OF PUNE

FOR THE DEGREE OF

DOCTOR OF PHILOSOPHY

IN

INSTRUMENTATION SCIENCE

BY

BHAGYASHREE PARESH JOSHI

Under the Guidance of

Dr. S. R. Gowariker
(Research Guide)

Dr. Murali Sastry
(Research Co-guide)

Mrs. Neelima Iyer
(Research Supervisor)

PHYSICAL CHEMISTRY DIVISION
NATIONAL CHEMICAL LABORATORY
PUNE 411 008
INDIA

DECEMBER 2006

Dedicated to
My Father…

CERTIFICATE

This is to certify that the work discussed in the thesis entitled "To design and develop Brewster Angle Microscope coupled with LB trough for observing and analyzing monolayers formed at air-water interface" by Mrs. **Bhagyashree Paresh Joshi**, for the degree of Doctor of Philosophy was carried out under my supervision. As per my guidance and suggestions the work was carried out in the Physical Chemistry Division, National Chemical Laboratory, Pune. Such materials, as has been obtained by other sources, have been duly acknowledged in this thesis. To the best of my knowledge, the present work or any part thereof, has not been submitted to any other University for the award of any other degree or diploma.

Date: Dr. S. R. Gowariker

(Research Guide)

Place:

CERTIFICATE

This is to certify that the work discussed in the thesis entitled "To design and develop Brewster Angle Microscope coupled with LB trough for observing and analyzing monolayers formed at air-water interface" by Mrs. **Bhagyashree Paresh Joshi**, for the degree of Doctor of Philosophy was carried out under my supervision in the Physical Chemistry Division, National Chemical Laboratory, Pune. Such materials, as has been obtained by other sources, have been duly acknowledged in this thesis. To the best of my knowledge, the present work or any part thereof, has not been submitted to any other University for the award of any other degree or diploma.

Date:

Dr. Murali Sastry
(Research Co-guide)

Place:

CERTIFICATE

This is to certify that the work discussed in the thesis entitled "To design and develop Brewster Angle Microscope coupled with LB trough for observing and analyzing monolayers formed at air-water interface" by Mrs. **Bhagyashree Paresh Joshi**, for the degree of Doctor of Philosophy was carried out under my supervision in the Physical Chemistry Division, National Chemical Laboratory, Pune. Such materials, as has been obtained by other sources, have been duly acknowledged in this thesis. To the best of my knowledge, the present work or any part thereof, has not been submitted to any other University for the award of any other degree or diploma.

Date:

Mrs. Neelima Iyer
(Research Supervisor)

Place:

DECLARATION

I, **Bhagyashree Paresh Joshi**, hereby declare that the work incorporated in this thesis entitled "To design and develop Brewster Angle Microscope coupled with LB trough for observing and analyzing monolayers formed at air-water interface" carried out by me at Physical Chemistry Division, National Chemical Laboratory, Pune, has not been submitted for the award of any other degree or diploma.

Date: (Bhagyashree Paresh Joshi)

Place:

Acknowledgement

I extend my sincere gratitude and appreciation to many people who made this Ph.D. thesis possible. First and foremost, I would like to extend my sincere thanks to my research guide Dr. S. R. Gowariker, Director, Tolani Education Foundation, Pune and Former Director, CSIO, Chandigarh, for his valuable advice, inspiration and encouragement during the course of my research work. His constant support was invaluable and went a long way towards the completion of this thesis.

I take this opportunity to express my deep sense of gratitude and sincere thanks to my research co-guide, Dr. Murali Sastry, for his inspiring guidance and valuable and critical suggestions during experimentation. His enthusiasm, positive approach and constant support has always been a source of inspiration for me.

With a deep sense of gratitude, I express my sincere thanks to my supervisor, Mrs. Neelima Iyer, Scientist and Head, Instrumentation and Communication Group, National Chemical Laboratory, Pune, for her invaluable guidance, support and encouragement throughout the duration of my work. I express my sincere gratitude to her for exposing me to this exciting and interesting field of research. I am greatly indebted for her insightful advice and active participation in every development stage of this research work.

I am thankful to Mrs. Rupali Waichal, Technical Assistant, Instrumentation and Communication Group, who has always helped in one way or the other. My sincere thanks to her for giving me the initial exposure on working in LabVIEW and for her advice during the mechanical fabrication and software development part of the research work.

I express sincere thanks to Dr P. Ratnaswamy and Dr. S. Sivaram, former and present Directors of NCL, Pune, for giving me the opportunity to

work in this institute and making all the facilities available for my research work.

I am grateful to Dr. P. Ganguly, Dr. S. K. Date and Dr. S. Pal, former and present Heads, Physical Chemistry Division, NCL, for their constant support and encouragement.

I am thankful to Mr. A. M. Patil, Technical Officer, Workshop, Engineering Services Unit, NCL, and his team for the fabrication of the Langmuir trough as per the design parameters.

I am thankful to Mr. Anand Bhave for his kind help and advice during the initial phases of my research.

I am grateful to Mr. Potdar, M/s Swaraj Engineering, Pune, for carrying out some critical mechanical fabrications.

I take this opportunity to thank my former colleagues from Nanoscience Group, Anita, Sumant, Kanan, Shivshankar who helped me to get familiarized with the physical chemistry part of the work during my initial days.

I take this opportunity to thank all my friends from Nanoscience Group, Hrushikesh, Tanushree and Deepti who have helped me in all possible ways.

A special mention of thanks to my friend in NCL, Rajashree, for her help and support. Her timely support and friendship shall always be remembered.

I feel a deep sense of gratitude for my mother and late father who formed part of my vision and taught me good things that really matter in life. My special thanks to Paresh, my dear husband, who was extremely patient and tolerant towards my erratic hours of work. His continued support has seen me through my thesis. I owe my special thanks to him for giving me the moral support and time when I needed the most. My sincere thanks to my mother-in-law for helping me in one way or the other. As always, it is impossible to mention everybody who had an impact on my work. However, I take this opportunity to thank all my family members, friends and relatives for their blessings and well wishes throughout my life.

I must thank all the people who, in their own way, helped and supported me along the way, and I wish to express a debt of gratitude to all those whose efforts have contributed in no small way to the success of this thesis.

Finally, I am thankful to the library and the administrative staff of NCL for their co-operation and to CSIR for the financial support in the form of Senior Research Fellowship.

Abstract

The thesis discusses the indigenous design, development and fabrication of the Brewster angle microscope and its coupling with Langmuir trough. The developed instrument allows the user to perform the real-time measurement and plotting of surface pressure and simultaneously imaging the monolayer formed at the air-water interface. The developed instrument is compact, economical and does not include heavy and bulky parts.

Chapter 1 of the thesis is an introduction to the thesis and briefly describes the background and motive behind developing the system. From amongst the various techniques available for the characterization of the surfaces, Brewster angle microscope and measuring pressure area isotherm were found to be the best suitable techniques for studying the morphological and phase changes of the Langmuir films. Chapter 2 covers the theoretical concepts behind the Brewster angle microscope and Langmuir films. Chapter 3 details the indigenous design, development and fabrication of the instrument. Interfacing of the frame grabber add-on card and the CCD camera, required for real-time imaging, storing and processing of the images, has been explained. The state-of-the-art design of single barrier Langmuir trough has been discussed. A pressure sensor has been integrated with the system for simultaneous measurement of surface pressure along with Brewster angle microscope. Interfacing of the pressure sensor and the AD/DA add-on card has been elaborated. Chapter 4 discuses about the real-time software developed for controlling and interfacing with the system. LabVIEW environment has been used for this development. This chapter describes the GUI design and vision system implementation for real-time operation of the entire system. It also describes the GUI design for implementation of other features for control and data acquisition. Chapter 5 discusses about the design validation experimentation and few systems that were studied on the developed instrument. The design validation was done by using standard surfactants to form the Langmuir monolayers. Their pressure area isotherm and Brewster angle microscopy images were captured and compared with the available reference images. The results were found to be satisfactory and reproducible. A few systems studied on the developed instrument include: time dependent complexation of sodium borohydride reduced gold nanoparticles and lemon grass reduced gold nanoparticles with

octadecylamine, assembly formation of hydrophobized Ni nanoparticles as a function of surface pressure and assembly of thiol capped gold nanoparticles on octadecylamine. Chapter 6 summarizes the work presented in the thesis. The specifications of the developed system have been mentioned. Finally, it discusses the scope of research for future developments in this area.

Table of Contents

List of Tables

List of Figures

CHAPTER 1

INTRODUCTION

This chapter is an introduction to the thesis and gives a brief idea about the importance of the Brewster angle microscopy technique. It presents the background of the thesis and discusses the objectives that have been taken during this research work. Finally, an outline of the thesis is given.

1.1 Introduction

Surface science and surface engineering have developed since the early sixties in the last century. Surface science and surface engineering include studies on formation of surfaces with defined chemical composition, structure and physical characteristics as well as studies on phenomena and chemical reactions at the surface. The morphologies of monolayers at air-water interface are striking examples of the spontaneous self-organization of materials in nature. The patterns formed by these films can be remarkable, ranging from the intertwined spiral-shaped island seen in phospholipid films to the fan textures formed by fatty acids and liquid crystalline materials [1-3]. The results make it possible to select the technology to obtain materials with well-defined surface parameters. Surface phenomena on boundaries of solids, liquids and gases play an important role in industrial technology and their recognition can influence the engineering projects. In order to obtain necessary information of the surface properties, many different and complementary techniques are currently used in the field of surface and thin film analysis [4]. Most of these techniques involve bombarding the sample with an incident particle and monitoring an ejected particle and are then destructive in nature. Some of these techniques are listed in Table 1-1.

Sr. No	Incident particle	Ejected Particle	Technique name	Acronym
1	X-ray	Electron	X-ray Photoelectron Spectroscopy	XPS
2	X-ray	X-ray	X-ray Fluorescence Spectroscopy	XRF
3	Electron	Electron	Auger Electron Spectroscopy	AES
4	Ion	Sample ion	Secondary ion mass spectrometry	SIMS

Table 1-1 Surface and thin film characterization techniques

It is very important to note that these techniques all require that the analysis be performed in an ultra high vacuum apparatus and that each of the techniques wherein the incident particle is either an electron or an ion, measures must be taken to insure that the sample surface is electrically conductive. Thus, for insulating materials and films such as oxides, glasses and polymers, the experiments are not straightforward. Also, these techniques give information about the elemental and chemical

composition of the surfaces and often the main interest lies in the information of the morphology or phase behavior of thin films. In such cases, imaging of thin films is generally considered to be of great importance. Following are some available techniques:

1. Transmission Electron Microscopy (TEM)
2. Scanning Electron Microscopy (SEM)
3. Imaging Ellipsometry
4. Atomic Force Microscopy (AFM)
5. Fluorescence Microscopy
6. Brewster Angle Microscopy (BAM)

Most of the above techniques are suitable only for characterization of films on a solid substrate (as in case of AFM and TEM, a Langmuir-Blodgett (LB) film has to be formed) and are not available for liquid surfaces. Also, there is always an uncertainty of whether the system under study is in its original state or not. In such cases, direct imaging of thin film at solid-solid, solid-liquid, solid-gas, liquid-liquid and liquid-gas interface is considered to be of great importance.

Only fluorescence microscopy techniques and Brewster angle microscopy (BAM) are the surface characterization techniques with the advantage that they can be used for characterizing both solid and liquid interfaces. These techniques are well suited for the in-situ characterization of the monolayers on air-water interface. The monolayer of insoluble amphiphilic molecules at air-water interface is known as a Langmuir film [5]. The Langmuir film formation on water surface plays an important role in the application of Langmuir–Blodgett (LB) technique [6-8]. In the case of fluorescence microscopy study on Langmuir films [9, 10], a fluorescent amphiphilic molecule is added to the amphiphilic monolayer. This fluorescent probe behaves like an impurity in the monolayer, i.e., its solubility in the coexisting phases can be very different. The contrast in the fluorescence images is sufficient to visualize the coexisting domains of different phases. However, this powerful technique has a number of drawbacks. First, dense and well-ordered phases are difficult to observe because they reject the fluorescent molecules almost completely. Secondly, in some cases, the addition of an impurity in the system can modify its behavior rather

strongly. Brewster angle microscopy, that was developed independently by Henon and Meunier [11] and Honig and Mobius [12] more than a decade ago, is a sensitive and effective method available for studying the organization in spread monolayers at the air-water interface at the microscopic level. The main advantage of the BAM technique, apart from being non-invasive, is that it allows the direct observation of ultra-thin films on air-water interface or on dielectric substrates without using any fluorescent probes in the studied materials. BAM has proven to be an extremely valuable tool for the characterization of the morphology of Langmuir monolayers of surfactant molecules at the air-water interface. Such films, which are prepared on water surface in Langmuir trough, are transferred from the water surface to the glass or silicon plate or on carbon coated grids (for TEM) for further analysis. The quality of the film depends on the morphology of the floating films on the trough and it is therefore of much interest to observe such floating Langmuir films in-situ during the transfer process.

BAM provides information on the morphology of amphiphilic monolayers [13-19], including the inner structure of condensed domains [20] and phase transitions [21-23] in monolayers, the orientation order of the monolayer domains, 2D-3D transformation of amphiphilic monolayer [24] and relaxation phenomena [25-28] in monolayer domains caused by compression-expansion cycles.

1.2 Background and Purpose

The first indigenous development of Brewster Angle Microscope has been carried out at our laboratory. Figure 1.2-I shows the principle of the BAM instrument. This technique allows the researcher to draw inference about the molecular orientation by direct visualization of the monolayer. When *p*-polarized light is used and incidence takes place at the Brewster angle, no light is reflected from the pure air-water interface. However, changes in the molecular density and /or refractive index by the condensed phase of a monolayer on the aqueous subphase leads to a measurable change in the reflectivity and allows one to visualize and record the monolayer morphology.

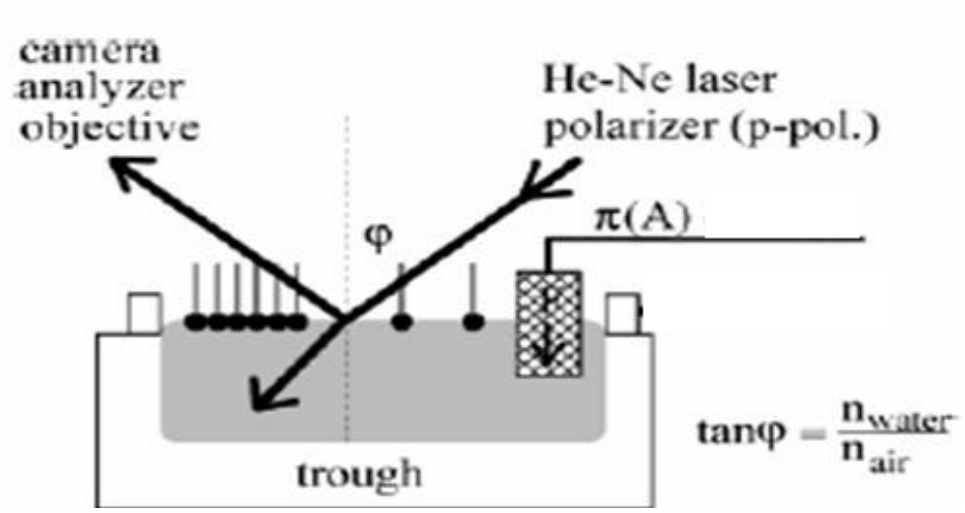

Figure 1.2-I Principle of Brewster Angle Microscopy

The project was sponsored by Department of Atomic Energy, BRNS, Mumbai. The development was carried out by Instrumentation and Communication Group of Physical Chemistry Division, NCL, during September 2000–March 2003 under the guidance of Mrs. Neelima Iyer. The preliminary testing was carried out by Nanoscience Group, NCL, under the guidance of Dr. Murali Sastry. Figure 1.2-II shows the preliminary setup that was built for the first development stage. In the setup, He-Ne laser source was used that emitted 1 mW at 623.8 nm. The emitted beam passed through the collimator and illuminated a spot of about 2 mm^2 on the surface. The reflected light passed through the objective and finally was detected by a CCD camera (KCC 310, Kocom). The CCD camera was coupled to the frame grabber card (FlashBUS, MVLite) for real-time capturing of the monolayer images. A teflon trough (5x10 cm^2) was fabricated. It had a single barrier to compress and decompress the monolayer. A stepper motor was attached to the barrier for its movement in forward and reverse direction and for speed control. Microcontroller module using AT89C51 was developed for controlling the direction and speed of the barrier. A driver circuitry for the stepper motor was developed using L297 (stepper motor controller) and L298 (stepper motor driver). Assembly software development was carried out for the microcontroller module. The graphical user interface (GUI) software for real-time capturing of the monolayer images was developed in VC++ using Microsoft SDK. PC controlled the direction and speed of the barrier. Serial protocol RS232 was established between PC and microcontroller module.

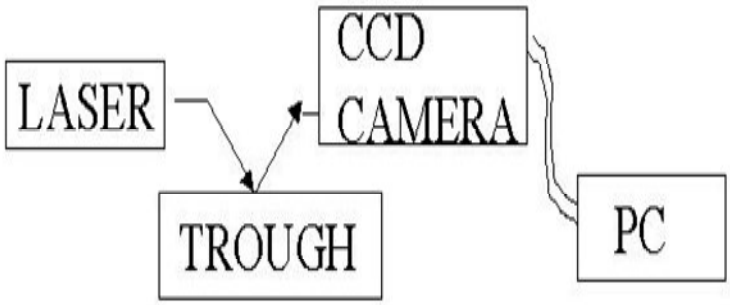

Figure 1.2-II Scheme of the setup built for the first development

Apart from Brewster angle microscopy, the most important indicator of the monolayer properties of an amphiphilic material is given by measuring the surface pressure as a function of area of water surface available to each molecule. This is carried out at constant temperature and is known as *surface pressure area isotherm*. Usually an isotherm is recorded by compressing the film at constant rate while continuously monitoring the surface pressure. After the development of BAM instrument, the next step was to integrate the pressure sensor along with the Brewster angle microscopy for real-time plotting of pressure area isotherm while simultaneously imaging the monolayer.

We used the Langmuir trough (Model 611D) from NIMA Technology, England [29] for preparation of the Langmuir films. The base intelligence of the instrument was the microcontroller AT89C552. The communication between microcontroller module and PC was established through RS232 serial protocol for controlling and passing the parameters to the instrument. Once the parameters were set and data was acquired, it was communicated to the PC and a real-time plot of pressure area isotherm was plotted on the PC. It was decided that developed Brewster angle microscope should be coupled with existing Langmuir trough for combined application of pressure area isotherm and imaging. The problem faced for this coupling was that the communication protocols of NIMA LB trough to PC were totally unknown and the company did not provide any information. So, it was decided that a new Langmuir trough with pressure sensor attachment should be designed and fabricated at NCL that will be interfaced with the BAM setup. It was also decided that the development should be a complete PC based solution and controlling software should be developed using LabVIEW.

1.3 Objectives

To complete the BAM and Langmuir trough development, following objectives were taken into consideration.

- Design and development of Brewster angle microscope.
- Design and fabricate Langmuir trough consisting of single barrier.
- Interfacing pressure sensor Model PS4 from Nima Technology, England for measuring pressure area isotherm.
- Mechanical assembly for pressure sensor holder.
- Design and fabricate necessary mechanical assembly for DC motor to be coupled with barrier.
- Design and develop DC motor driver circuitry for bi-directional motion of the barrier.
- Real-time system software development using LabVIEW.
- Creating a graphical user interface using LabVIEW.
- Interfacing of data acquisition card with LabVIEW.
- Implementing the vision system in LabVIEW.

1.4 Overseas market study

Brewster angle microscope instruments are available in international market, mainly from Nanofilm Technology, Germany, NIMA Technology, England and KSV Instruments, Finland. Following are the models available from the international companies:

1. MiniBAM: This is the BAM from Nanofilm Technology. It has a resolution of < 20 μm. The field of view is around 4x6 mm^2. Black and white CCD camera with monitor is being provided for real-time video monitoring. It has a massive tripod with mounting post and fine adjustment screws for vertical alignments. With this instrument, only aqueous sub phases can be studied as the angle adjustment range is from 52^0 - 54^0 and that is not suitable for solid substrate. It is a separate unit that can be fitted to any existing trough available from NIMA Technology.

2. MiniBAMplus: This is an upgradation of MiniBAM model. In addition to all above features, it has a PC visualization version for image acquisition and analysis.

3. MicroBAM: MicroBAM is the latest development from Nanofilm Technology and NIMA Technology to monitor mono-molecular layers at air-water interface. It has imaging system resolution of 8 μm and field of view of 3.6x4.8 mm^2. It has motorized rotation of polarizer and analyzer via software control. This is only suitable for aqueous sub phases.

4. EP3-BAM or BAM2plus: This is high end, high resolution instrument available from Nanofilm Technology, Germany. The lateral resolution is ~1 μm with the field of view of around 0.44 mm. A colored CCD is incorporated in it. PC controlled software is available for image acquisition, monitoring and adjusting optical components. With this instrument, it is also possible to study non-aqueous sub phases. It can be upgraded to imaging ellipsometer by adding a compensator and special software with additional cost.

5. KSV Optral300: This is the recently available BAM instrument from KSV Instruments, Finland. It has a lateral resolution of 2 μm. It includes an image processing software. It has a very massive vertical arrangement for BAM that can be fitted to variety of troughs available from KSV Instruments.

All above mentioned models are mainly available in the international market. The cost of the above instruments is more than Rs 10-12 lacs.

While designing the instrument, a detailed study has been done and all the designing criteria have been taken into consideration. The developed instrument is an indigenous development that is very compact and economical. It has comparable lateral resolution and field of view with the commercially available instruments. It includes the pressure sensor for simultaneous operation. Real-time system software has been developed for controlling, imaging and storing the data. Detailed specifications of the instrument will be discussed in Chapter 6.

1.5 Highlights of subsequent chapters

The outline of the thesis is as follows:

Chapter 2: Theory - Brewster angle microscope and Langmuir films

This chapter of the thesis gives the theoretical understanding of Brewster angle microscope and Langmuir films. It covers the basics of Brewster angle and its derivation, principle behind Brewster angle microscopy and its applications. It also includes the basics of the Langmuir films and pressure area isotherm, which is most common way to study the Langmuir films.

Chapter 3: Design, development and fabrication of BAM and Langmuir trough

This chapter is about the indigenous development of the instrument that has been carried out during this research work.

Designing of vertically mounted compact Brewster angle microscope has been discussed in detail. The selection and the specification of different optical components that are used in the setup have been explained. The add-on frame grabber card has been incorporated for real time imaging, storing and further processing of the images. The detail interfacing of the card and CCD camera has been explained.

A state-of-the-art design of Langmuir trough has been done. Langmuir trough consists of single barrier with DC motor coupled to it for barrier movement. Along with Brewster angle microscopy, measurement of pressure area isotherm is the best suitable way to study the Langmuir films. The necessary interfacing of the pressure sensor and AD/DA add-on card to measure surface pressure has been elaborated.

The developed instrument is controlled through the real-time system software explained in Chapter 4.

Chapter 4: Development of real-time system software

Real-time system software for controlling and interfacing with the system has been developed. 'G' language in LabVIEW (Laboratory Virtual Instrument Engineering Workbench) environment has been used for this development. This chapter describes the basics of LabVIEW, creating a Graphical User Interface (GUI) and vision system implementation for real-time imaging of the monolayer. It also describes the implementation of other features for control, data acquisition and user interface.

Chapter 5: Experimental results and analysis

The design validation was done by using standard surfactants to form the Langmuir monolayers. Their pressure area isotherm and Brewster angle microscopy

images were captured and compared with the available reference images. The results were found to be satisfactory and reproducible.

Following systems were further studied on the developed instrument:

1. Time dependent complexation of sodium borohydride reduced gold nanoparticles with octadecylamine Langmuir monolayers: the system was studied and BAM images clearly indicated that the density of particles increases at the surface as a function of time of complexation.
2. Assembly of hydrophobized Ni nano particles as a function of surface pressure has been studied: Brewster angle microscopy and pressure area isotherm measurements have been employed for this study.
3. Study of thiol capped gold nanoparticles on octadecylamine and on stearic acid monolayers.

Chapter 6: Conclusions

This chapter summarizes the work presented in the thesis. It lays emphasis on the importance of the Brewster angle microscopy technique. This chapter describes the specifications of the developed system and it also discusses the scope of research for future developments in this area.

References

1. R. Volinsky, F. Gaboriaud, A. Berman and R. Jelinek, *J. Phys. Chem. B* **2002**, 106, 9231-9236.
2. Nilashis Nandi, Dieter Vollhardt, *Chem. Rev.* **2003**, 103, 4033.
3. Marc N. C. de Mul, J. Adin Mann. Jr., *Langmuir* **1998**, 14, 2455-2466.
4. "Surface and Thin film Analysis Methods" Technical note 26, Patrick Chapon, Jobin Yvon S.A.S., Horiba Group, Longjumeau, France.
5. "Insoluble Monolayers at Liquid Gas Interface", G. L. Gaines Jr., *Interscience*, New York, 1966.
6. Ariga K., Shin J. S., Kunitake T., *J. Colloid Interface Sci.* **1995**, 170, 440-448.
7. Brinks B. P., *Ad*V. *Colloid Interface Sci.* **1991**, 34, 343.
8. R. M. Morelis, A. P. Girard-Egrot, P. R. Coulet, *Langmuir* **1993**, 9, 3101-3106.
9. Knobler C. M., *Adv. Chem. Phys*. **1990**, 77, 397.
10. McConnell H. M., *Annu. Rev. Phys. Chem*. **1991**, 42, 171.
11. S. Henon and J. Meunier, *Rev. Sci. Instruments* 62, 936 (**1991**).
12. Dirk Hoenig, Dietmar Moebius, D. Honig and D. Mobius, *J. Phys. Chem.* 95, 4590 (**1991**).
13. Yuh-Lang Lee, Yaw-Chia Yang, and Yu-Jen Shen, *J. Phys. Chem. B*. **2005,**109, 4662-4667.
14. D. Vollhardt, S. Siegel, D.A. Cadenhead, *J. Phys. Chem. B* **2004**, 108, 17448-17456.
15. Werkman P. J., Schouten A. J., Noordegraaf M. A., Kimkes P., Sudho¨lter E. J. R., *Langmuir* **1998**, 14, 157.
16. Gehlert U., Weidemann G., Vollhardt D., Brezesinski G., Wagner R., Mo¨wald H., *Langmuir* **1998**, 14, 2112.
17. Deschenaux R., Megert S., Zumbrunn C., Ketterer J., Steiger R., *Langmuir* **1997**, 13, 2363.

18. Vollhardt D., *Adv. Colloid Interface Sci.* **1996**, 64, 143.

19. Ho¨nig D., Overbeck G. A., Mo¨bius D., *Adv. Mater.* **1993**, 4, 419.

20. Ho¨nig D., Mobius D., *Thin Solid Films* **1992**, 210/211, 64.

21. Vollhardt D., Melzer V., *J. Phys. Chem. B* **1997**, 101, 3370.

22. Melzer V., Vollhardt D., *Phys. Rev. Lett.* **1996**, 76, 3770.

23. Overbeck, G. A.; Ho¨nig, D. Mo¨bius, D. *Thin Solid Films* **1994**, 242, 213.

24. Angelova A., Vollhardt D., Ionov R., *J. Phys. Chem.* **1996**, 100, 1071.

25. Lee Y.-L., Liu K.-L., *Langmuir* **2004**, 20, 3180.

26. Gehlert U., Vollhardt D., *Langmuir* **1997,** 13, 277.

27. Lautz C., Fisher Th. M., Kildea J., *J. Chem. Phys.* **1997**, 106, 7448.

28. Reda T., Hermel H., Ho¨ltje H.-D., *Langmuir* **1996**, 12, 6452.

29. http://www.nima.co.uk/equipment/equipindex.htm.

CHAPTER 2

THEORY – BREWSTER ANGLE MICROSCOPE AND LANGMUIR FILMS

This chapter covers the principle of the Brewster angle and Brewster angle microscopy. It also discusses the basics of the Langmuir films, for which this technique is extensively used.

2.1 Brewster angle and Brewster angle microscopy

Light waves are electromagnetic waves and electromagnetic waves are transverse waves, meaning that the directions of the vibrating electric and magnetic vectors are at right angles to the direction of propagation.

Sunlight and almost every other form of natural and artificial illumination produces light waves whose electric field vectors vibrate in all planes that are perpendicular with respect to the direction of propagation.

When the light is reflected from a flat surface of a dielectric (or insulating) medium, it becomes partially polarized. This means the electric vectors of the reflected light vibrate in a plane that is parallel to the surface of the material.

Figure 2.1-I illustrates how polarization of light is changed on reflection from a dielectric or insulating media.

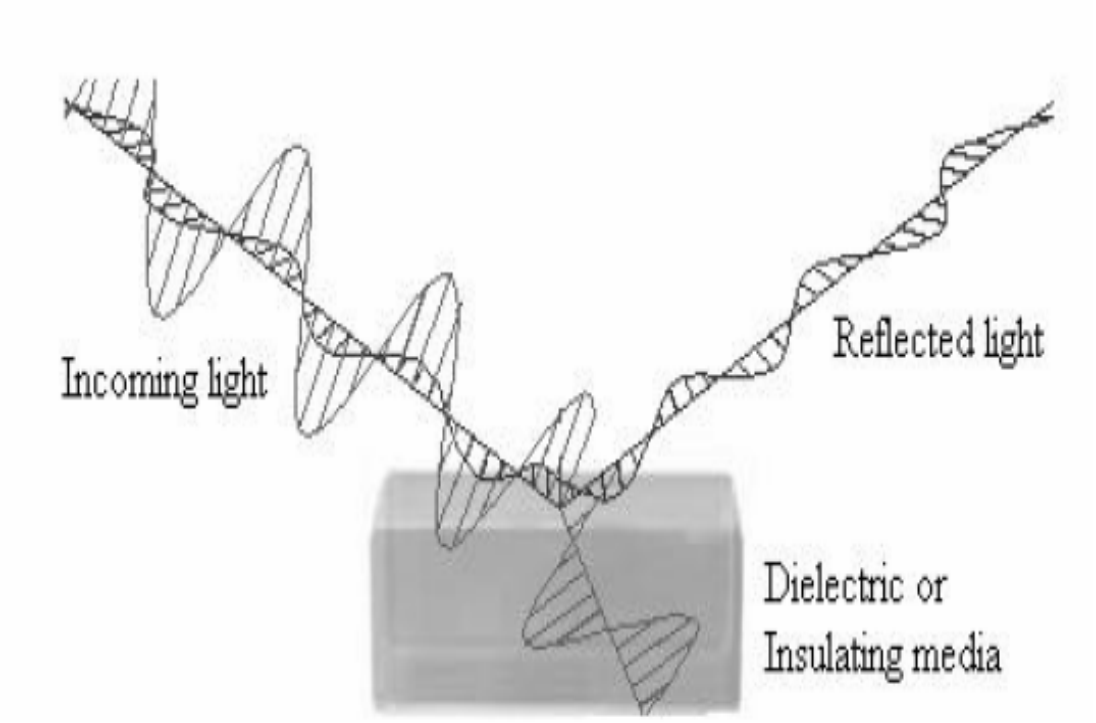

Figure 2.1-I Polarization of light

Common examples of naturally occurring sources of polarized light are; light reflected from undisturbed water, glass, plastic and paper sheets and highways. Bright

reflections originating from these kinds of horizontal surfaces are partially polarized with the electric field vectors vibrating in a direction that is parallel to the ground. In these instances, light waves that have the electric field vectors parallel to the surface are reflected to a greater degree than those with different orientations.

In the beginning of the 19th century, Sir David Brewster, a Scottish physicist, discovered the polarization phenomenon of light reflected at specific angles. In his studies on polarized light, Brewster discovered that when light strikes a reflective surface at a certain angle, the light reflected from that surface is polarized into a single plane. This angle is commonly referred to as *Brewster angle* [1].

The principle behind the Brewster angle is illustrated in Figure 2.1-II [2]. This shows a single ray of light reflecting from a flat surface of a transparent medium having a higher refractive index than air. The incident light is unpolarized in nature, i.e., light having vibrations in all planes perpendicular to the direction of propagation. When the beam arrives on the surface at a critical angle, the Brewster angle, the polarization degree of the reflected beam is 100 percent with the orientation of the electric vectors lying perpendicular to the plane of incidence and parallel to the reflected surface. The refracted ray is oriented at an angle of 90° from the reflected ray and is only partially polarized.

At the Brewster angle of incidence, the reflected and refracted beams are perpendicular to each other. The polarization '*p*' is not reflected because the dipole moments induced in the second medium n_2, by this polarization *p*, point exactly in the direction of reflection. The plane of the figure is the plane of incidence.

From geometry of the Figure 2.1-II:

$\angle CBD = 90°$

We have,

$$\varphi_2 + \varphi_p = 90^o$$

$$\varphi_2 = 90^o - \varphi_p$$

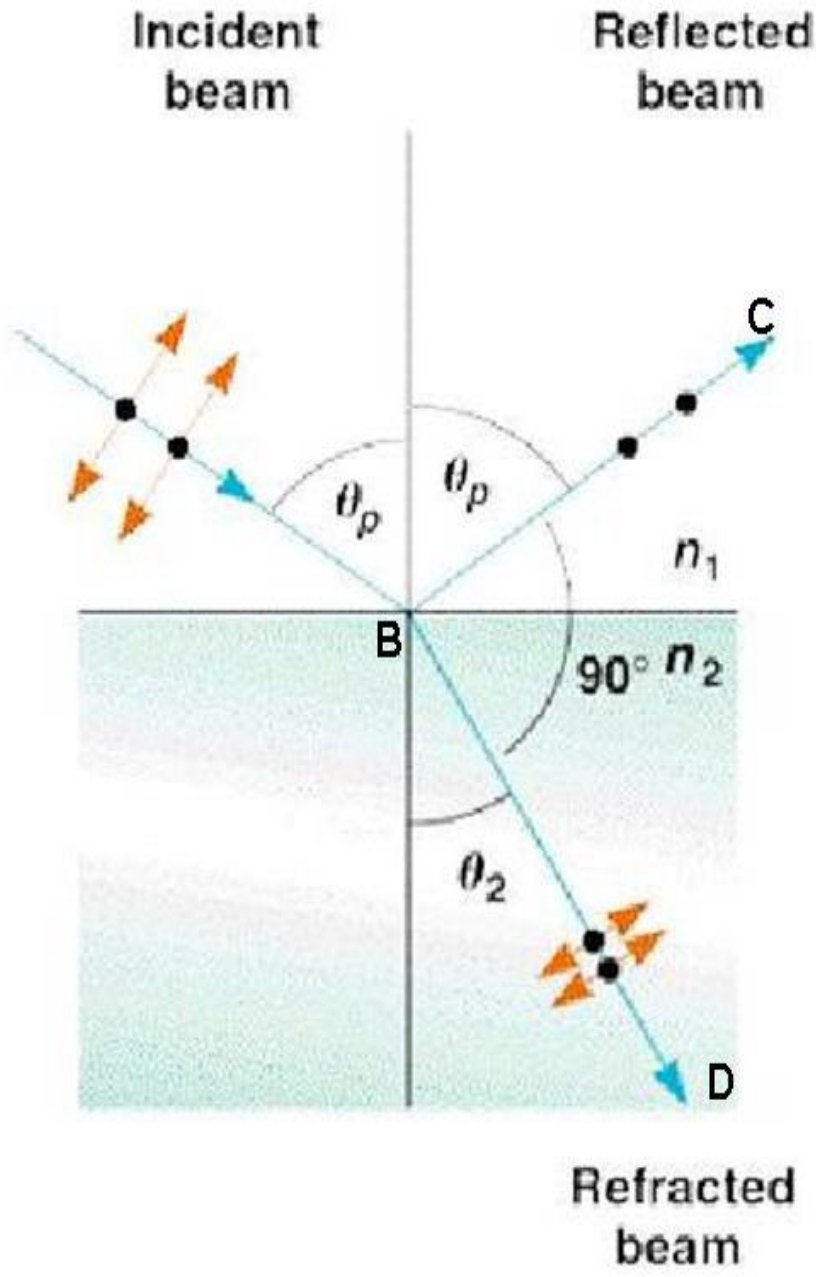

Figure 2.1-II Illustration of the Brewster angle

If μ is the refractive index, then, by Snell's law,

$$\frac{\eta_2}{\eta_1} = \mu = \frac{\sin\varphi_p}{\sin\varphi_2}$$

$$\mu = \frac{\sin\varphi_p}{\sin(90-\varphi_p)} = \frac{\sin\varphi_p}{\cos\varphi_p}$$

$$\mu = \tan\varphi_p$$

$$\varphi_p = \tan^{-1}(\mu)$$

ϕp = Brewster Angle

Light reflected from a highway surface at the Brewster angle often produces annoying and distracting glare that can be demonstrated quite easily by viewing the distant part of a highway or the surface of a swimming pool on a hot and sunny day. Modern lasers commonly take advantage of Brewster angle to produce linearly polarized light from reflections at the mirrored surfaces positioned near the ends of the laser cavity.

2.1.1 Fresnel's equations and the Brewster angle

Fresnel's equations describe the reflection and transmission of electromagnetic waves at an interface [3]. They give the reflection and transmission coefficients for waves parallel and perpendicular to the plane of incidence.

In general, when a wave reaches a boundary between two different dielectric constants, part of the wave is reflected and part is transmitted, with the sum of the energies in these two waves equal to that of the original wave.

Since the electromagnetic waves are transverse, there are separate coefficients in the directions perpendicular to and parallel to the surface of the dielectric. The coefficients for reflection and transmission of the *transverse electric* field (TE) are denoted $r_\perp$ and $t_\perp$ respectively, while the coefficients for reflection and transmission of the *transverse magnetic* field (TM) are denoted $r_\parallel$ and $t_\parallel$ respectively.

For TE radiation

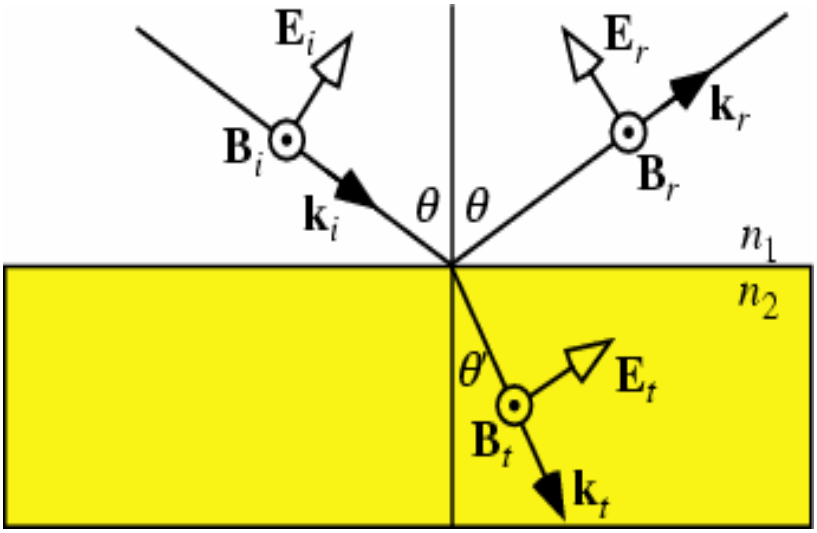

Figure 2.1-III TE radiation

$$r_{\perp} \equiv \frac{E_r}{E_i} = \frac{\frac{n_1}{\mu_1}\cos\theta - \frac{n_2}{\mu_2}\cos\theta'}{\frac{n_1}{\mu_i}\cos\theta + \frac{n_2}{\mu_2}\cos\theta'} \quad (1)$$

$$t_{\perp} \equiv \frac{E_t}{E_i} = \frac{2\frac{n_1}{\mu_1}\cos\theta}{\frac{n_1}{\mu_1}\cos\theta + \frac{n_2}{\mu_2}\cos\theta'}, \quad (2)$$

where, n_1 is the dielectric constant in the original medium, n_2 is the dielectric constant in the second medium, θ is the angle to the normal in the initial medium, θ' is the angle in the second medium (which is different from θ due to refraction), μ_1 is the magnetic permeability in the original medium, and μ_2 is the permittivity in the second medium.

For TM radiation

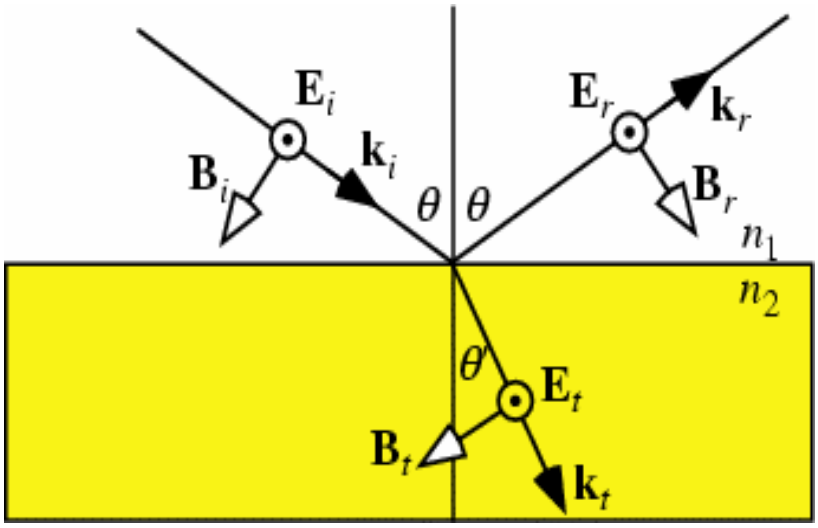

Figure 2.1-IV TM radiation

$$r_{\parallel} \equiv \frac{E_r}{E_i} = \frac{\frac{n_2}{\mu_2}\cos\theta - \frac{n_1}{\mu_1}\cos\theta'}{\frac{n_1}{\mu_1}\cos\theta' + \frac{n_2}{\mu_2}\cos\theta} \tag{3}$$

$$t_{\parallel} \equiv \frac{E_t}{E_i} = \frac{2\frac{n_1}{\mu_1}\cos\theta}{\frac{n_1}{\mu_1}\cos\theta' + \frac{n_2}{\mu_2}\cos\theta}. \tag{4}$$

For $\mu_1 \approx \mu_2$, these simplify to,

$$r_{\parallel} = \frac{\tan(\theta-\theta')}{\tan(\theta+\theta')} = \frac{\sin\theta'\cos\theta' - \sin\theta\cos\theta}{\sin\theta\cos\theta + \sin\theta'\cos\theta'} \tag{5}$$

$$t_{\parallel} = \frac{2\sin\theta'\cos\theta}{\sin(\theta+\theta')\cos(\theta-\theta')}. \tag{6}$$

The angle θ_B at which $r_{\parallel} = 0$, resulting in completely polarized reflected light, is called the Brewster angle.

2.1.2 Derivation of Brewster Angle from Fresnel's equations

From Fresnel's equations, it can be determined that the parallel reflection coefficient is zero when the incident and transmitted angles sum to 90°. The use of Snell's law gives an expression for the Brewster angle.

From Fresnel's equations, the reflection coefficient $r_{\parallel}$ (TM radiation) will be equal to zero when the indices of refraction are equal, so, $\eta_1 = \eta_2$ or

$$n_2 \cos\theta = n_1 \cos\theta'$$

$$\cos^2\theta' = \left(\frac{n_2 \cos\theta}{n_1}\right)^2 \tag{7}$$

Solving for $\sin^2\theta'$ in Snell's law,

$$n_1 \sin\theta = n_2 \sin\theta'$$

$$\sin^2\theta' = \left(\frac{n_1 \sin\theta}{n_2}\right)^2 \tag{8}$$

Adding (7) and (8) yields

$$\sin^2\theta' + \cos^2\theta' = 1 = \sin^2\theta + \cos^2\theta$$

$$= \frac{n_2^2}{n_1^2}\cos^2\theta + \frac{n_1^2}{n_2^2}\sin^2\theta$$

$$\sin^2\theta\left(\frac{n_2^2 - n_1^2}{n_2^2}\right) = \cos^2\theta\left(\frac{n_2^2 - n_1^2}{n_1^2}\right)$$

$$\tan^2\theta = \frac{n_2^2}{n_1^2}$$

$$\theta_B = \tan^{-1}\left(\frac{n_2}{n_1}\right).$$

where, θ_B is the angle from the normal.

Figure 2.1-V shows the reflection coefficient *r* for the electric field of a Fresnel interface between two media similar to air (η_1 = 1) and water (η_2 = 1.33) versus incident angle.

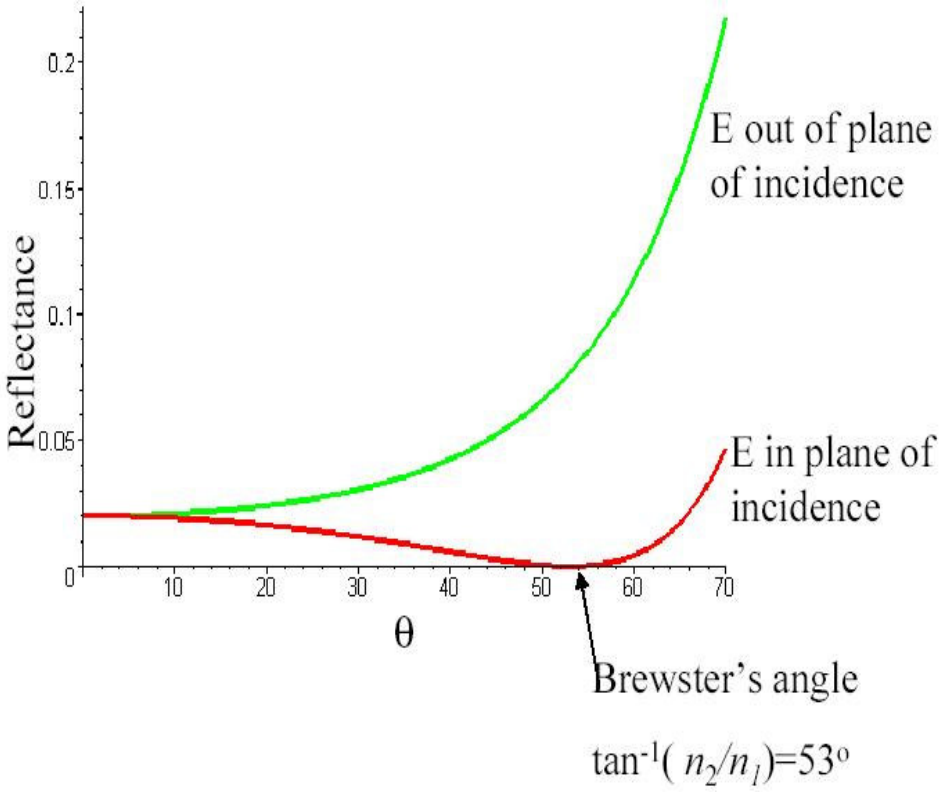

Figure 2.1-V Reflection coefficient r versus incident angle [4]

2.1.3 Brewster angle microscopy

The principle behind the Brewster Angle Microscope (BAM) makes use of the zero reflectance of an air-water interface or dielectric substrate for vertically linearly polarized light at the Brewster angle of incidence.

Brewster angle is determined by the refractive indices of the substrates involved, for example, air-water interface (refractive index of 1.333), air-glass interface (refractive index of 1.515), and air-diamond interface (refractive index of 2.417), the critical angles (Brewster angles) are 53, 57 and 67.5 respectively.

When a condensed phase of a monolayer with different refractive index is spread or deposited on the interface of interest, a measurable change in reflectivity will occur. The reflected light can then be used to form a high contrast image of the lateral morphology of the spread or deposited layer.

A monolayer spread at an air-water interface is extremely thin, approximately 0.5 % of the wavelength of visible light. The relative effect it has on the electric field

reflected from a water surface is therefore very small and the monolayer is under normal conditions quite invisible. However, if the water surface is illuminated with pure vertically linearly polarized light at the Brewster angle before spreading the monolayer at the air-water interface, there is no reflection from the water surface. The background is then completely dark and after spreading the monolayer and compressing it, the tiny effect of the monolayer can be visualized. Figure 2.1-VI illustrates the change in reflectivity due to a thin film on a substrate or at air water interface [5] and leads to significant contrast.

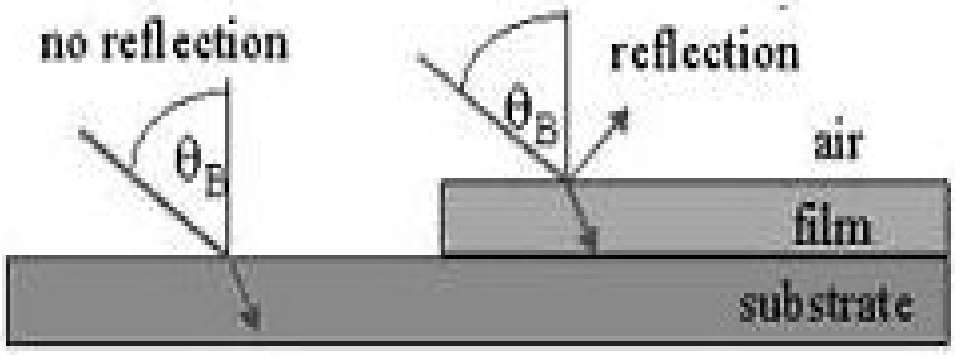

Figure 2.1-VI Schematic illustration of the change in reflectivity due to a thin film on a substrate or air-water interface

2.1.4 Applications of Brewster angle microscopy

In an increasing number of publications, researchers use BAM to monitor the monolayer phases. List of the other application areas of the BAM are mentioned below:

1. Phase behavior of monolayers, i.e., domains and order phenomena [6-10].
2. Influence of sub phase compositions on monolayer structures [11-13].
3. Phase separation in monolayers and thin films [14, 15].
4. Transformation of monolayer into multilayered structure [16, 17].
5. Determining the quality and homogeneity of thin (organic) films and LB films [18- 21].

Brewster angle microscopy is the surface characterization technique that is well suited for the in-situ characterization of the monolayer formed at the air-water

interface. These monolayers are known as Langmuir films. Section 2.2 gives the details regarding the basics of the Langmuir films, their importance and about pressure area isotherm, which is the most promising way to study these monolayers.

2.2 Langmuir films

Langmuir films [22] consist of surface active materials or *surfactants* trapped at the interface between two dissimilar phases, either liquid-liquid or liquid-gas. Surfactants are molecules, which are amphiphilic in nature (Figure 2.2-I) and consist of a hydrophilic (water soluble) and hydrophobic (water insoluble) part. The hydrophobic part usually consists of hydrocarbon or fluorocarbon chains and the forces acting upon them are predominantly van der Waal's force. The hydrophilic part consists of a polar group (-OH, -COOH, $-NH_3^+$, $-PO_4^-(CH_2)_2NH_3^+$ etc.) and the forces acting upon them are predominantly Coulomb forces.

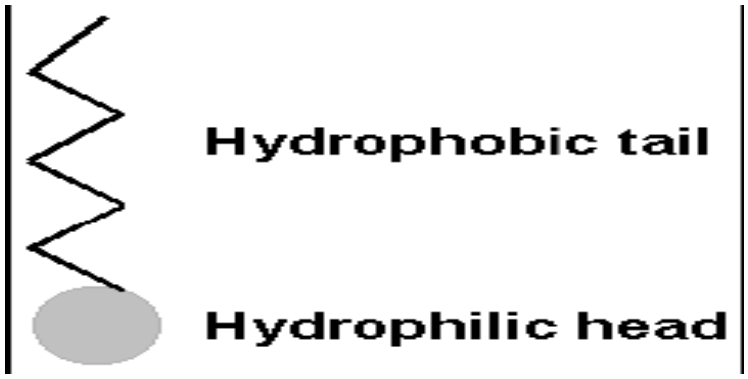

Figure 2.2-I Schematic of an amphiphilic molecule showing hydrophobic (long hydrocarbon chain) and hydrophilic (polar group) parts

Amphiphilic molecules are trapped at the interface because they possess two different types of bonding within the one molecular structure. The driving force behind the association is the reduction of the free energy of the system. Therefore, when a surfactant comes in contact with water, it accumulates at the air-water interface causing a decrease in the surface tension of water. Many of these amphiphilic molecules insoluble in water can (with the help of a volatile and water insoluble solvent) be easily spread on the water surface with hydrophilic *head* groups pulling the molecule into the bulk of the water and the hydrophobic *tail* groups pointing into the air. One molecule thick surface monolayer will only be achieved if

the amphiphilic balance (balance between hydrophilic and hydrophobic parts) of the molecule is correct. Sweeping a barrier over the water surface causes the molecules to come closer together and eventually form a compressed and an ordered monolayer. The film produced by such a method is known as a Langmuir film [23]. The amphiphilic nature of the surfactants dictates the orientation of the molecules at the air-water interface in such a way that the polar head group is immersed in the water and the long hydrocarbon chain is pointing towards air (Figure 2.2-II).

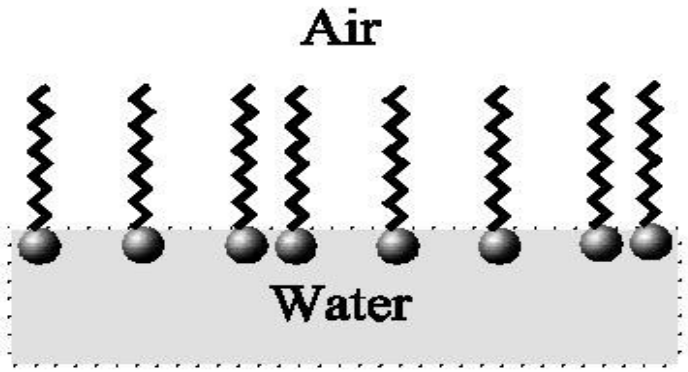

Figure 2.2-II showing a spread monolayer at the air-water interface

The hydrocarbon chain of the substance used for monolayer studies has to be long enough to form an insoluble monolayer. There should be minimum 12 hydrocarbons or groups in the chain. If the chain is shorter, though still insoluble in water, the amphiphile on the water surface tends to form micelles. These micelles are water soluble, which prevents the build-up of a monolayer at the interface. On the other hand, if the length of the chain is too long, the amphiphile tends to crystallize on the water surface and consequently does not form a monolayer. Furthermore, the amphiphile has to be soluble in some organic solvent that is highly volatile and water insoluble. Chloroform or hexane is commonly used for this purpose.

The most important indicator of the monolayer properties of an amphiphilic material is given by measuring the surface pressure area isotherm. Section 2.2.1 gives the details about the pressure area isotherm.

2.2.1 Surface pressure area isotherms

The most important indicator of the monolayer properties of an amphiphilic material is given by measuring the surface pressure as a function of the area of water

surface available to each molecule. This is carried out at constant temperature and is known as a surface pressure area isotherm or simply *isotherm*.

When a solution of an amphiphile in a water insoluble solvent is placed on the water surface with a micro syringe, the solution spreads rapidly to cover the available area. As the solvent evaporates, a monolayer is formed. When the available area for the monolayer is large, the distance between adjacent molecules is large and their interactions are weak. Then, the monolayer can be regarded as a two-dimensional gas. Under these conditions, the monolayer has little effect on the surface tension of water. If the available surface area of the monolayer is reduced by a barrier system, the molecules start to exert a repulsive effect on each other. This two-dimensional analogue of pressure is called surface pressure [23], and is given by the following relationship

$$\pi = \gamma - \gamma_o$$

where, γ is the surface tension of pure water surface and γ_o is the surface tension with the monolayer.

Usually an isotherm is recorded by compressing the film (reducing the area with the barriers) at a constant rate while continuously monitoring the surface pressure. Depending on the material being studied, repeated compressions and expansions may be necessary to achieve a reproducible trace. Figure 2.2-III shows the typical pressure area isotherm and various phase transitions of the floating monolayer.

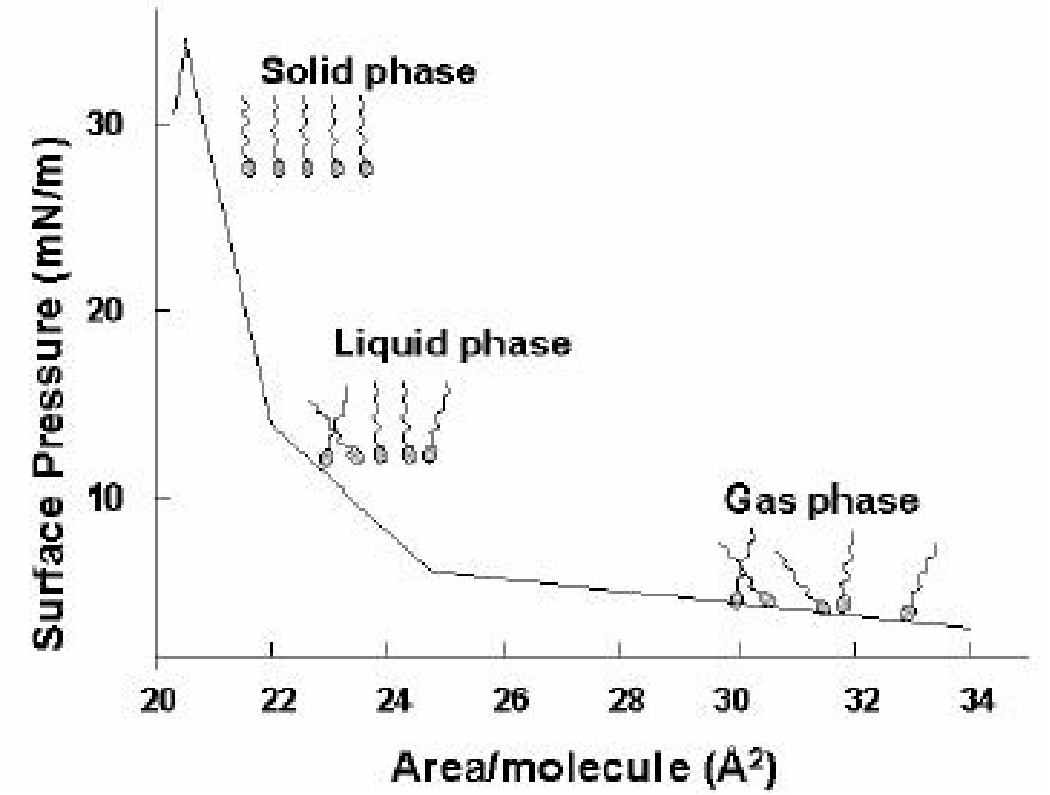

Figure 2.2-III Typical pressure area (ð-A) isotherm showing the various phase transitions of the floating monolayer

As early as 1952, W. D. Harkins proposed a simple terminology to classify different monolayer phases of an amphiphile molecule [24]. Initially, the monolayer exists in the gaseous state (G) and on compression can undergo a phase transition to the liquid-expanded state (LE). Upon further compression, the LE phase undergoes a transition to the liquid-condensed state (LC), and at even higher densities, the monolayer finally reaches the solid state (S). If the monolayer is further compressed after reaching state S, the monolayer will collapse into three-dimensional structures. The collapse is generally seen as a rapid decrease in the surface pressure or as a horizontal break in the isotherm if the monolayer is in a liquid state. This collapse pressure is a function of the temperature, the pH of the sub phase and the speed by which the barrier is moved.

An isotherm gives the information about the stability of the molecules in the two-dimensional system, phase transitions and conformational transitions. It also gives some idea of the amount of pressure that has to be applied to the film on the sub

phase to enable deposition of the LB film in the solid phase. Thus, at appropriate pressure, the film can be transferred to the substrate.

2.2.2 Measurement of surface pressure using Wilhelmy plate

The surface pressure is measured by the Wilhelmy plate method [25]. In this method, measurement is made by determining the force due to surface tension on the plate that is partially immersed in the sub phase.

Then, this force is converted into surface tension (mN/m or dynes/cm) with the help of the dimensions of the plate.

The plate is often very thin and made of platinum, but even plates made of glass, quartz, mica and filter paper can be used.

When the Wilhelmy plate is immersed in the water (Figure 2.2-IV), there are generally three forces acting upon it.

1. Weight of the plate.
2. Up thrust on the submerged part of the plate.
3. Surface tension of the plate.

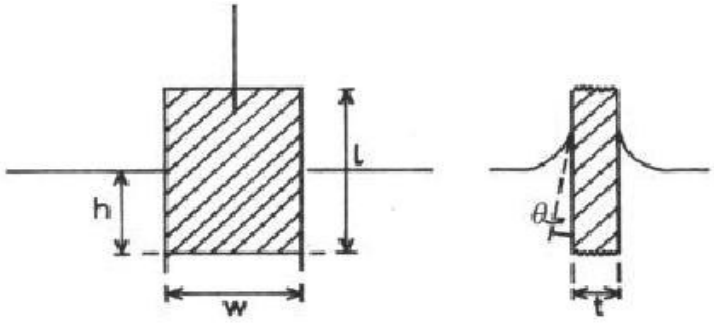

Figure 2.2-IV Wilhelmy plate partially immersed in a water surface

If the dimensions of the plate are l, w and h, the net force acting on the plate is:

Force = weight – up thrust + Surface tension

$$= (\partial p * l * w * t) * g - (\partial l * h * w * t) * g + 2 * (w + t) * ST * \cos \phi \qquad (1)$$

Where, ∂p = density of the plate.

∂l = density of the liquid.

ST = surface tension of the liquid

ϕ = contact angle of the liquid with the plate

Before making any measurements, the pressure is zeroed, thereby eliminating the weight term from equation (1).

F = - up thrust + Surface tension

While making the measurements, the plate is drawn up out of the liquid, so that its lower edge is at the level of the liquid surface. This eliminates the up thrust.

Force = $2 * (w + t) * (ST) * \cos \phi$

Finally, if the contact angle is zero, $\cos \phi = 1.0$

Force = $2 * (w + t) * (ST) * 1.0$

ST = Force / $2 * (w + t)$

ST = Force / perimeter (mN/m)

References

1. "Why Brewster angle microscopy – BAM", Technical note, KSV instruments Ltd., Finland.
2. Serway, College Physics, 5/e, Text Figure 24.21.
3. http://scienceworld.wolfram.com/physics/FresnelEquations.html
4. Phys 114 – Lecture 25, Natalie Holzwarth
5. http://users.otenet.gr/~garof/Bam
6. Ruiz-Garcia J., Qui X., Taso M. W., Marshall G., Knobler C. M., Overbeck G. A., Mobius D., *J. Phys. Chem.* **1993**, 97, 6955.
7. Werkman, P. J.; Schouten, A. J.; Noordegraaf, M. A.; Kimkes, P.; Sudho¨lter, E. J. R. *Langmuir* **1998**, 14, 157.
8. Gehlert, U.; Weidemann, G.; Vollhardt, D.; Brezesinski, G.; Wagner, R.; Mo¨wald, H. *Langmuir* **1998**, 14, 2112.
9. Deschenaux, R.; Megert, S.; Zumbrunn, C.; Ketterer, J.; Steiger, R. *Langmuir* **1997**, 13, 2363.
10. Cohen Stuart, M. A.; Wegh, R. A. J.; Jroon, J. M.; Sudho¨lter, E. J. R. *Langmuir* **1996**, 12, 2863.
11. Vollhardt, D.; Melzer, V. *J. Phys. Chem. B* **1997**, 101, 3370.
12. Melzer, V.; Vollhardt, D. *Phys. Rev. Lett.* **1996**, 76, 3770.
13. Overbeck, G. A.; Ho¨nig, D. Mo¨bius, D. *Thin Solid Films* **1994**, 242, 213.
14. Vollhardt, D.; Melzer, V. *J. Phys. Chem. B.* **1997**, 101, 3370.
15. Melzer, V.; Vollhardt, D. *Phys. Rev. Lett.* **1996**, 76, 3770.
16. De Mul, M. N. G.; Mann, J. A., *Langmuir* **1994**, 10, 2311.
17. Friedenberg, M. C.; Fuller, G. G.; Frank, C. W.; Robertson, C. R. *Langmuir* **1994**, 10, 1251.
18. Yuh-Lang Lee, Yaw-Chia Yang, and Yu-Jen Shen, *J. Phys. Chem. B.* **2005**, 109, 4662-4667.
19. D. Vollhardt, S. Siegel, D.A. Cadenhead, *J. Phys. Chem. B.* **2004**, 108, 17448-17456.
20. Werkman, P. J.; Schouten, A. J.; Noordegraaf, M. A.; Kimkes, P.; Sudho¨lter, E. J. R. *Langmuir* **1998**, 14, 157.

21. Gehlert, U.; Weidemann, G.; Vollhardt, D.; Brezesinski, G.; Wagner, R.; Mo¨wald, H. *Langmuir* **1998**, 14, 2112.
22. "Insoluble Monolayers at Liquid Gas Interface", G. L. Gaines Jr., *Interscience*, New York, 1966.
23. "Langmuir and Langmuir Blodgett films: What and How?", Application note #107, KSV instruments Ltd., Finland.
24. Ulman A., *An introduction to Ultrathin Organic Films: from Langmuir-Blodgett to Self-Assembly*, Academic Press, San Diego, CA, 1991.
25. Technical manual from Nima technology, England.

CHAPTER 3

DESIGN, DEVELOPMENT AND FABRICATION OF BAM AND LANGMUIR TROUGH

This chapter describes the indigenous development of the BAM instrument that has been carried out during this research work.

3.1 Design, development and fabrication of Brewster angle microscope

The principle behind Brewster angle microscopy has been discussed in the previous chapter. The advent of this technique has allowed for detailed studies of Langmuir monolayers at the air-water interface. Such films that are prepared on the water surface in the Langmuir trough can be transferred from the water surface to solid support by the Langmuir-Blodgett technique. The quality of the transferred film depends crucially on the morphology of the floating film from which it is formed. Therefore, the in-situ qualitative visual inspection of these monolayers is of much interest. BAM has proven to be an extremely valuable tool for characterization of the morphology of insoluble monolayers of surfactant molecules at air-water interface. Instruments that are presently commercially available (comparative study in section 1.4) have good performance but are rather heavy and very expensive. The designed BAM instrument along with Langmuir trough is compact, economical and easy to use.

3.1.1 Design objective

In Chapter 1, the initial development of the BAM instrument that was carried out in our laboratory has been discussed. In the setup, the incident laser light source and camera along with the imaging optics were tilted at the Brewster angle of the subphase. The collimator designed for that setup was heavy.

In the typical setup of BAM, the air-water interface is illuminated at the Brewster angle with polarized light in the plane of incidence. The incidence angle has to be adjusted with high accuracy. This is achieved either by mirrors or by an optical fiber, which allows one to adjust the incidence keeping the same part of the film illuminated. One problem inherent to BAM is that the surface must be viewed under an angle and only a narrow strip of the area will be focused. The surface elements which are far away from this narrow strip appear fuzzy and unfocused. In the case of a BAM instrument developed by Meunier [1], the area of interest was scanned, retaining only a narrow strip around the focal line. The final image was then composed of these strips after they had been treated digitally to remove the compression. This leads to a good quality image but it takes a long time to capture and process the images. It is also mandatory that the image object does not move

during the capture. However, this is practically not possible. The depth of field of objective allows for a narrow strip of the film to be in focus. To enlarge this strip, one can increase the depth of field by decreasing the aperture of the objective. One can thus take images in focus on a strip a few tens of micrometer wide, and with an in-plane resolution of about 5-10 μm. But increasing the depth of field decreases the in-plane resolution of the microscope. To avoid all these drawbacks, in the current setup the laser source, camera and the imaging optics are mounted vertically [2]. The aperture of the objective is big enough to allow light reflected at the Brewster angle and the light scattered around this direction to be collected to form an image. Because the symmetry axis of the objective is vertical, the film is in focus and images are taken at video rate and hence reconstruction of the image is not required.

The incident light beam in a Brewster angle microscope comes from a laser beam. This is the only light source because the light must have high intensity and the incident beam must have a well defined direction (parallel beam) to illuminate the surface at the Brewster angle as precisely as possible, otherwise the contrast of the images would be decreased. However, the drawback is that laser light produces interference fringes. Another difficulty is that, the reflectivity, even in the presence of molecules on the surface, is very low, typically of the order 10^{-6}. This is a small value and very thin layers or low density monolayers will be difficult to observe in Brewster angle microscopy. In order to cope with this, a high power laser and a sensitive video camera are needed and the parasitic light must be carefully eliminated. Meunier used a sensitive CCD camera in combination with Ar^{+} ion laser, but the drawback of this is a rather bulky instrument. Use of small compact laser diode in the current setup removes these limitations.

In our design, we wanted to achieve good contrast and good sensitivity without using heavy or bulky parts. Section 3.1.2 describes the current BAM setup.

3.1.2 Description of the BAM setup

In the developed setup of BAM, the light source, collecting optics and the camera were mounted vertically. The incident p-polarized beam is directed onto the sample surface by a front surface silver mirror M1 of diameter 0.5 inch. The second mirror M2 directs the reflected beam into the lens system. The mirrors are supported

by a screw for adjusting the incidence and reflected angle. Figure 3.1-I shows the schematic of the vertical BAM set-up.

The light source for the instrument is a laser diode (LaserMax LDM-4-650-25-G, 25 mm long, 11 mm diameter) which emits 35 mW at 650 nm. The emitted beam passes through the Glan Thompson prism polarizer. A high level of polarization is important for obtaining high quality images. The lens system consists of a lens with focal length of 28 mm. The lens focuses the image on to a charge-coupled device (CCD). A working distance of at least 30-40 mm is required so that the barrier used for compression of the monolayer could easily pass under the microscope. A 60 mm extension tube is inserted in front of the CCD camera to vary the magnification. The rack and pinion assembly is coupled to for fine movement of this extension tube. Mounts for laser diode, polarizer and mirror holder are fabricated from local industries as per our design. Figure 3.1-II and Figure 3.1-II shows the photograph of the entire setup of the instrument.

The first step in aligning the microscope is to set the angles of the two mirrors close to the Brewster angle. The polarizer is turned 90^0 from the plane of incidence and the laser diode is then rotated on the beam axis until no light is transmitted to the polarizer. The polarizer is then returned to the plane of incidence and the mirror M1 is then carefully set at the Brewster angle of water by adjusting the screw mechanism until no reflection is observed on the target. However, for real interfaces, the refractive index does not change abruptly from one value to the other, and these interfaces are more or less rough. As a consequence, the reflection is minimal but does not vanish at the Brewster angle. As the angle of the mirror M1 is changed, the alignment of the mirror M2 may have to be adjusted to ensure that the beam continues to be directed in the lens system and on the camera. The exact position of the spot of measurement was marked by calibrating with the reflected light from a TEM grid positioned under the microscope.

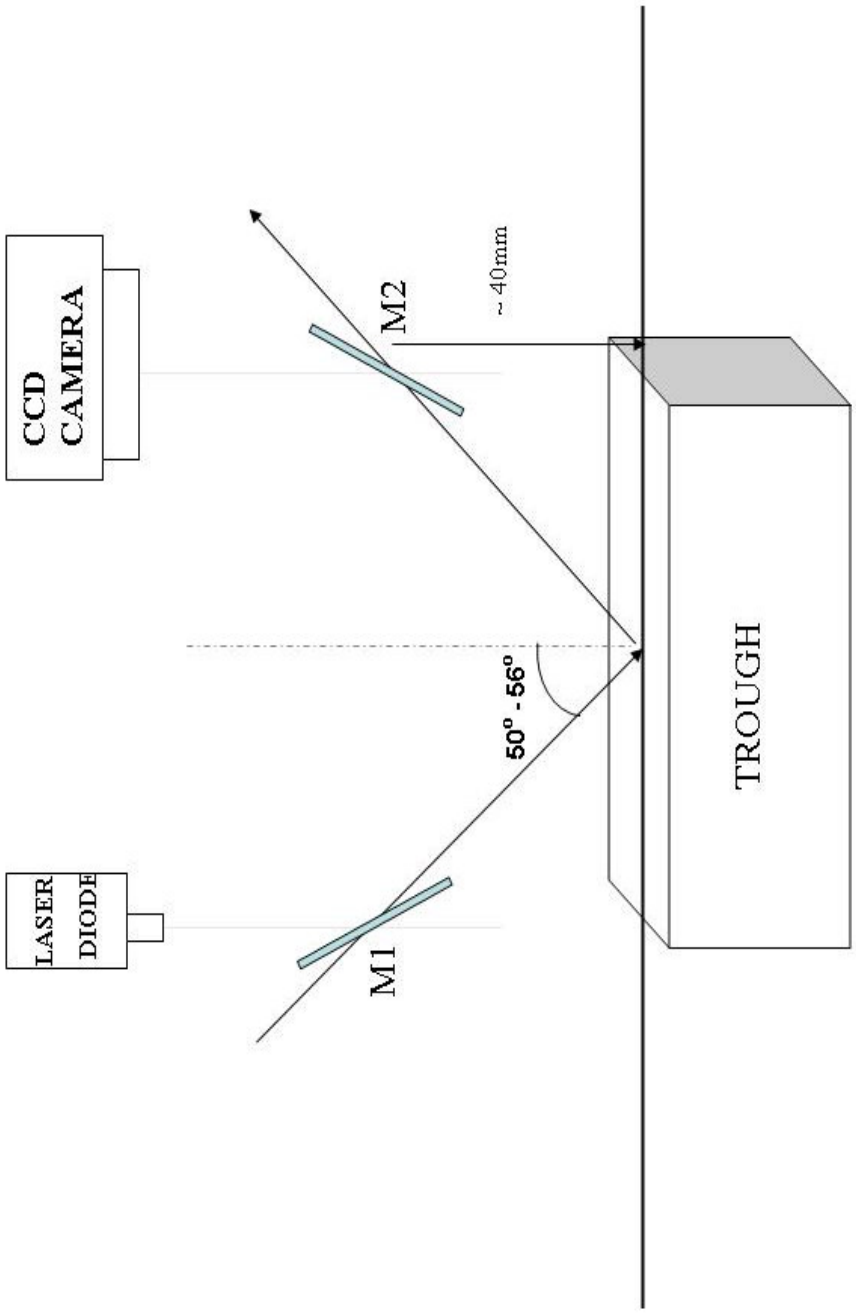

Figure 3.1-I Schematic of the vertical BAM set-up

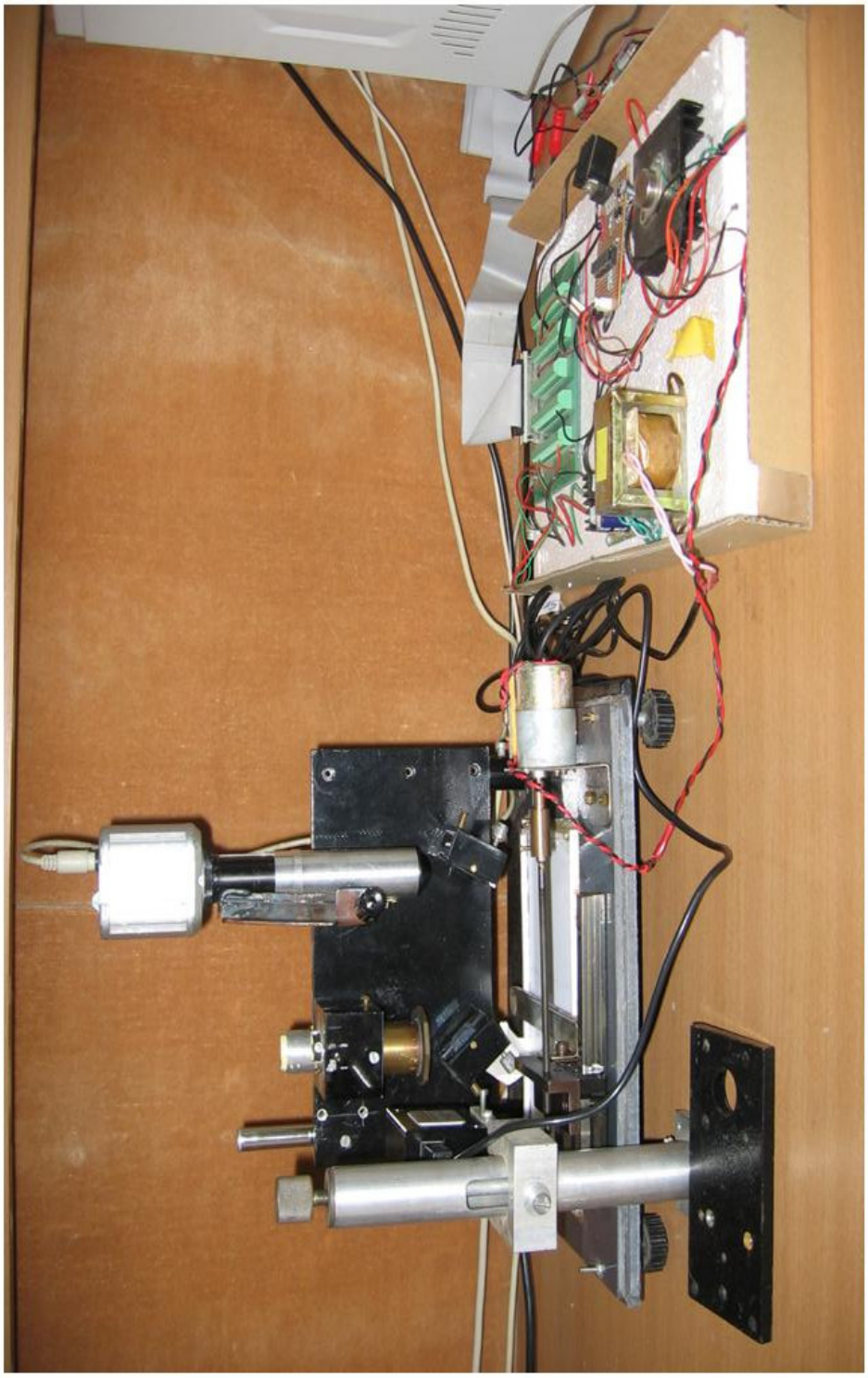

Figure 3.1-II Photograph of the setup of the instrument with electronics

Figure 3.1-III Photograph of the entire setup of the instrument

The camera used is a CCD camera (Kocom KCC 310). The camera has its maximum response at 650 nm and has a lower detection limit of 0.1 lux. The horizontal resolution of the camera is 450 TV lines. The output terminal contains both S-Video and a BNC connector. The detail specifications of the CCD camera are given in Appendix A. For real-time capturing of the images and also for storing the images, camera is coupled to the frame grabber add-on card. National Instrument NI IMAQ PCI 1411 frame grabber card is used for this application. The IMAQ PCI 1411 is an analog image acquisition (IMAQ) board designed to acquire color and grayscale images. The accompanied NI IMAQ driver software supports LabVIEW as a development environment. Chapter 4 discusses interfacing and programming of frame grabber card in detail.

3.2 Langmuir trough design

Agnes Pockles [4] first designed a trough with barriers for manipulation of the film at the air-water interface. In that design, the barriers were placed across the edges of the trough. Since then, the trough has been dramatically changed and developed. Today, the trough is fully computerized with the state-of-the-art electronics. Figure 3.2-I presents a schematic of one barrier trough [5].

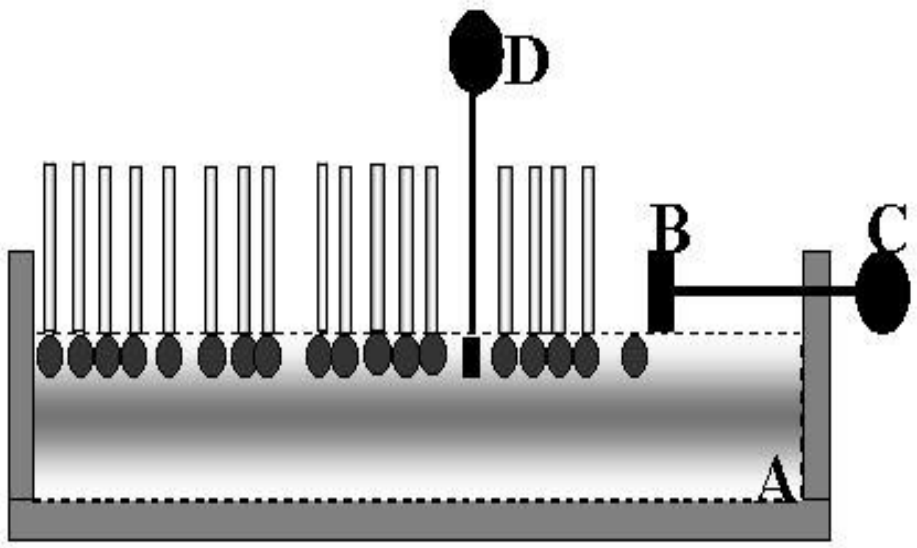

Figure 3.2-I Schematic of the trough for deposition of monolayer

In Figure 3.2-I,

A, a trough, usually made up of teflon;

B, a moving barrier that controls the pressure applied on the monolayer;

C, a motor that moves the barrier;

D, a balance that measures the pressure;

While designing trough, few points should be taken into consideration.

1. Leakage of the film must be prevented: In order to prevent the leakage of the film between the barriers and the trough edges, a good fit between the trough and the barrier is required. This is usually obtained by using barriers of square or rectangular cross-section and trough edges carefully machined flat.
2. Spilling over of the sub phase must be prevented: To prevent spilling over of the subphase liquid, the trough edges must be non wetting. Either the trough must be constructed of a hydrophobic material or the edges must be coated to prevent wetting.
3. Contamination must be prevented: The materials forming the trough must not contribute to the contamination of the system. Also, the liquid subphase should not affect the trough.
4. The surface should be accessible for manipulation: The liquid surface is made accessible by making it rise slightly above the brim of the trough. The barriers for manipulation of the film can then rest across the edges of the trough.
5. Choice of material: A solid piece of teflon is widely used for the trough and barriers. This is mainly because of cleanliness advantages, since it can be treated with strong oxidizing agents such as sulfochromic acid, or a mixture of nitric and hydrochloric acid to ensure a complete removal of organic contaminates.

Taking into consideration all above points, a Langmuir trough has been designed and fabricated for depositing Langmuir films. A trough is made up of teflon that is a chemically inert material. It consists of a single barrier for compressing and decompressing the monolayer. Generally, the barrier mechanism is driven along the trough by a toothed belt. A precision DC motor and a gearbox move the belt mechanism. The combination turns the pulley at one end of the belt and barrier position is detected by a potentiometer attached to a second pulley at the other end of the belt. This becomes a more complex system to drive the barrier of the Langmuir trough and also generates heat and wastes power. So, at NCL, we designed a state-of-

the-art LB trough [6] for horizontal barrier movement that totally eliminates belt and pulley mechanism. Figure 3.2-II shows the photograph of the developed trough.

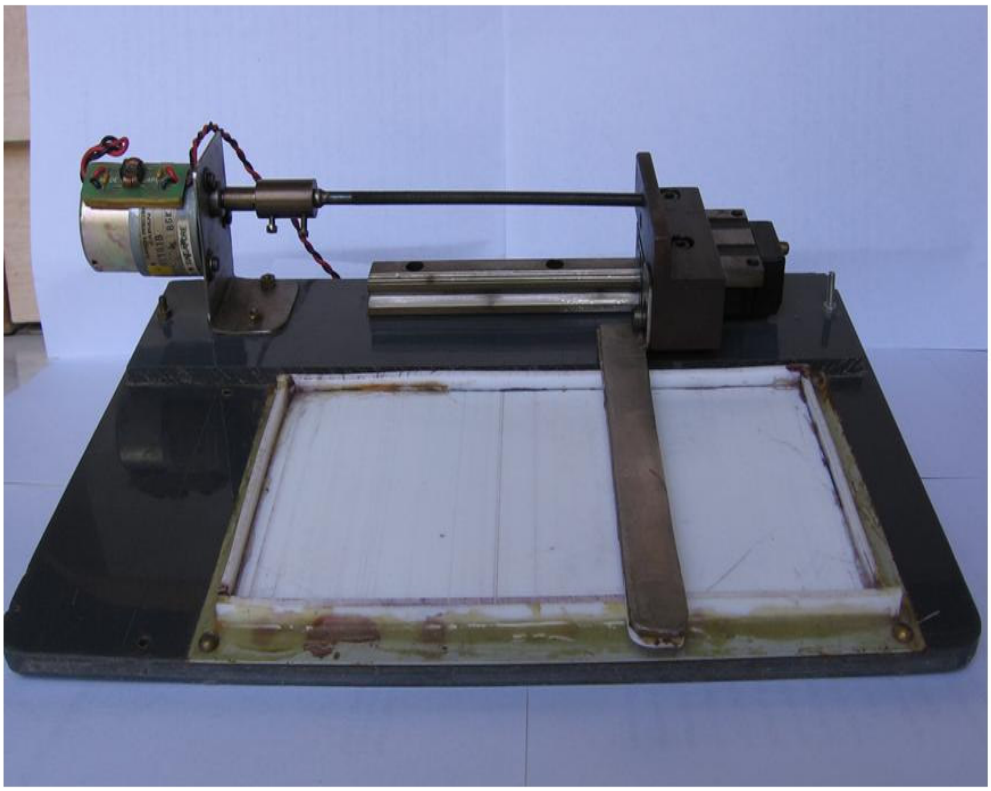

Figure 3.2-II Photo of the developed Langmuir trough

3.3 Choice of motor for barrier movement

Stepper motor and a DC motor are the two options that can be used for the barrier movement. A stepper motor uses frequency as input. The stepper motor has a permanent magnetized core surrounded by a magnetic field. Sending current to different phases of the motor alters the field, which makes the motor to take steps. A motor driver is used to translate a pulse train into phase current for the required motion. The current is set by the driver according to an excitation sequence. By using different sequences, the number of steps per revolution for the motor axis can be altered. On the other hand, a DC motor provides movement that is directly proportion to the voltage applied to it. The control signal to the dc motor is a voltage level. In the initial setup, stepper motor and driver circuitry with microcontroller module was used for controlling the direction and speed of the barrier. The approach of complete PC based solution has enabled us to choose a dc motor for the barrier movement. The advantage of using a dc motor is smooth movement and that the signals from the AD/DA card can be directly used to control the direction and speed of the motor.

A dc motor is coupled to the barrier assembly with some mechanical arrangement is shown in figure. The forward, reverse direction and speed of the motor has been controlled through the real-time system software (Chapter 4: Section 4.9).

3.4 Pressure sensor

The pressure sensor used for this application is Model PS4 [3] obtained from NIMA Technology, England. Figure 3.4-I shows the mechanical setup of the pressure sensor.

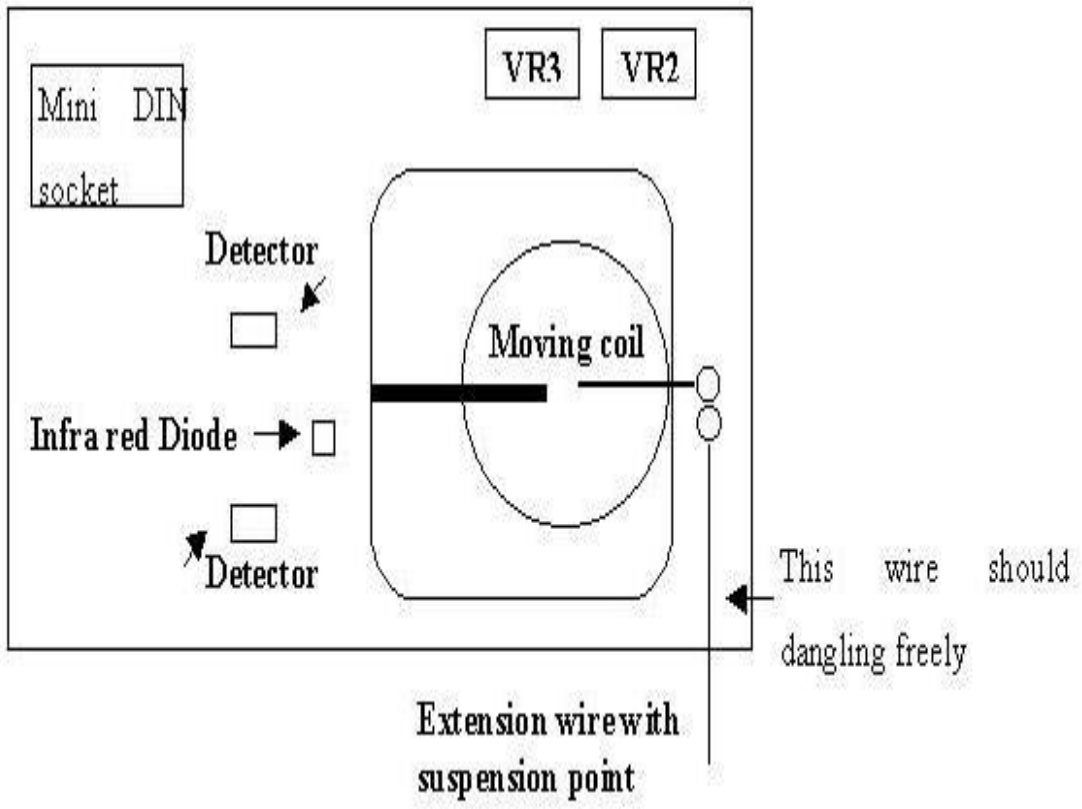

Figure 3.4-I Mechanical setup of pressure sensor

The pressure sensor has a magnetic coil, a moving arm of which is illuminated by IR-diode. A shadow cast by the arm falls on two IR detectors and the control electronics holds the arm in place, so that the shadow falling on each detector is always the same. The force required to hold the arm steady is then simply read off by measuring the current through the coil. Figure 3.4-II and Figure 3.4-III shows the actual photograph of the pressure sensor.

Figure 3.4-II Photo of pressure sensor

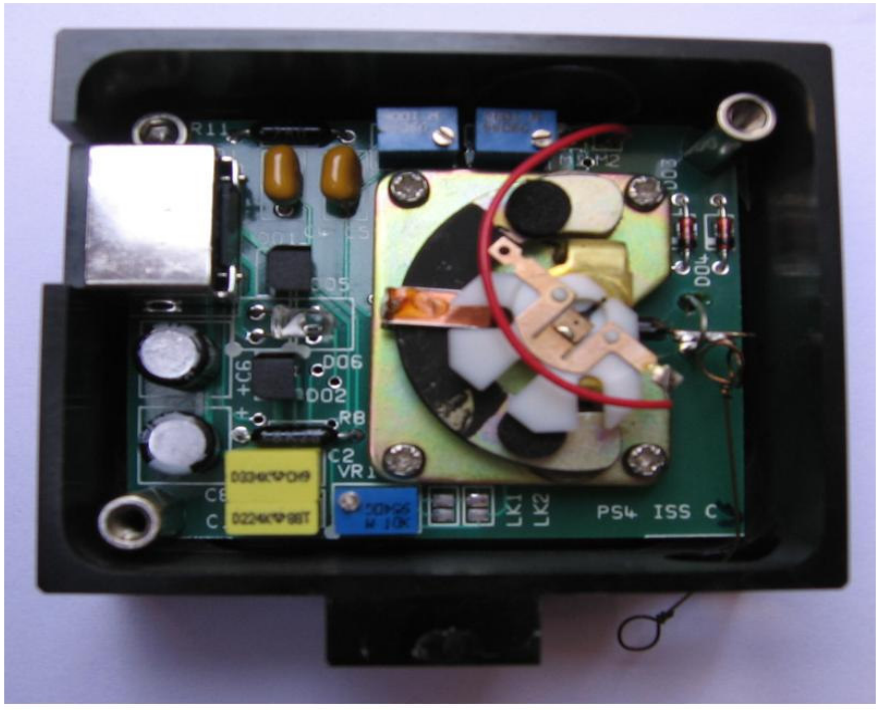

Figure 3.4-III Pressure sensor with signal conditioning circuitry

PS4 can support up to 500 mg load. This is equivalent to a range of more than 240 mN/m for a 21 mm perimeter of Wilhelmy plate. The dimensions of the pressure sensor are 62 mm x 28 mm.

Accuracy of the sensor is determined by the width of the plate, for 10 mm wide plate, the accuracy is 0.1 mN/m.

The output from the pressure sensor is in volts and is terminated to a 5-pin DIN socket (Figure 3.4-IV).

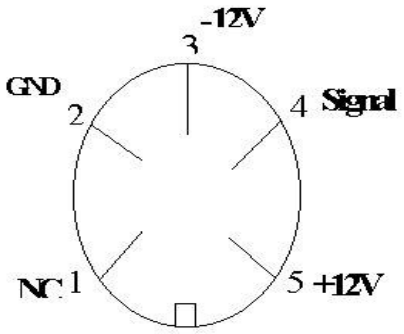

Figure 3.4-IV 5-pin DIN Socket

3.4.1 Calibration of the sensor

1. Calibration

Force suspended from sensor	**Approximate output (volts)**
Output with empty weighing pan	0.2 V
Output with pan + 100 mg:	0.6 V

Procedure: (Figure 3.4-I)

(a) Adjust VR2 potentiometer until 0.2 V is displayed.

(b) Add 100 mg weight and adjust VR3 potentiometer until 0.6 V is displayed.

(c) Remove the weight and verify whether 0.2 V is displayed.

(d) Adjust VR2 again, if necessary.

2. Calibration check

For calibration check, use the developed software (Chapter 4: Section 4.5) for measuring the surface pressure.

(a) Attach the empty weighing pan to the sensor and "Zero" the reading with control software.

(b) Then, add the 100 mg calibration weight and display should show 46.7 mN/m. This value is the equivalent of 100 mg force when measured with the standard 21.0 mm paper plate.

Surface tension = Force / Perimeter
= 100 mg / 21 mm
= 0.981 mN / 0.021 m
= 46.7 mN/m

The pressure sensor is mounted on specially designed and fabricated holder (Figure 3.4-V). It can be moved vertically to adjust the height of the pressure sensor from trough.

Figure 3.4-V Pressure sensor along with holder

3.5 Hardware Design

This section describes in detail the hardware used to implement the interface between the National Instruments AD/DA card NI 6014 and the DC motor drivers for the generation and reading of motor signals. It also describes the interfacing of pressure sensor with NI 6014 AD/DA card for measuring surface pressure. Need to use single multi I/O card for the entire application was the main criterion for selecting the add-on AD/DA card. Hence, the same card (NI 6014) is used in Analog input (AI), Analog output (AO) and digital input/output (DIO) mode. The card acts as true input-output card and can generate signals and can receive the data from external system.

3.5.1 Data Acquisition Card PCI-6014

NI 6014 device is a high performance multifunction analog, digital and timing I/O device for PCI. NI 6014 has a 68 pin connector and features 16 channel (eight differential) of 16 bit AI, two channels of 16 bit AO and eight lines of digital I/O (DIO).

Because of the NI standard architecture for data acquisition and standard specification, the NI 6014 is completely software configurable.

I/O connector detail and pin assignment of the card is given in Appendix B.

3.5.1.1 Analog Input section

AI of the card is being used for measuring surface pressure. The AI section of the NI 6013/6014 is software configurable. The following sections describe in detail each AI setting.

The AI signals for NI 6014 are ACH0 (0 … 15), AISENSE and AIGND.

Input modes: It has two input modes.

1. *NRSE: Non referenced single ended*

A channel configured in NRSE mode uses one AI line, which connects to the positive input of Programmable Gain Instrumentation Amplifier (PGIA). The negative input of the PGIA connects to AISENSE.

2. *DIFF: Differential mode*

A channel configured in DIFF mode uses two lines. One line connects to the positive of Programmable Gain Instrumentation Amplifier (PGIA) and other connects to the negative of PGIA.

Input Range

The NI 6013/6014 has a bipolar input range that changes with the programmed gain. Each channel may be programmed with a unique gain of 0.5, 1.0, 10, or 100 to maximize the A/D converter (ADC) resolution.

With the proper gain setting, the full resolution of the ADC can be set to measure the input signal. Table 3-1 shows the input range and precision according to the gain used.

Gain	Input Range	Precision
0.5	–10 V to +10 V	305.2 µV
1.0	–5 V to +5 V	152.6 µV
10.0	–500 mV to +500 mV	15.3 µV
100.0	–50 mV to +50 mV	1.53 µV

Table 3-1 Input range and precision

The output from the pressure sensor is connected to the AD/DA card in NRSE mode as shown in Figure 3.5-I.

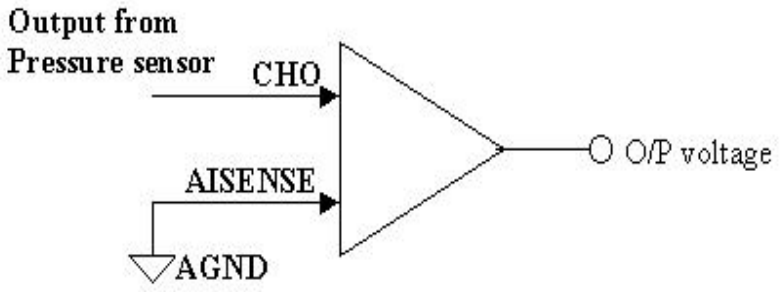

Figure 3.5-I NRSE mode

Other two signals required for pressure sensor connector are +12 V and –12 V. These signals are generated by the power supply.

3.5.2 Interfacing of DC motor

NI 6014 card in Analog output (AO) mode and in Digital input-output (DIO) mode is used to interface DC motor with barrier.

3.5.2.1 Analog out for NI 6014

The NI 6014 has two channels of 16-bit AO voltage at the I/O connector. This has a fixed bipolar output range of ±10 V. For controlling the speed of the motor, this signal is used.

3.5.2.2 Digital I/O

The NI 6013/6014 contains eight lines of digital I/O (DIO 0 ... DIO 7) for general purpose use. Each line of DIO can be configured as input or output. At system startup and on reset, all DIO ports are in high-impedance state.

For controlling direction of the dc motor, DIO 4 and DIO 5 are used as control signals for the dc motor driver circuitry.

3.6 DC motor driver

L298, a dual full bridge driver, is used to control the dc motor in bi-directional mode. L298 is an integrated monolithic circuit in a 15-lead multiwatt and Power SO20 packages. It is a high voltage, high current dual full bridge driver designed to accept standard TTL logic levels and drive inductive loads, such as relays, solenoids, dc and stepping motors. Two inputs are provided to enable or disable the device independently of the input signals.

A bi-directional dc motor control schematic is shown in appendix C, in which only one bridge is needed. The brake function (fast motor stop) requires that the absolute maximum rating of 2 Amperes must never be overcome.

3.7 Input Signals for the Hardware

Table 3-2 summarizes the input/output signals for the hardware that are generated by the AD/DA card, NI 6014, and the voltage supply. The signals are used for measuring the voltage from the pressure sensor and for controlling the speed and direction of the motor. All signals are wired to the main circuit card.

I/O Signals:

Mode	Channel number	Input or Output	Description
Analog Input	A0 – Channel 1	Input	Pressure sensor connector
Analog Output	DAQ 0	Output	Control the speed of the motor
Digital I /O	DIO 4 and DIO 5	Input	Control the forward and reverse direction of the barrier

Table 3-2 Input and output signals from hardware

Signals (From power supply)

Aplab model L236:

+ 15 V supply voltage to Op1, 2 and 3 pin 7

- 15 V supply voltage to Op1, 2 and 3 pin 4

+ 5V logical supply voltage to L298 pin 9

+ 5V supply voltage to L298 pin 11 (Enable signal)

+10 V collector voltage of 2N355

All ground references, both internally and externally are coupled together to insure signal levels.

The developed instrument is controlled through the real time system software. The details about the software and its functioning will be discussed in Chapter 4.

References

1. S. Henon and J. Meunier, *Rev. Sci. Instruments* 62, 936, 1991.
2. Gray Marshall, Michael D., Charles M. Knobler, *Review of Scientific Instruments*, Volume 69, Number 10, 3699.
3. "Model PS4" Pressure sensor technical manual. http://www.nima.co.uk/Literature/Help-pdf/Pressure Sensor Information.pdf
4. Pockels A., *Nature* **1891**, 43, 437
5. Ulman, A. *An introduction to Ultrathin Organic Films: from Langmuir-Blodgett to Self-Assembly*, Academic Press, San Diego, CA, **1991**.
6. "State of art intelligent system for barrier movement of LB trough", Neelima Iyer, Rupali Khatavkar, Bhagyashree Joshi at International Conference on Global Signal Processing and Embedded Application GSPx at Santa Clara, USA, September 27-30, **2004.**

CHAPTER 4

DEVELOPMENT OF REAL-TIME SYSTEM SOFTWARE

Real time system software for controlling and interfacing with the system has been developed using LabVIEW. This chapter describes the basics of LabVIEW, creating a Graphical User Interface (GUI) and vision system implementation for real-time imaging of Langmuir monolayers. It also describes the implementation of other features for control, data acquisition and user interface.

4.1 Choice of Software

In the initial development of the BAM instrument, Windows programming using Microsoft SDK was used for controlling and interfacing of the add-on cards and assembly language programming for microcontroller based stepper motor module. It was further decided that the current setup should be entirely a PC based solution for which the developed BAM instrument along with the Langmuir trough should be controlled and interfaced through LabVIEW software. Head, Instrumentation and Communication Group made PDS (Professional Development System) LabVIEW 7.0 available to me for this development. Instrumentation and Communication Group, National Chemical Laboratory gave initial training on LabVIEW development. Compatible add-on card for data acquisition (NI 6014) and frame grabber card (NI 1411) for real-time imaging of the monolayer has been selected. The details of the add-on card have been discussed in Chapter 3. All the controls and commands for data acquisition and vision system implementation with frame grabber card are developed in LabVIEW.

4.2 LabVIEW environment

4.2.1 Basics

National Instruments LabVIEW [1] is a highly productive graphical programming environment that combines easy to use graphical development with the flexibility of a powerful programming language. LabVIEW offers an intuitive environment, integrated with measurement hardware, for the user to quickly produce solutions for acquisition, analysis, and presentation of data.

4.2.2 Building the Virtual Instrument

The Virtual Instrument is an important feature in LabVIEW. A VI is used in the same way as traditional sub procedures. All programs that are written in LabVIEW are called VI's. With LabVIEW, the user can quickly build virtual instruments consisting of a front panel user interface and a block diagram. These user interfaces give interactive control of the software system.

Several predefined VI's are included in the basic LabVIEW package. Two separate windows, the front panel and the diagram build up the programming environment in LabVIEW. Into these window variables, controls and VI's can be imported from palettes. Appendix D gives more information on the LabVIEW environment.

4.2.3 LabVIEW Features

LabVIEW uses a patented dataflow programming model. It is the flow of data between objects on a block diagram, and not sequential lines of text. It determines execution order in LabVIEW and user can easily create diagrams that execute multiple operations simultaneously. Consequently, LabVIEW is a multitasking system capable of running multiple execution threads and multiple VI's concurrently.

LabVIEW VI's are modular in design, so, any VI can run on its own or be used as part of another VI (sub VI). With this modularity, user can design a hierarchy of VI's and sub VI's that serve as building blocks in any number of applications.

In many applications, execution speed is a critical consideration. LabVIEW is the only graphical programming system with a compiler that generates optimized code with execution speeds comparable to compiled C programs. To further improve performance, user can analyze and optimize time-critical sections of code with the built-in profiler. In this way, it increases productivity with graphical programming without sacrificing execution speed.

4.2.4 Instrument Control

The LabVIEW GPIB, VISA (Virtual Instrument Software Architecture), VXI, and Serial VI libraries use National Instruments' industry-standard device driver software for complete instrumentation control. With the LabVIEW Instrument Wizard, immediate detection of any instrument connected to computer, including GPIB, VXI, Serial, and computer-based instruments, is possible. The wizard installs appropriate instrument drivers and helps to communicate with instruments. LabVIEW instrument drivers translate instrument capabilities into a set of high-level functions to reduce development time and simplify instrument control by eliminating the need to learn the complex low-level programming protocol for each instrument.

4.2.5 Data Acquisition and Control

The data acquisition (DAQ) VI library acquires waveforms and generates signals with all National Instruments' plug-in and remote data acquisition products. The plug-in boards are ideal for high-speed, direct control applications. LabVIEW also has drivers for I/O devices such as PLC's, data loggers and single-loop controllers.

4.2.6 Standalone Applications

LabVIEW Application Builder is a feature to create and distribute standalone executable applications. These executable applications run at compiled execution speeds. For Windows platforms, the LabVIEW Application Builder features a Distribution Kit Builder for easily creating installation disks for executables.

4.2.7 LabVIEW Competitive Advantage

LabVIEW gives significant productivity gains when compared to traditional development tools. LabVIEW:

- Reduces development time by a factor of 4 to 10.
- Preserves capital investment in computer and instrumentation hardware.
- Empowers a larger group of users to develop their own solutions.
- Completes the entire application without the addition of more complicated development tools.
- Simplifies complicated development tasks with powerful add-on tools for tasks such as data analysis and visualization, report generation, and corporate database connectivity.

4.3 Development of Graphical User Interface (GUI)

A Graphical User Interface (GUI) should be intuitive and easy to understand. BAM application is a scientific application that includes real-time imaging, recording and storing of the monolayer images along with real-time measuring, plotting and storing the data of surface pressure. To plot the pressure area isotherm, some inputs from user like molecular weight, concentration of the sample used and volume of the surfactant spread on the sub phase are required. In the similar way, motor configurations for direction and speed of the barrier need to be set by the user. For some experiments, user might be interested in finding pressure area isotherm or some times only in Brewster Angle Microscopy results. Considering the varied requirements from the user, it was decided to design GUI application that should have three different experimentation options for the user. These three options are:

1. Combined application for BAM and for measuring and plotting pressure area isotherm.
2. Plotting pressure area isotherm.
3. Brewster Angle Microscopy and post processing function.

In order to systematically integrate the user demands in the development phase, necessary inputs from the BAM instrument users of the Nano Science Group were taken. Also, a detailed study of the GUI functionality of the software available with LB trough from NIMA Technology was done. Furthermore, common guidelines regarding interface design were gathered from the literature [2]. The main GUI windows used in this application are shown in Appendix E.

Two guiding principles were used in the implementation of the GUI. Firstly, the GUI was made simple. Only the information and choices that are necessary for the system to perform correctly are displayed. Secondly, the different windows follow a predefined template. The same gray background color is used in all windows, and all input fields are white. Additionally, all buttons have the same appearance, and buttons with similar functionality are situated at the same place in the different windows. Numbers of sub VI's were created so as to minimize the controls and indicators on the front panel. All these aspects give a uniform view of the system and thereby make the program easier for the users to understand. Moreover, to get an even more clarified

GUI, information about that particular VI is situated in respective window. In case user wants to stop the application, an emergency stop button is provided on main GUI.

4.4 LabVIEW software development for data acquisition

This section describes the programming of AD/DA card NI 6014 with LabVIEW. The developed system in LabVIEW lets the user to configure some input parameters and then acquire, process and save the data on disk. Measurement of surface pressure, plotting of real-time pressure area isotherm and controlling and configuring DC motor parameters are the tasks which are to be performed by data acquisition card and LabVIEW software. Figure 4.4-I shows the data flow for data acquisition in LabVIEW.

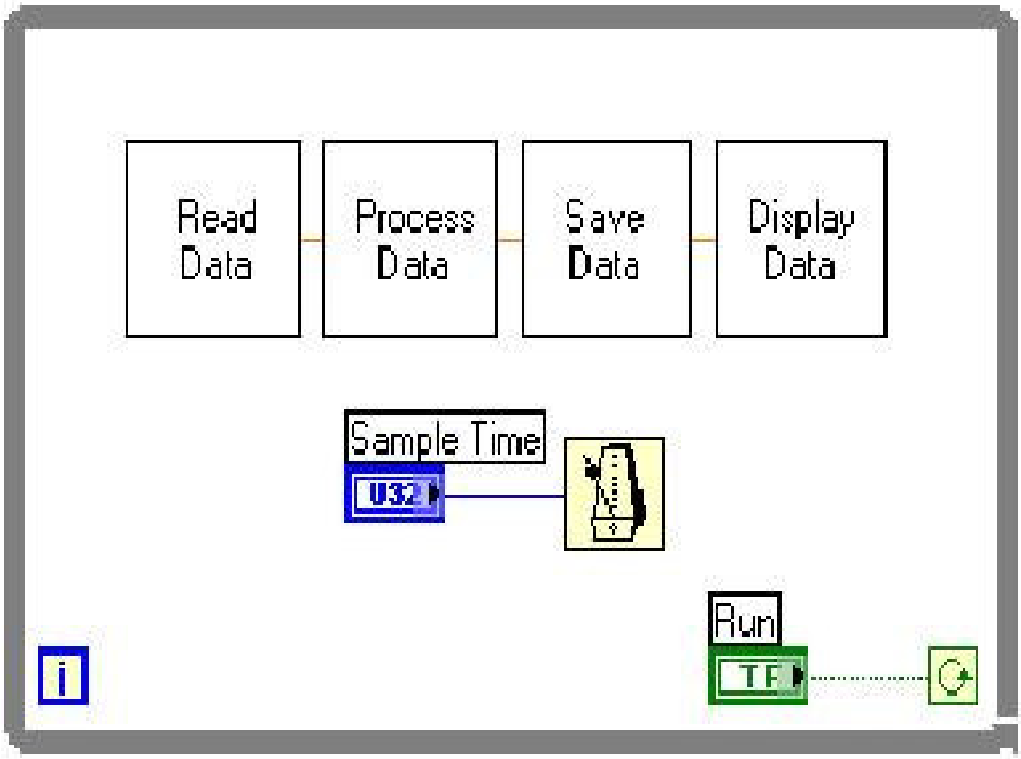

Figure 4.4-I Data flow for Data acquisition in LabVIEW

4.4.1 NI–DAQ 7.0 software

National Instruments' measurement device NI 6014 supports NI-DAQ driver software that is an extensive library of functions and VI's. All these functions can be

call from LabVIEW. Driver software has an application programmer's interface (API), which is a library of VI's, functions, classes, attributes, and properties for creating applications for the NI measurement device.

NI–DAQ 7.0 includes two NI-DAQ drivers, each with its own API, hardware configuration and software configuration.

1. Traditional NI-DAQ
2. NI-DAQmx

The data acquisition card NI 6014 used for this application supports traditional NI-DAQ driver.

4.4.2 Programming channels using Traditional NI-DAQ

Figure 4.4-II shows the data acquisition palette in LabVIEW.

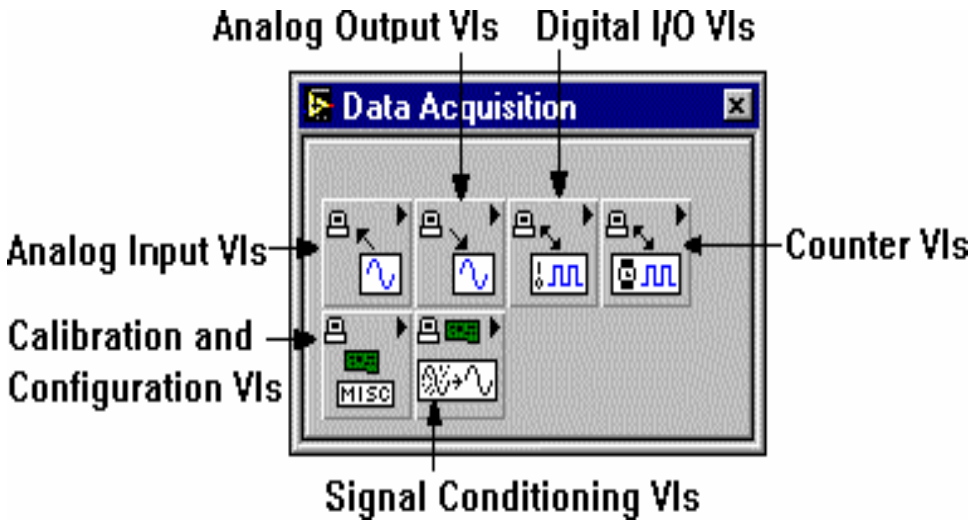

Figure 4.4-II Data acquisition palette

Measuring Surface pressure:

The voltage output from the pressure sensor model PS4 is terminated to 5 pin DIN socket and directly coupled to the channel [1] of NI 6014. The interfacing of the pressure sensor has been discussed in chapter 3.

The function "*AI Sample channel*" (Figure 4.4-III) is used for reading the channel value. The function measures the signal attached to the specified channel and

returns the measured data. The AI Sample Channel VI performs a single, untimed measurement of a channel.

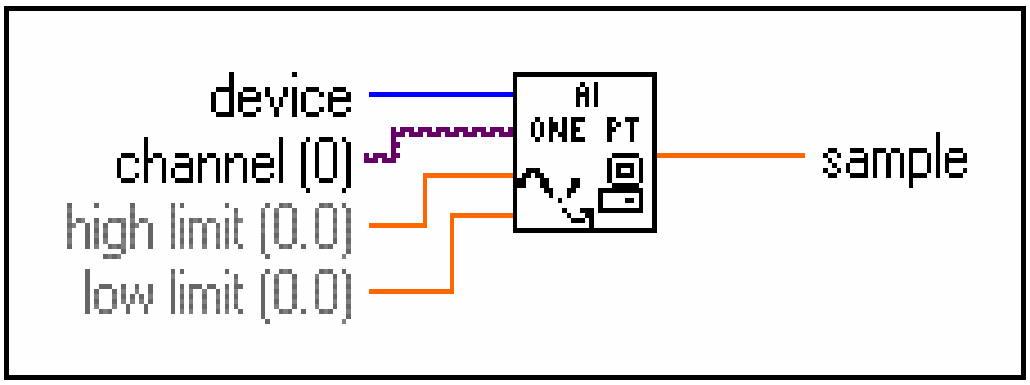

Figure 4.4-III AI Sample channel API

In Figure 4.4-III,

Device is the device number assigned to the DAQ device during configuration.

Channel identifies the analog input channel. The default input is channel 0.

High limit is the highest expected level of the signal. The default input is 0.

Low limit is the lowest expected level of the signal. The default input is 0.

Sample contains the scaled analog input data for the specified channel.

4.5 Plotting of pressure area isotherm

4.5.1 Input for X-axis

On the X-axis either molecular area in A^{0^2} /molecule or trough area is plotted. To calculate the molecular area following inputs are required from the user.

1. Concentration of the surfactant used. For example, 1 mg/ml or 2.5 mg/ml
2. Molecular weight of the compound
3. Amount of the solution spread on the sub phase to form a monolayer
4. Target pressure for pressure control isotherm

After the user provides the inputs, the software calculates the amount in gram of solution spread on sub phase. Then, the software calculates the number of molecules in a given amount of solution using Avagadro's number.

Molecular area = Area of the trough / Number of molecules

As we are compressing the trough with barrier, area of the trough gets reduced by a factor of 1.03 cm^2/sec.

Therefore, the final input for the x-axis is given by the equation,

(Area of the trough) – (number of seconds * 1.03) / number of molecules)

4.5.2 Input for Y-axis

On the Y-axis, the surface pressure in mN/m is plotted.

Calibration of the pressure sensor has been discussed in chapter 3. To measure the surface pressure following steps have to be followed.

1. Clean the trough and fill it with pure Millipore water to be used as sub phase. Dip Wilhelmy plate in the water and press *ZERO* on the GUI front panel.

2. To measure the surface tension of pure water, the plate is drawn up out of the liquid.

Press *WATER ST* to measure the surface tension of the pure water. The display should show the value of ≈72 mN/m.

Spread the surfactant on the surface of the water with the help of micro syringe and place the lower edge of the plate on the water surface. Press *START* to start acquiring different potentials from pressure sensor.

Using equation,

((X * 46.7 mN/m) / 0.8 V) – surface tension of the pure water

where, X are the different potentials acquired in step 3.

Every data point is then converted into surface pressure. This data is then plotted on y-axis of the graph and is stored in the file (*.xls or *.txt) on user specified path. For pressure control experiment it is compared with target pressure input by the user and stops if the required pressure has been reached. At the same time, barrier that compresses the film stops and maintains the pressure at that point.

Figure 4.5-I represents the block diagram of the VI for real-time plotting of pressure area isotherm.

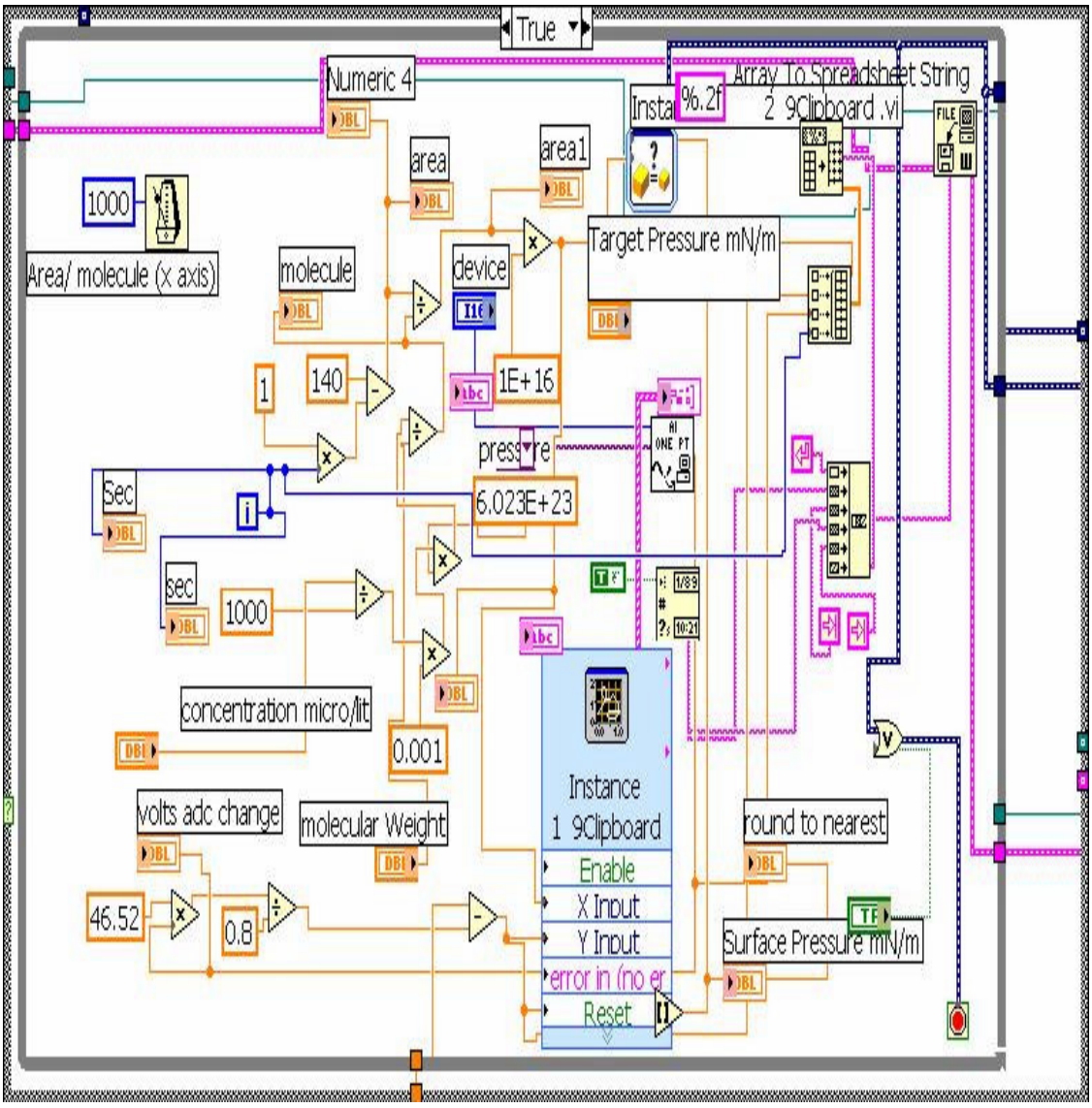

Figure 4.5-I Block diagram of VI developed for pressure area isotherm

In the combined application, real-time imaging and storing of the monolayer images, motor configuration for barrier movement, sensing and plotting the input pressure and comparing it with targeted pressure executes in a single loop.

4.6 LabVIEW software development for image acquisition

Following section describes the programming of frame grabber card NI 1411 in LabVIEW using integrated NI IMAQ software for real-time capturing, storing and processing of monolayer images.

4.6.1 About NI IMAQ software

National Instruments' image acquisition device (IMAQ) includes NI-IMAQ software. NI-IMAQ is a set of functions that controls the National Instruments' plug-in IMAQ devices for image acquisition. NI-IMAQ contains methods for performing tasks ranging from device initialization to advanced high-speed image acquisition. The NI-IMAQ VI Library, a series of virtual instruments (VI's) for using LabVIEW with IMAQ device are included with the NI-IMAQ software.

4.6.2 Programming with NI-IMAQ

The NI-IMAQ application programmer's interface (API) is divided into three groups: (a) high-level functions, (b) low-level functions and (c) generic functions.

With the high-level functions, programs can be written quickly without having to learn the details of the low-level APIs and driver. The low-level functions give finer granularity and control over the image acquisition process. However, greater understanding of API and driver is required. Generic functions allow setting up of the interfaces and sessions. They also close the interfaces and sessions when application is finished.

To acquire images using the high-level or low-level functions, first establish a connection to an interface and create a session. This can be done with MAX (Measurement and Automation software) that is part of LabVIEW. All parameters configured in MAX for an IMAQ device are associated with an interface name. One device can be associated with more than one interface name, which allows several different configurations for one device. Interface name is used to refer to the device in the programming environment. Interface name information is stored in an interface (.iid) file and includes the device serial number, the camera file associated with each channel on the device, and the default channel. NI-IMAQ specifies all interfaces by a

name. By default, the system creates default names for the number of devices in the system.

4.6.3 NI IMAQ VI palette

Figure 4.6-I shows the IMAQ palette on the function palette of LabVIEW.

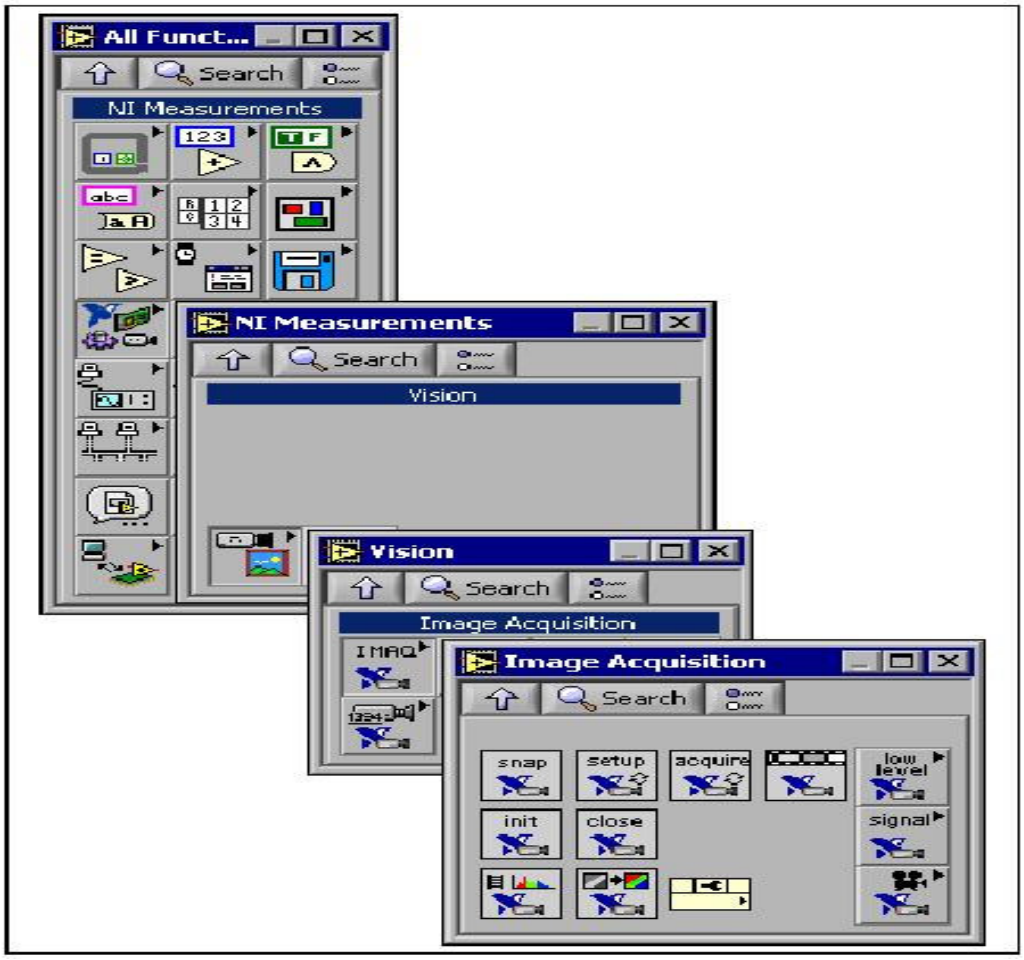

Figure 4.6-I LabVIEW 7.0 function palette with IMAQ palette

The most commonly used IMAQ VI's are on the *Image Acquisition* palette. The image Acquisition → IMAQ Low Level palette contains VI's for more advanced applications.

4.6.4 Common NI-IMAQ VI Parameters

IMAQ Session is a unique identifier that specifies the interface file used for the acquisition. This identifier is produced by the *IMAQ Init* VI and used as an input to all other NI-IMAQ VI's. The NI-IMAQ VI's use *IMAQ Session Out,* which is identical to *IMAQ Session In*, to simplify dataflow programming.

The high-level acquisition VI's - *IMAQ Snap, IMAQ Grab Setup* and *IMAQ Sequence* are required to wire IMAQ Session In.

The acquisition VI's use the Region of Interest input to specify a rectangular portion of an image frame to be captured. Use Region of Interest to reduce the size of the image you wish to capture. Region of Interest is an array of four elements with the elements defined as Left, Top, Right and Bottom. If Region of Interest is not wired, the entire image acquisition window is captured. Configure the default acquisition window using Measurement and Automation Explorer (MAX).

Many acquisition VI's require an image buffer to receive the captured image.

IMAQ Create and *IMAQ Dispose* manage image buffers in LabVIEW. *IMAQ Create,* shown in Figure 4.6-II, allocates an image buffer. *Image Name* is a label for the buffer created. Each buffer must have a unique name. *Image Type* specifies the type of image being created. Use 8 bits for 8-bit monochrome images, 16 bits for 10-bit, 12-bit and 14-bit monochrome images, RGB for RGB color images, and HSL for HSL color images.

New Image contains information about the buffer, which is initially empty. When you wire New Image to the Image in input of an image acquisition VI, the image acquisition VI allocates the correct amount of memory for the acquisition. If you are going to process the image, you might need to wire to Border Size. Border Size is the width in pixels created around an image. Some image processing functions, such as labeling and morphology require a border. The input that receives the image buffer is *Image in.* The *Image out* output returns the captured image.

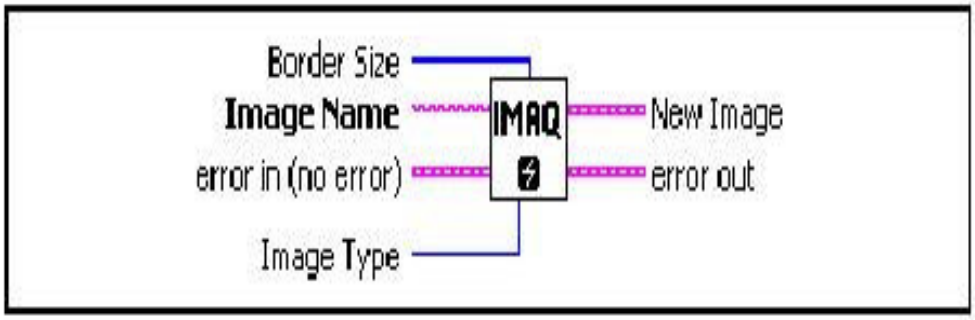

Figure 4.6-II IMAQ create VI

IMAQ Dispose, shown in Figure 4.6-III, frees the memory allocated for the image buffer. Call this VI only after the image is no longer required for processing.

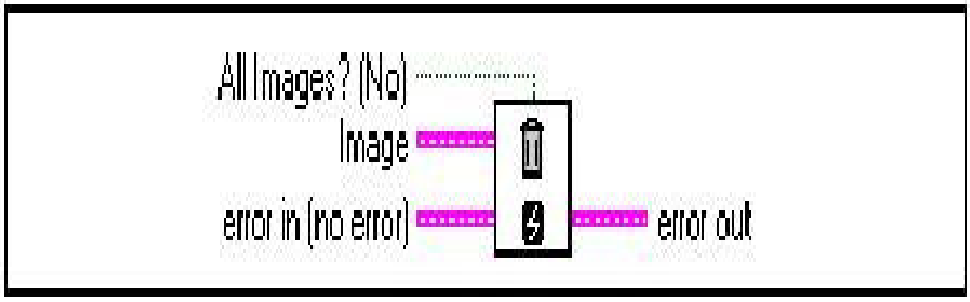

Figure 4.6-III IMAQ Dispose VI

4.7 VI created for real-time Image Acquisition

Figure 4.7-I shows the VI developed for real-time acquisition of monolayer images. This VI gets activated when user clicks Start video for Brewster Angle Microscopy GUI. In case of combined GUI where real-time plotting of pressure area isotherm is also to be activated, both the VI's are in a single loop. In this case, initialization process for both, frame grabber card and for AD/DA card will be executed outside the control loop.

Four NI-IMAQ image acquisition types are available in LabVIEW — snap, grab, sequence, and ring.

Snap: A snap acquires a single image into a memory buffer. Use this acquisition mode to acquire a single frame or field to a buffer.

Grab: A grab is a continuous, high-speed acquisition of data to a single buffer in host memory. This function performs an acquisition that loops continually on one buffer.

Sequence: A sequence initiates a variable-length and variable-delay transfer to multiple buffers. Use a sequence for applications that process multiple images.

Ring: A ring initiates a continuous high-speed acquisition to multiple buffers. Use a ring for high-speed applications where you need to perform processing on every image.

We are using *IMAQ Grab acquire* VI for this application and simultaneously we are recording and storing the image file (in *AVI* file format) in user defined path.

Following steps need to be completed for real-time continuous acquisition:

1. Call *IMAQ Init* to generate an *IMAQ Session*.
2. Use the IMAQ property node to find the image type and bits per pixel.
3. Create an image with *IMAQ Create* using the image type from the property node.
4. Use file dialog box to save the recorded image file.
5. Acquire the image with two VI's, *IMAQ Grab Setup* and *IMAQ Grab Acquire*, for a grab acquisition in LabVIEW.

   IMAQ Grab Setup, that will be called only once, initializes the acquisition and starts capturing the images to an internal software buffer.

   IMAQ Grab Acquire, that will be called multiple times, copies the image currently stored in the internal buffer to a G image buffer. The *Immediate?* input to *IMAQ Grab Acquire* determines if the copy takes place immediately or waits for the next vertical blank.
6. Use the *write AVI* VI to write the file in AVI format.
7. After the program finishes copying images, call *IMAQ Close* once to shut down the acquisition.

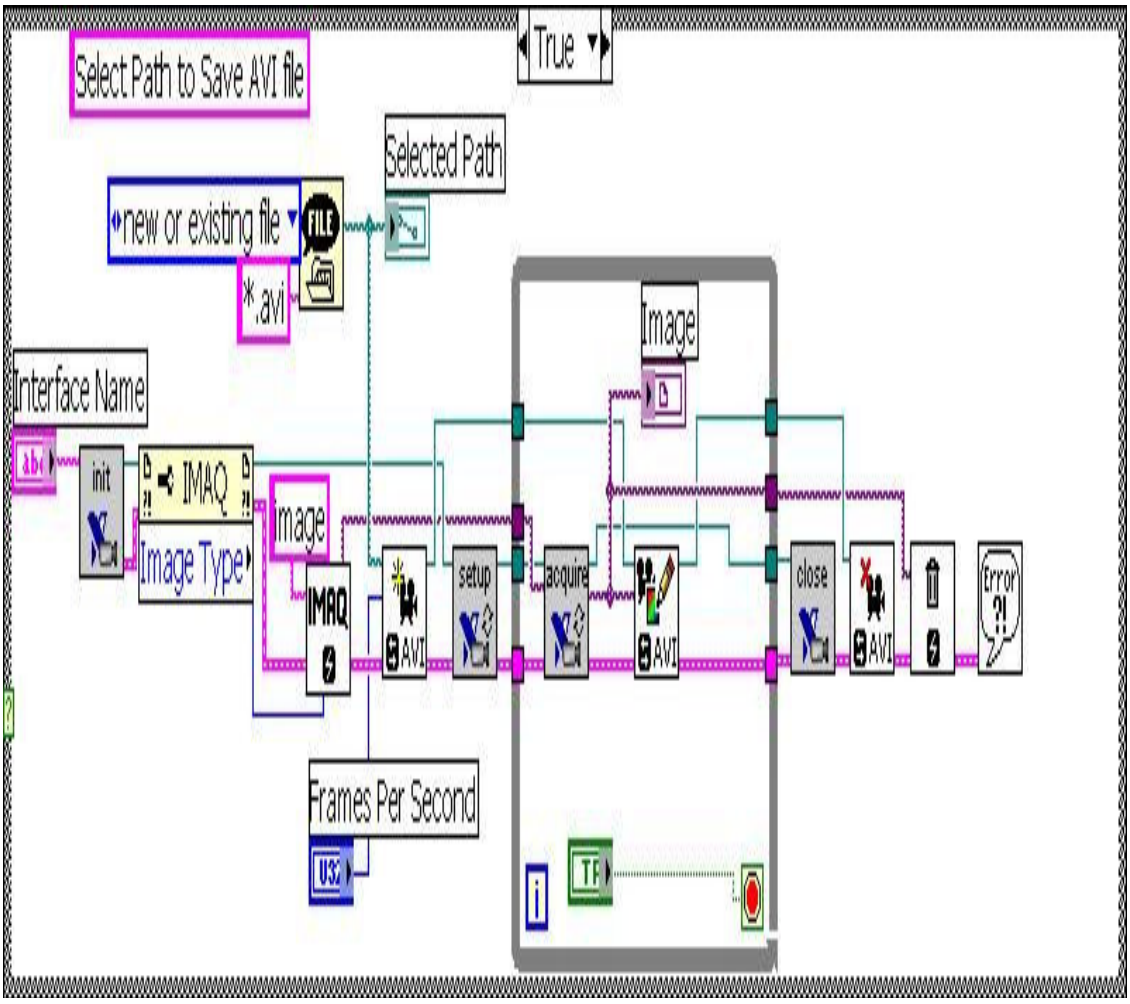

Figure 4.7-I VI for image acquisition

During the compression of the monolayer, images get recorded in AVI file with surface pressure value for each particular frame. For reading this AVI file, following VI's were developed.

Show video: This VI will read the specified AVI file and show video clip.

Read AVI and display pressure value: This VI will read specified AVI file and display it frame by frame along with the surface pressure value associated with frame. The same file can be read by changing BCG (Brightness, Contrast and Gamma) values if required. Figure 4.7-II shows the block diagram for this VI.

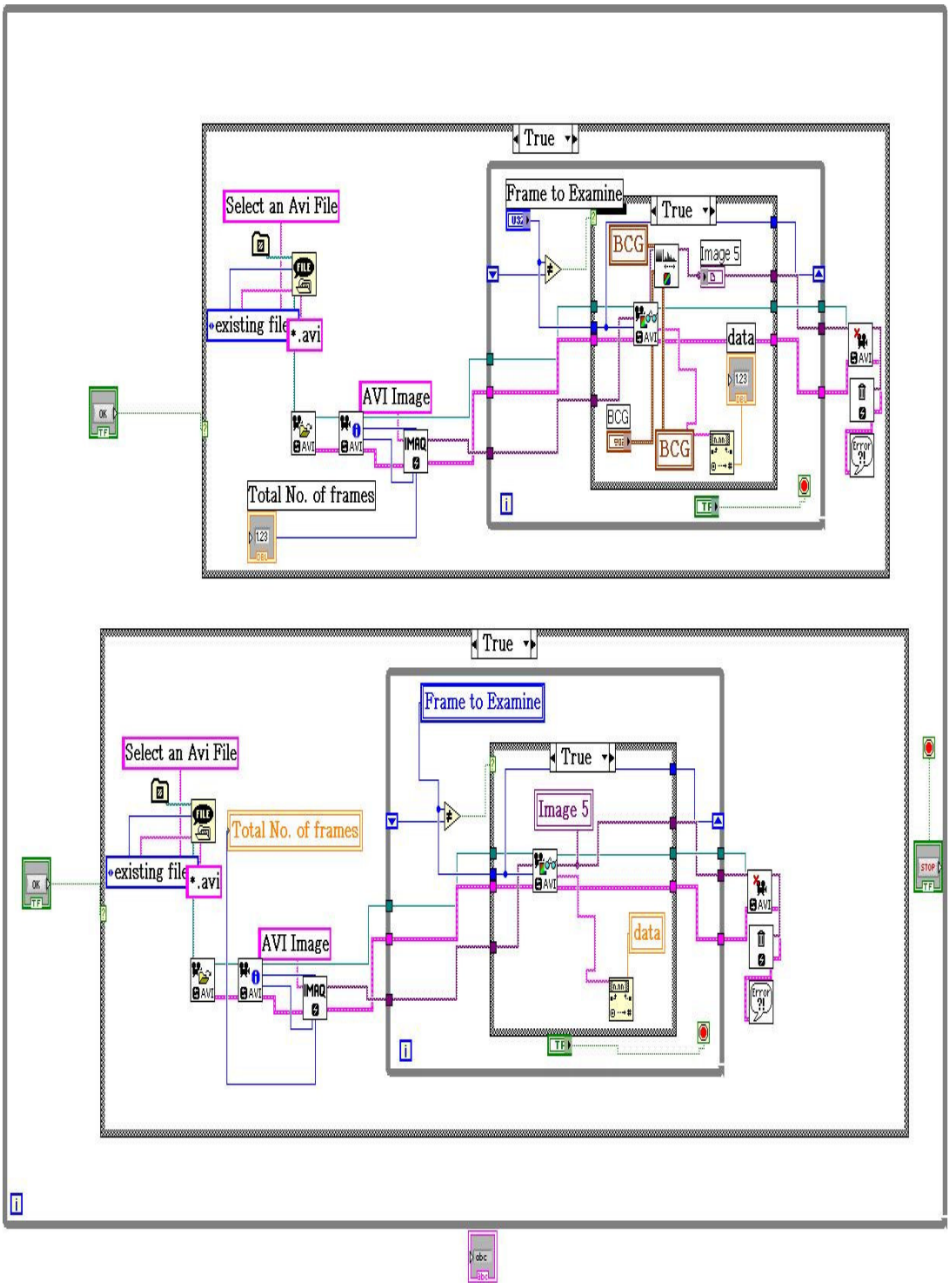

Figure 4.7-II VI developed for "read AVI file and display pressure value"

4.8 Image Display

Many image acquisition applications require one or more images to be displayed. In LabVIEW, an image can be displayed directly on the front panel using

the Image Display control. To display an image on the Image Display control, place the image control on the front panel of VI. On the block diagram, wire the *Image Out* from an acquisition VI to the Image Display control terminal. Figure 4.8-I illustrates the use of an Image Display control to display an image.

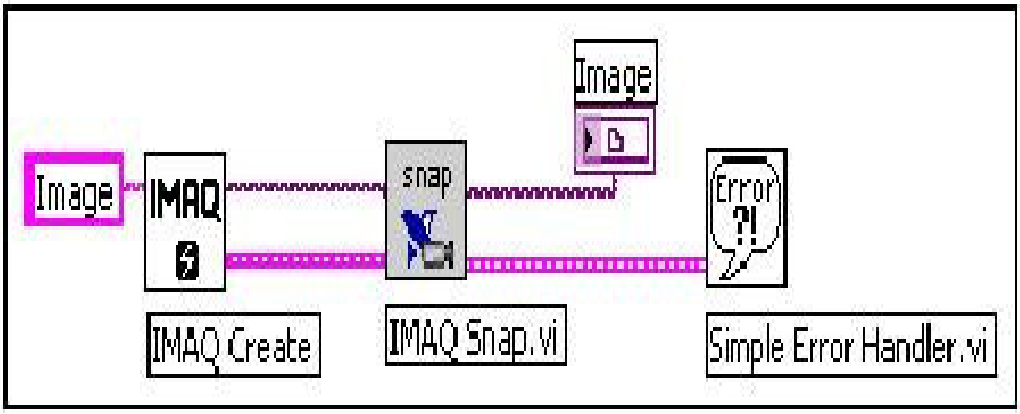

Figure 4.8-I Displaying an image using an image control

4.9 Controlling motor signals in LabVIEW

DC motor for barrier movement for compressing the monolayer is very important interface and needs to be controlled by software. Motor direction and speed are the two parameters that have to be controlled.

Analog out (AO) of NI 6014 AD/DA card is used for motor speed and DIO (4 and 5) are used for motor direction. (Chapter 3: Section 3.4.2).

Four VI's are developed: (a) for configuring the motor parameters, (b) forward barrier movement, (c) reverse barrier movement and (d) stopping the barrier.

4.9.1 VI for Configuration of motor parameters

Figure 4.9-I shows the VI that allows user to select the analog output channel and digital output channel that are configured in MAX. The direction for the motor is decided by setting bits 4 and 5 of the DIP switch on the front panel. This internally controls the hardware DIO. This VI is used as a sub VI for each GUI.

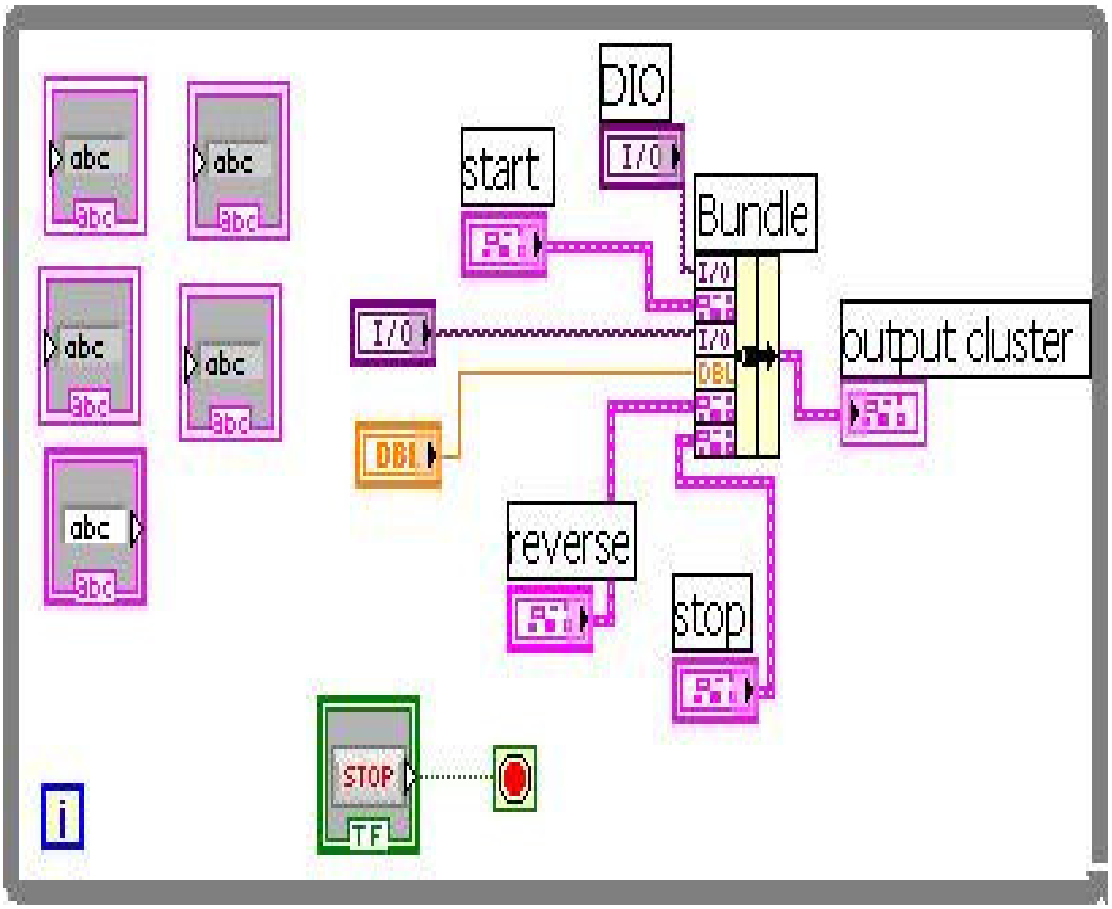

Figure 4.9-I Block diagram for motor configuration VI

All the parameters from user are stored in the output cluster. These parameters are passed to main window by using the *Unbundle* function. Forward, Reverse and Stop action of the barrier uses these parameters in their VI's.

4.9.2 VI for FORWARD action of the barrier

Figure 4.9-II explains the VI developed for Forward movement of the barrier. API's used for this VI are:

AO config: Configures the channel and allocates a buffer for analog output operation.

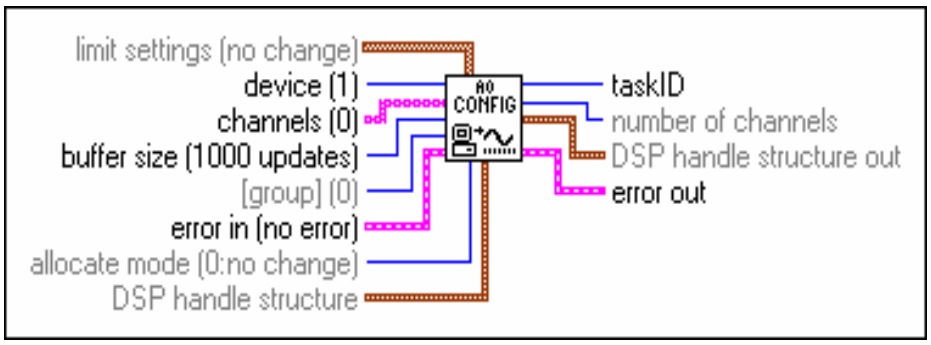

Figure 4.9-II AO configuration API

AO Single update: Performs an immediate update of the channels in the group (Figure 4.9-III).

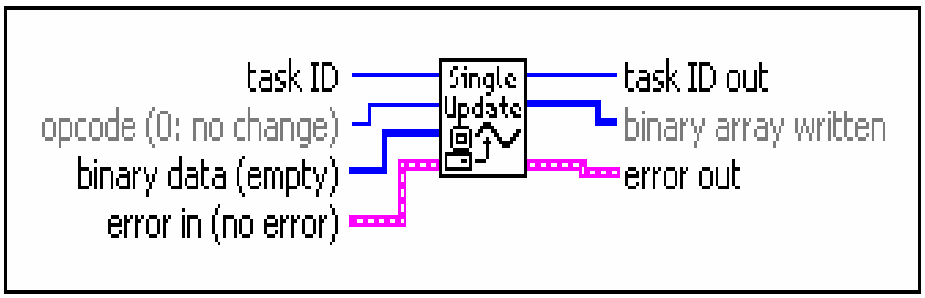

Figure 4.9-III AO single update API

Opcode specifies the type of data retrieval the VI performs

0 – Do not change the opcode setting.

1 - Output data and update DAC's (default setting).

2 - Output data only, do not update DAC's.

3 - Update DAC's.

4 - Do not output data. Translate voltage or current to binary data only.

DIO port config: Establishes a digital channel configuration. You can use the task ID that this VI returns only in digital port VI's. (Figure 4.9-IV)

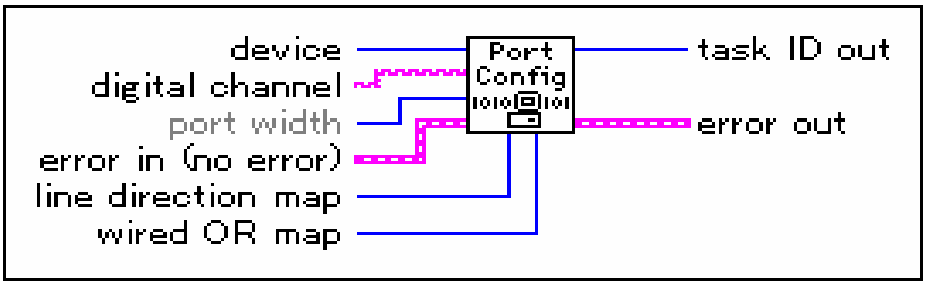

Figure 4.9-IV DIO port configuration API

In Figure 4.9-IV,

device is the device number you assigned to the DAQ device during configuration;

digital channel is the channel name or port number that this VI configures;

port width is the total width or the number of lines of the port in bits;

line direction map specifies the direction of each line in the port. If a bit is 0 in the line map, the line is an input line. If a bit is 1, the line is an output line. Set line direction map to -1 to make all the lines in a port as output lines. Set line direction map to 0 to make all the lines in a port as input lines.

DIO port write: Writes the value in pattern to the digital channel identified by task ID. (Figure 4.9-V)

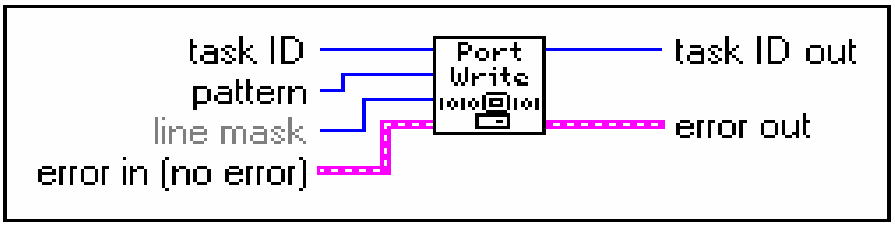

Figure 4.9-V DIO port write API

In Figure 4.9-V,

task ID identifies the group and the I/O operation.

pattern is a bit pattern representing the desired state of the lines in the port.

Figure 4.9-VI shows the block diagram developed for FORWARD action of motor.

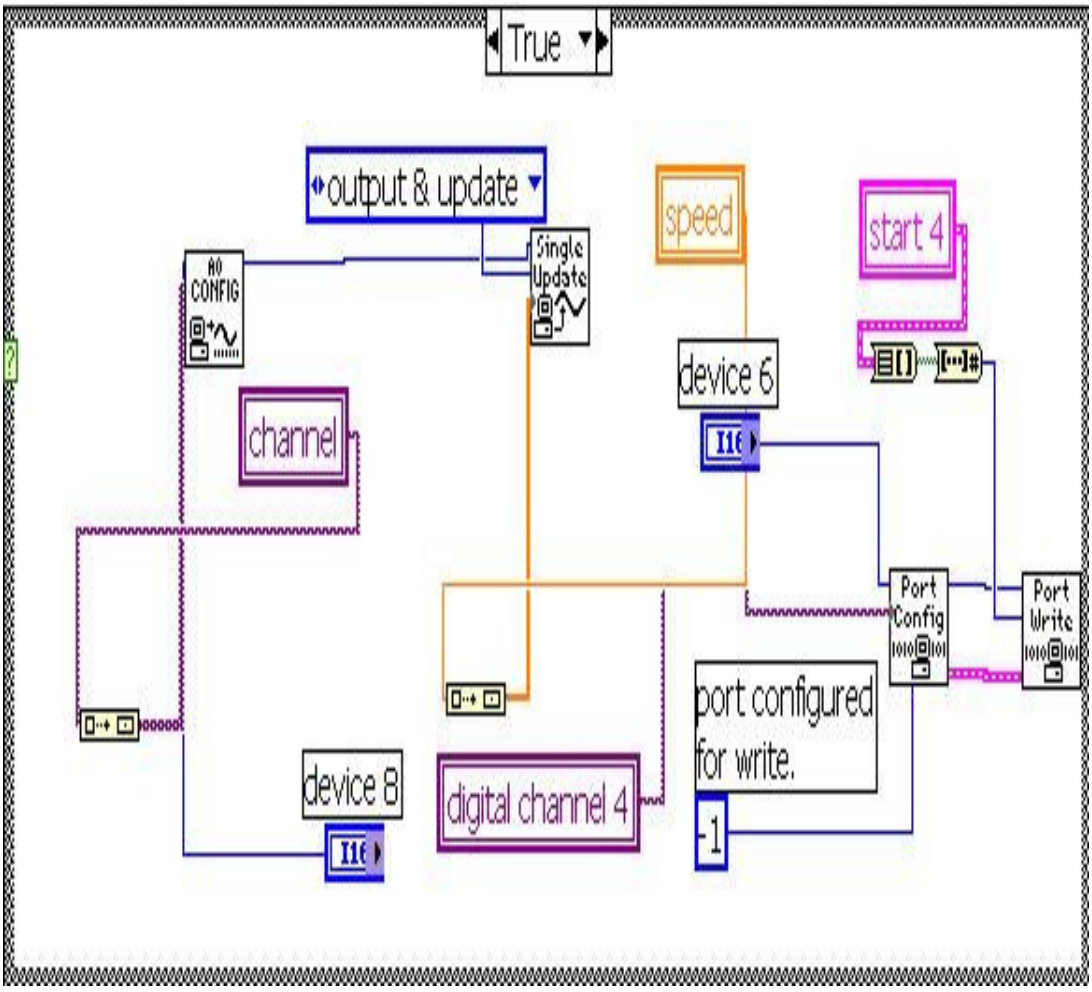

Figure 4.9-VI Block diagram for FORWARD action of motor

VI's for Reverse and Stop action of the barrier have been developed on the same line as the one for Forward action of the barrier (Figure 4.9-VI).

References

1. www.ni.com
2. LabVIEW development guide.

CHAPTER 5

EXPERIMENTATION AND ANALYSIS

This chapter covers the different systems that were studied with the developed BAM instrument.

5.1 Design Validation Experimentation

Design validation of the developed BAM was done using standard surfactants to form Langmuir monolayers. Langmuir monolayer formed by fatty acids (stearic acid (SA)) and fatty amine (Octadecylamine (ODA)) were used for this purpose.

Langmuir monolayers at the air-liquid interface play an important role in the application of the LB technique [1-3]. For a traditional LB film of amphiphilic molecule, the film quality is intimately determined by the characteristics of the precursor monolayer. As an alternative method, Langmuir monolayers have been used as a template to adsorb nanoparticles for the assembly of particulate thin film [4-6]. The behavior of monolayers of fatty acids and fatty amines and their related LB films are the most extensively studied systems for both research and application [7-10].

In this work, pressure area isotherm and Brewster angle images of SA and ODA were captured and compared with reference images and values reported in the literature [11-12].

Experimental section

Materials

Octadecylamine (ODA, > 99% pure) and stearic acid (SA, > 99% pure) were purchased from Aldrich Chemicals. Both chemicals were used as received. Chloroform (> 99% pure) was supplied by Aldrich Chemicals and was used as the spreading solvent for the amphiphilic molecules. The concentrations of ODA and SA solutions were 1 mg/ml. Pure water was used as the sub-phase. The water used was purified by a Milli-Q plus water purification system with an electric resistance of 18.2 MΩ.

Method

Pure water was used as the sub-phase, which has a pH value of 6.5 at the experimental temperature. Once the trough was filled with water sub-phase, the barrier was opened and closed once and all dust particles present on the surface were removed very carefully with a suction tube. The sample containing 1mg/ml of SA to form the monolayer was spread on the subphase by a microsyringe. Depending upon the trough area, approximately 25-30 µl of volume of surfactant solution was required. Care was to taken such that the monolayer did not get saturated. All the

parameters required for an experiment (like molecular weight, volume of the surfactant used, target pressure and motor configuration bits) were input through the interface software.

After allowing 20 minutes for solvent evaporation, the monolayer was compressed at the rate of 1.03 cm^2/min. The surface pressure area per molecule isotherm was plotted in real-time by continuous compression of the monolayer up to the defined targeted pressure.

Initially, the BAM was adjusted on pure water surface till a dark image is seen on the PC monitor and then the BAM images of the monolayer were captured. Figure 5.1-I shows the BAM image of pure water surface. It can be seen that the reflectivity does not vanish completely because of some surface roughness caused by capillary waves. When an insoluble monolayer is present at the air-water interface, the beam reflects and an image is shown according to the organization of the monolayer.

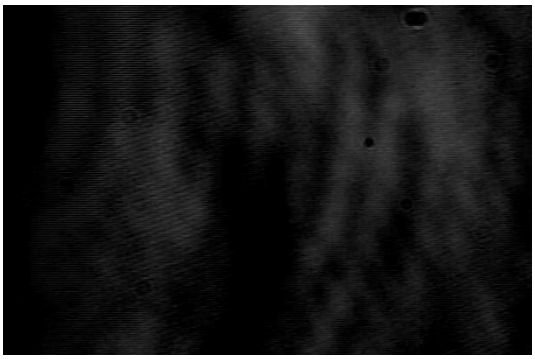

Figure 5.1-I BAM image of pure water subphase

The BAM images were obtained during the compression process and recorded along with the isotherm. Similar experiment was carried out for fatty amine. Octadecylamine was used for this purpose. Figure 5.1-II and Figure 5.1-III show the pressure area isotherm of the pure ODA and SA.

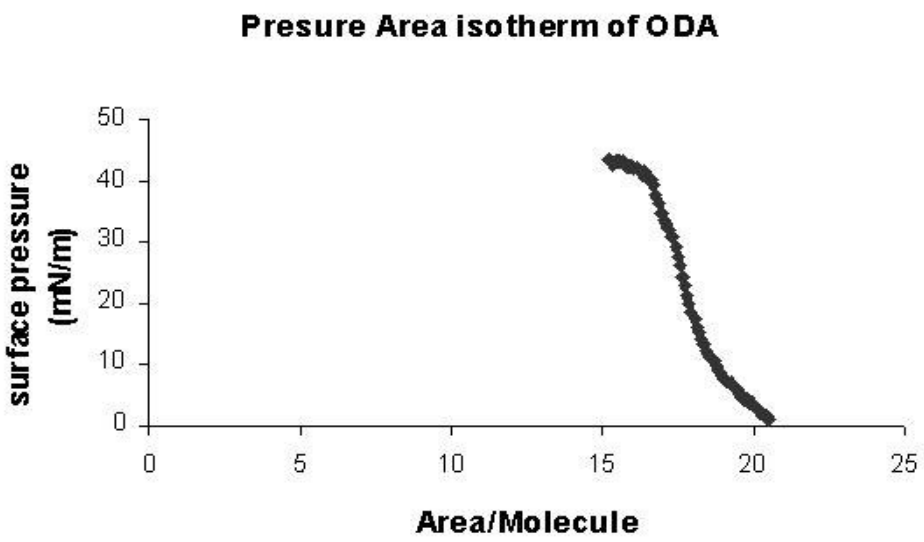

Figure 5.1-II Pressure area isotherm of pure octadecylamine

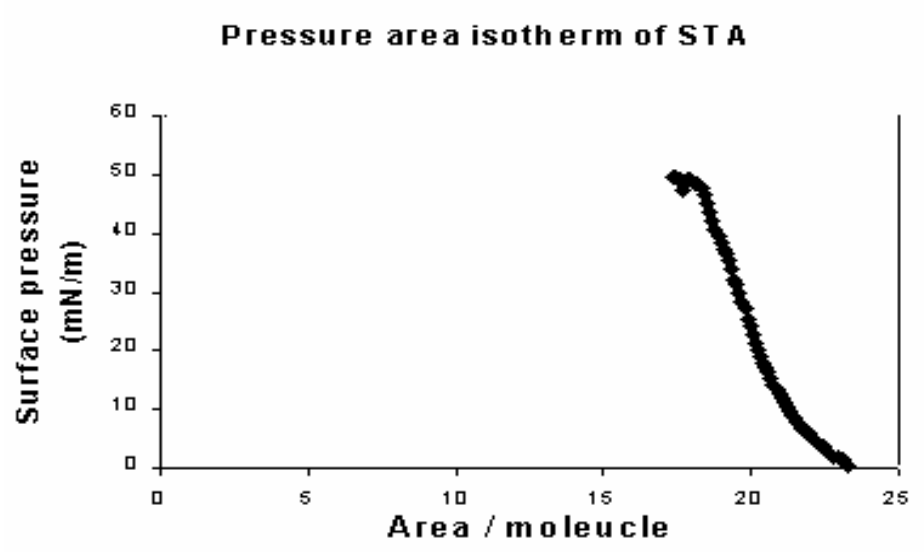

Figure 5.1-III Pressure area isotherm of pure stearic acid

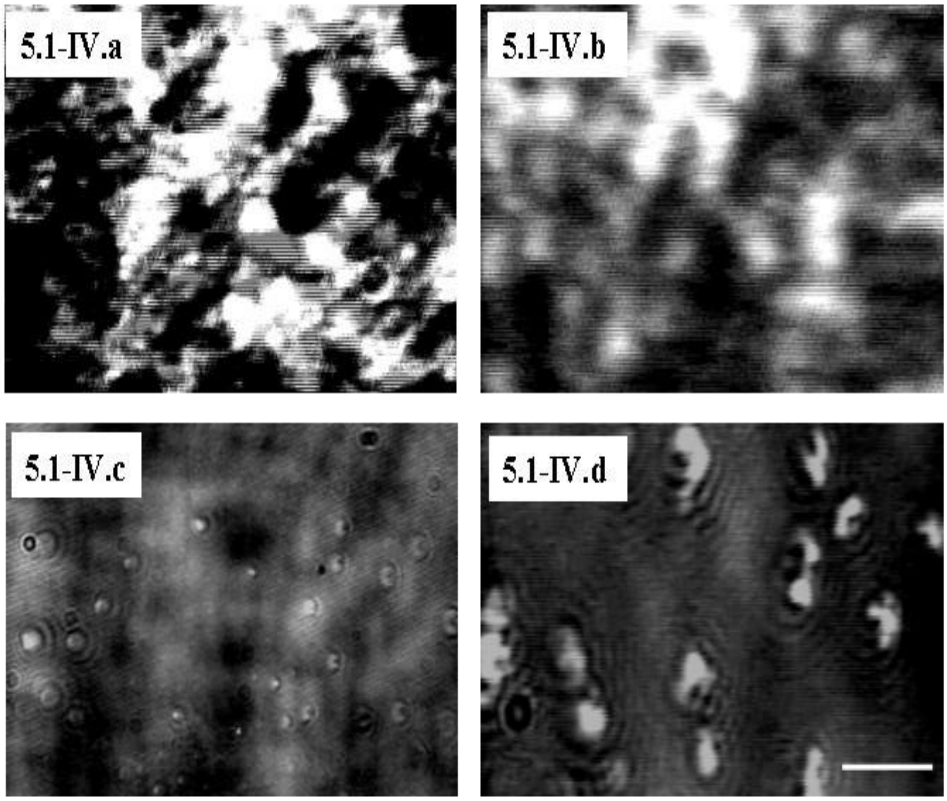

Figure 5.1-IV Images of pure SA monolayer at air-water interface. The images correspond to state of (5.1-IV.a) π=0 mN/m; (5.1-IV.b) π=1 mN/m; (5.1-IV.c) π=47 mN/m near collapse point; (5.1-IV.d) π=35 mN/m after collapse point. The length of bar corresponds to ~ 80πm.

Figure 5.1-IV illustrates the BAM images of pure stearic acid (SA) exhibiting the morphological information on SA monolayer at different surface pressures. When the occupied area of molecule is large, no light is reflected from the gas-water interface and a dark image is observed, which is identified to be the gas phase. On monolayer compression, bright zones of low contrast appear and the brightness and area of these zones increase gradually, indicating the increasing density of the monolayer and the formation of liquid phase. The bright zones tend to form a network structure, as shown in Figure 5.1-IV.a. The gas-liquid coexistence phases remain before the lift-off point of isotherm. As shown in Figure 5.1-IV.b, the liquid phase covers nearly the entire monolayer at surface pressure of 1mN/m. On further compression, the gas-phase zone disappears, but bright dots are seen instead of the sharp boundary (Figure 5.1-IV.c). Figure 5.1-IV.d, indicates the collapse of

monolayers to be 3-dimensional (3D) aggregates. The aggregates grow in size and density when the surface pressure decreases after collapse.

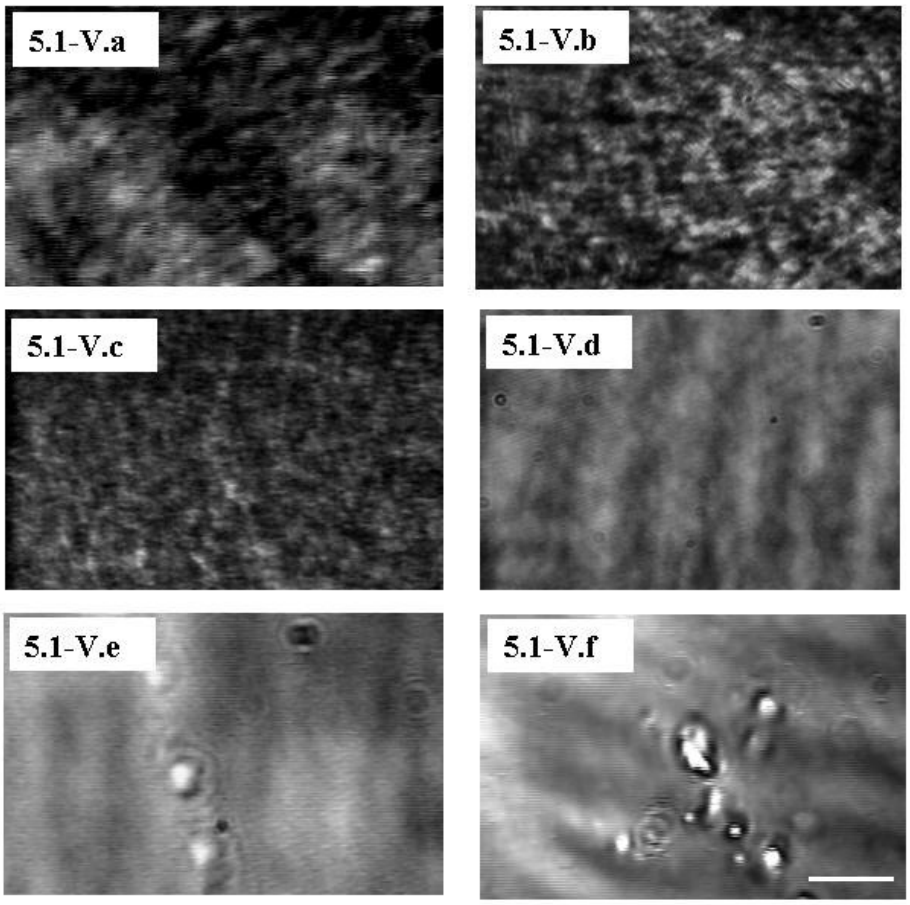

Figure 5.1-V BAM images of ODA monolayer on air-water interface. The images correspond to state of (5.1-V.a) π=0 mN/m; (5.1-V.b) π=1 mN/m; (5.1-V.c) π=10 mN/m; (5.1-V.d) π=38 mN/m; (5.1-V.e) and (5.1-V.f) π=42mN/m near collapse point. The length of bar corresponds to ~ 80 μm.

The BAM morphology of ODA is different from that of SA as illustrated in Figure 5.1-V. However, the ODA monolayer does not show condensed patch domains as for the SA monolayer, but exhibit a cloudy-like morphology. Such a behavior of ODA monolayer is attributed to the higher hydrophilic property of amine group compared to the carboxylic group of SA, which can be verified by the higher solubility of ODA in water [13]. The higher interaction between the amine group and water promotes the spreading of ODA molecules on the gas-water interface. That is,

the coherent interaction among hydrophobic tails of ODA molecules is less than the interaction between amine group and water. As a consequence, the liquid phase of ODA does not form condensed domains as that of SA. At higher surface pressure, aggregates dots gradually appear. More significant collapse phenomenon can be inspected near the collapse pressure (Figure 5.1-V.f).

Three different experiments were carried out to visualize the morphological change and assembly of the nanoparticles on Langmuir monolayers. The samples for these studies were provided by Nanoscience group at NCL, which is actively involved in the synthesis, surface functionalization and subsequent thin film formation of nanoparticles [14-17].

5.2 Experimentation 1

In order to build a nano device for practical applications, the individual nanoparticles need to be assembled in a desired fashion. Most of the current research interest lies in ordered two-dimensional (2D) assembly of nanoparticles.

Various attempts regarding the assembly of nanoparticles have been reported [18-22]. The Langmuir–Blodgett (LB) method [23-26] probably provides the best solution to the problem in the self-assembly process. It is also easy to transfer these films onto solid substrates and control the film thickness by varying the number of monolayers deposited on the substrate. The reports available for 2D assembly of nanoparticles using the LB technique discuss the assembly of hydrophobized (organically dispersible) nanoparticles at the air-water interface. The driving force for the 2D assembly is the hydrophobic interaction between the hydrophobized nanoparticles.

However, there are very few studies, which have probed the in-situ self-assembly process at the air-water interface and there is little knowledge on what controls the assembly process. In this context, BAM becomes a very handy tool to explore the assembly process at the air-water interface in-situ [27]. This may provide more details about the organization process, thus, providing the necessary impetus to understand this assembly process in-situ at a microscopic level.

In this work, synthesis of Ni nanoparticles in the aqueous phase, which were consequently phase transferred to organic phase in presence of stearic acid in the medium, has been discussed. Details regarding the sample preparation can be found in Ref [28]. Phase transferring the particles from aqueous to organic medium or the reverse can provide more flexibility as desired in their applications [29]. The aqueous colloidal nanoparticles have the potential of biological application [30] whereas, organic solvent based nanoparticles are preferred for catalysis [31-34]. The beauty of phase transfer is that the particles can be used in both the mediums without any appreciable change in their structure and properties. The hydrophobized Ni thus prepared, were organized at the air-water interface in the form of a Langmuir monolayer and it was observed that by controlling the pressure and concentration of hydrophobized Ni nanoparticles at the air-water interface, linear ribbon like assemblies could be obtained. The organization process was followed by surface

pressure area isotherm measurement, Transmission Electron Microscopy and BAM. BAM study was also performed to establish the assembled structure of the Ni nanoparticles at the air-water interface. This enabled us to understand the assembly process in-situ and suggests the importance of the concentration as well as surface pressure in obtaining the desired assembly of hydrophobized Ni nanoparticles.

Pressure area isotherm study:

The hydrophobized Ni nanoparticles capped with oleic acid and SA were weighed and dissolved in chloroform keeping the concentration as 1mg/ml. A known volume of this solution was spread on the surface of double distilled water at pH 6.5. Figure 5.2-I shows the π-A isotherm recorded from the Langmuir monolayer as a function of volume of nanoparticle solution added to the air-water interface. It is noticed that the surface pressure can be increased to 21 mN/m when the volume added is increased from 50 µl (curve 1) to 125 µl (curve 2). When the volume is further increased to 250 µl (curve 3) the monolayer could again be compressed up to a pressure of 25 mN/m beyond which the monolayer does not seem to be very stable as indicated by the change in the slope of the curve. The take-off area is increased with the increase in volume of the hydrophobized Ni nanoparticles added to the monolayer pointing to the presence of a more compact monolayer.

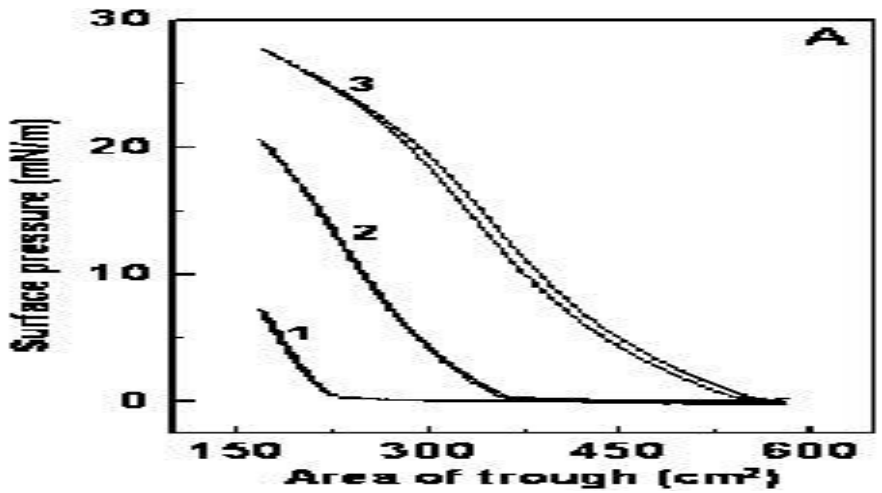

Figure 5.2-I Surface pressure-area isotherm of hydrophobized Ni nanoparticles of different concentrations

The long range assembly is a phenomenon that takes place at the air-water interface and is visualized in-situ using BAM. A real-time measurement of the domain structure formed at the air-water interface and the effect of pressure or

concentration of the Ni nanoparticles on the assembly pattern can also be studied using the same equipment.

Figure 5.2-II.a to Figure 5.2-II.d demonstrate the Brewster angle micrographs, which correspond to the morphology of the assembled Ni nanoparticles at air-water interface at different surface pressures. Figure 5.2-II.a illustrates that the particles at 0 mN/m pressure were not arranged in any patterns, but, with the increase of surface pressure to 15 mN/m, the particles showed an interesting linear arrangement (Figure 5.2-II.b and Figure 5.2-II.c). The concentration of the initial solution was then increased to 5 mg/ml and the hydrophobized nanoparticles were spread at the air-water interface in a similar way. Also, the surface pressure was increased to 15 mN/m. This did not produce any linear assembly at similar pressure and the whole surface appeared to be filled with the nanoparticles (Figure 5.2-II.d). This observation could be explained on the basis that due to such high concentration of the nanoparticles in chloroform the particles turned into clusters. The second reason could be the presence of large number of nanoparticles at the air-water interface bringing linear structures close to each other destroying the distinct linear type arrangement.

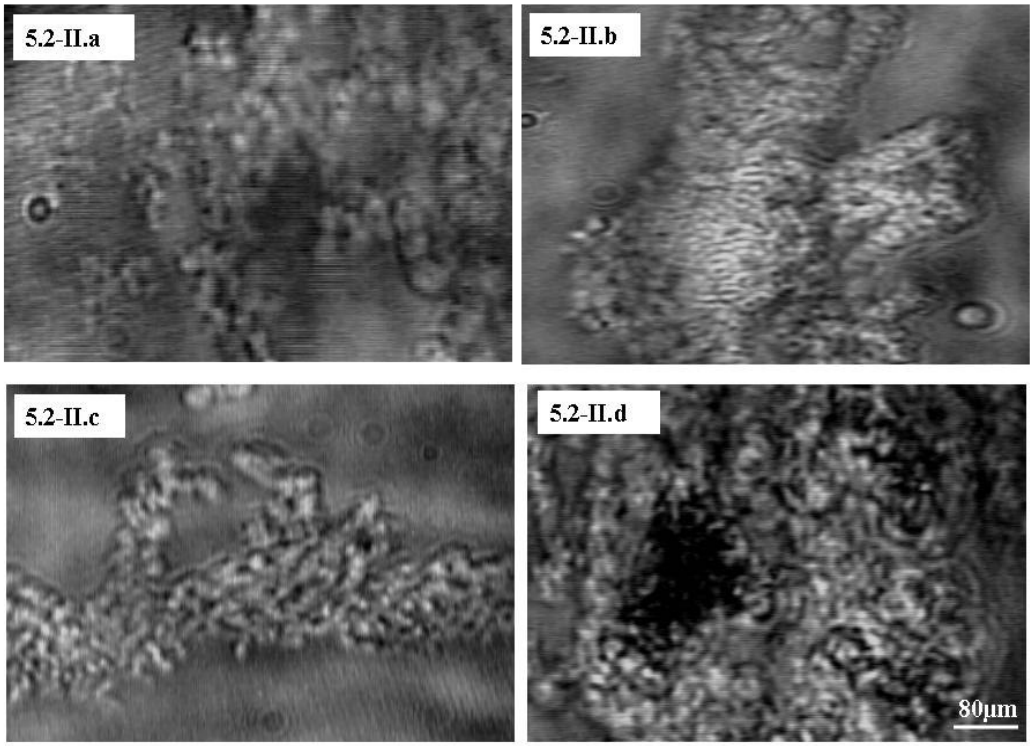

Figure 5.2-II Brewster angle micrographs of hydrophobized Ni nanoparticles assembled at air-water interface

Correlating the results with TEM results

Figure 5.2-III shows the TEM pictures when the monolayer was compressed at 15 mN/m surface pressure and was transferred to the TEM grid by dipping it vertically. The images showed long range compact linear ensemble of the Ni nanoparticles at the air-water interface, which can be correlated with the BAM pictures in Figure 5.2-II.b and Figure 5.2-II.c.

The difference in the scale of BAM was basically due to the difference in the resolution of the two imaging techniques. The closely spaced area of the Langmuir film of Ni nanoparticles as observed on TEM can not be resolved by BAM and thus appeared as a thicker assembly.

The TEM grid when lifted vertically from the Langmuir film, obtained by spreading Ni nanoparticles with the initial concentration of 5 mg/ml, was found to have no linear assembly, but disordered polydisperse particles all over the grid (Figure 5.2-IV). It could be linked to the BAM image observed for this case (Figure 5.2-II.d). The particles appeared to be more aggregated and linear structures were very scarce.

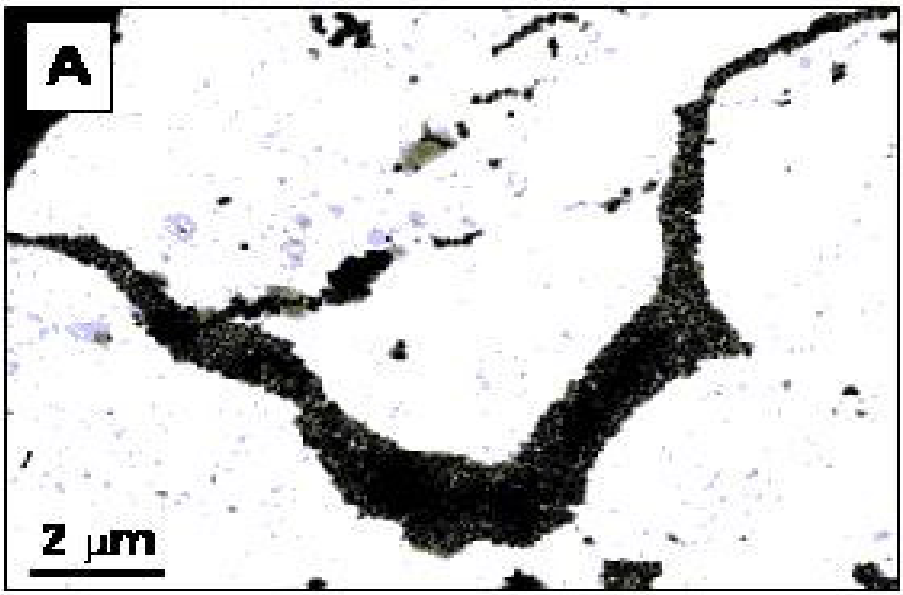

Figure 5.2-III TEM images obtained when the Ni nanoparticles monolayer was transferred on to a TEM grid at 15 mN/m pressure

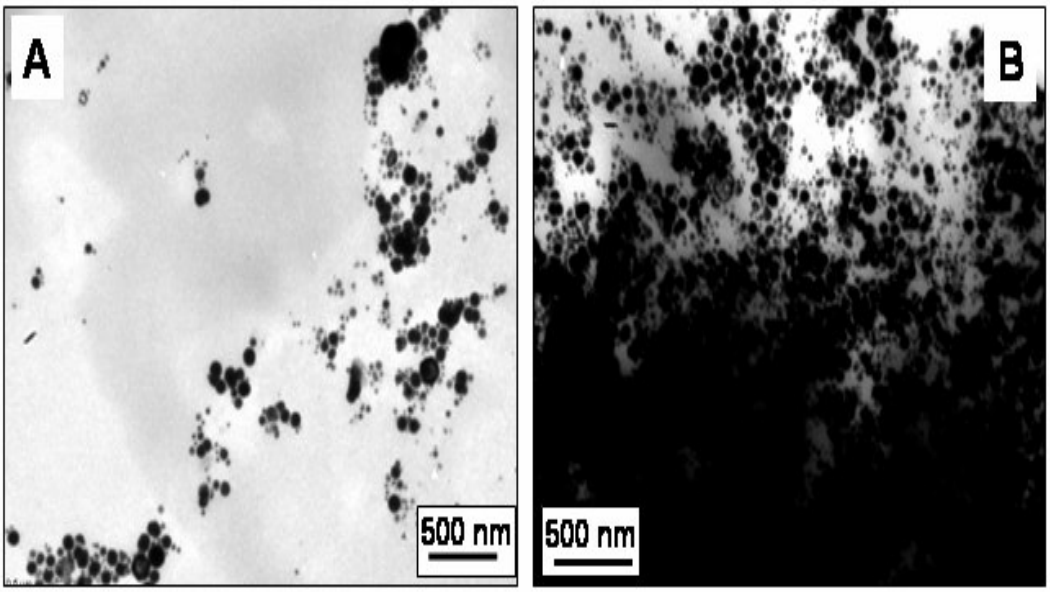

Figure 5.2-IV TEM images when the monolayer was compressed at surface pressure 15 mN/m with the solution of initial concentration 5mg/ml

Thus, it has been shown that the hydrophobized Ni nanoparticles can be assembled at air-water interface to yield closely packed nanoparticles' Langmuir monolayer. We have shown that the BAM studies could be effectively used to get important information on factors that determine the assembly of the nanoparticles at the air-water interface. Availability of data like these can give us great control in assembling the nanoparticles in desired superstructure and can address many fundamental issues related to the assembly of nanoparticles at the air-water interface.

5.3 Experimentation 2

The key technologies of the past half-century, transistors and semiconductors, all have been reducing in size, materials and costs while increasing power.

Within the area of nanoscale electronics, research is currently focused on development of a "bottom up" approach to fabricate nanometer scale electronic devices. The motivation for the preparation of gold nanoparticles includes their potential utility in nanoelectronics, sensors and the vast basic knowledge we can gain from these novel materials [35].

Nanoscience group at NCL has been actively involved in preparing and controlling the size and shape of the nanoparticles to form the linear assemblies. In such cases, apart from other characterization techniques, BAM is used as a qualitative method to probe into in-situ characterization of these nanoparticles at air-water interface.

For this experimentation work, thiol capped gold nanoparticles were prepared. These particles were made using reverse micelle technique in the presence of thiol to get hydrophobized nano particle [36]. These particles have very narrow size distribution, i.e., in the range of 5-7 nm. These hydrophobized thiol capped gold nanoparticles were assembled at the air-water interface using the Langmuir technique. The main aim to use BAM was to observe in-situ images of the assemblies formed. For the assembly formation, these hydrophobized nanoparticles were spread on ODA monolayer on pure millipore water surface.

It was observed that as soon as these particles were spread on the surface, without significant surface pressure, they self assembled in a linear fashion. Figure 5.3-I shows some of the BAM images of these particles. These images indicate that linear structures are being formed but further analysis is yet to be done. Figure 5.3-I.a shows the ODA monolayer at the pure water surface for comparison. Figure 5.3-I.b shows the images of thiol capped gold nanoparticles immediately after spreading. Figure 5.3-I.c and Figure 5.3-I.d show the self assembled BAM images of thiol capped gold nanoparticles. Scale bar is $\approx 80\ \mu m$.

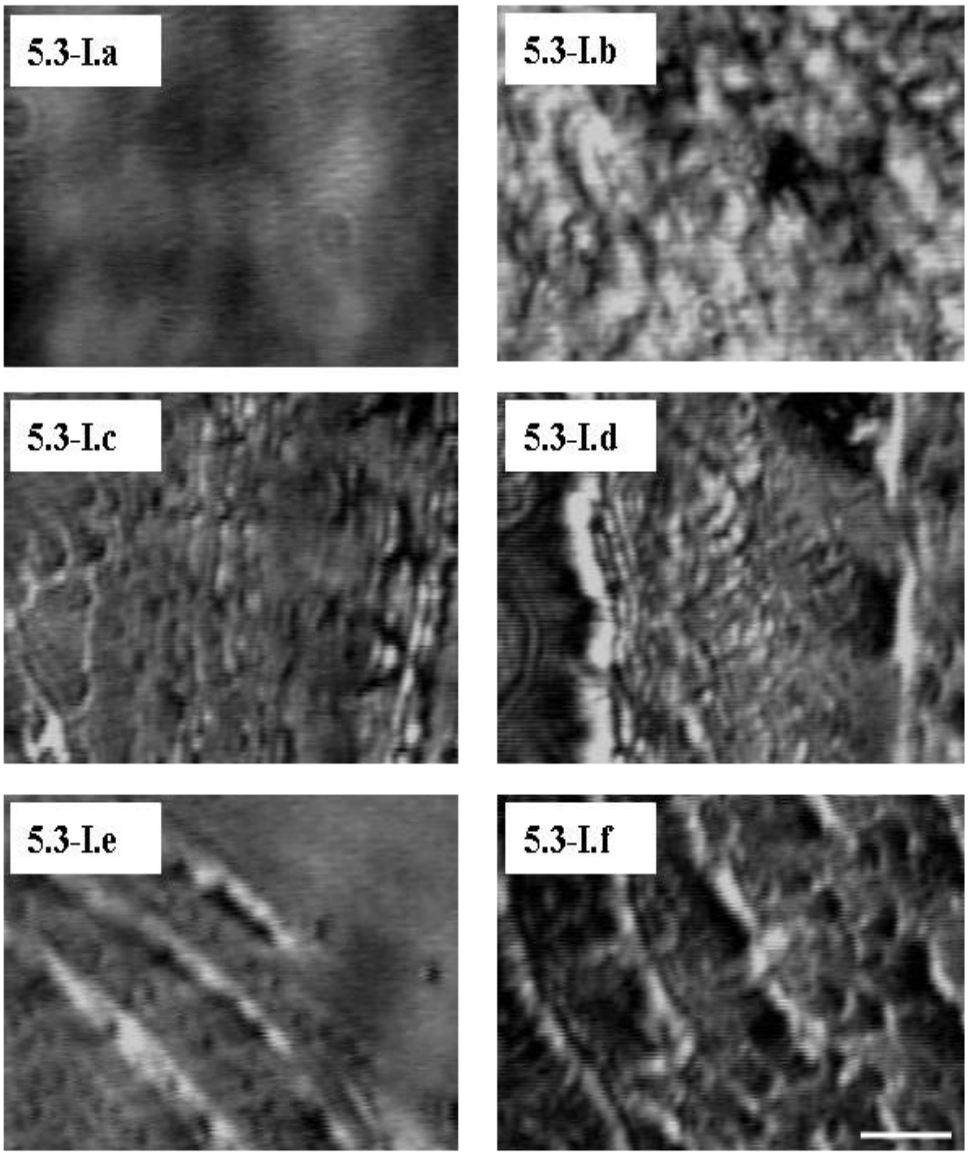

Figure 5.3-I Brewster angle microscopy images of hydrophobized thiol nanoparticles assembled at air-water interface. Scale bar is ~80 µm.

5.4 Experimentation 3

In this work, time dependent complexation of sodium borohydride ($NaBH_4$) reduced gold nanoparticles and lemon grass reduced gold nano clusters with ODA Langmuir monolayers were studied.

Sodium borohydride reduced gold nanoparticles were prepared as per Patil et al. [37]. These nanoparticles were spherical in shape and 7.5 nm in diameter. These nanoparticles have net negative charge on their surface [38]. Strong attractive electrostatic interaction between the negatively charged gold nanoparticles and positively charged ODA monolayer drives the complexation process.

Lemon grass reduced gold nanoparticles were prepared as per Rai et al. [39]. These nanoparticles were triangular in shape and are of the size ≈ 567 nm. These nanoparticles have net negative charge on their surface. In order to confirm the charge on the gold nanoparticles, gel electrophorisis measurement was conducted. It was confirmed that there was a negative charge on the gold nanoparticles as we see them moving towards positive electrode under the influence of electric field.

Complexation process depends upon the size, shape and charge of the nanoparticles. These three factors contribute for the mobility of the nanoparticles in solution. The kinetics of time dependent complexation of the nanoparticles at the interface was monitored by BAM technique.

Brewster angle measurement:

BAM was primarily used to monitor the topographic variations in the ODA monolayer as a function of complexation of gold nanoparticles. These images of ODA gold nanoparticles monolayer at the air-water interface were recorded as a function of time holding the barrier at a constant predetermined area.

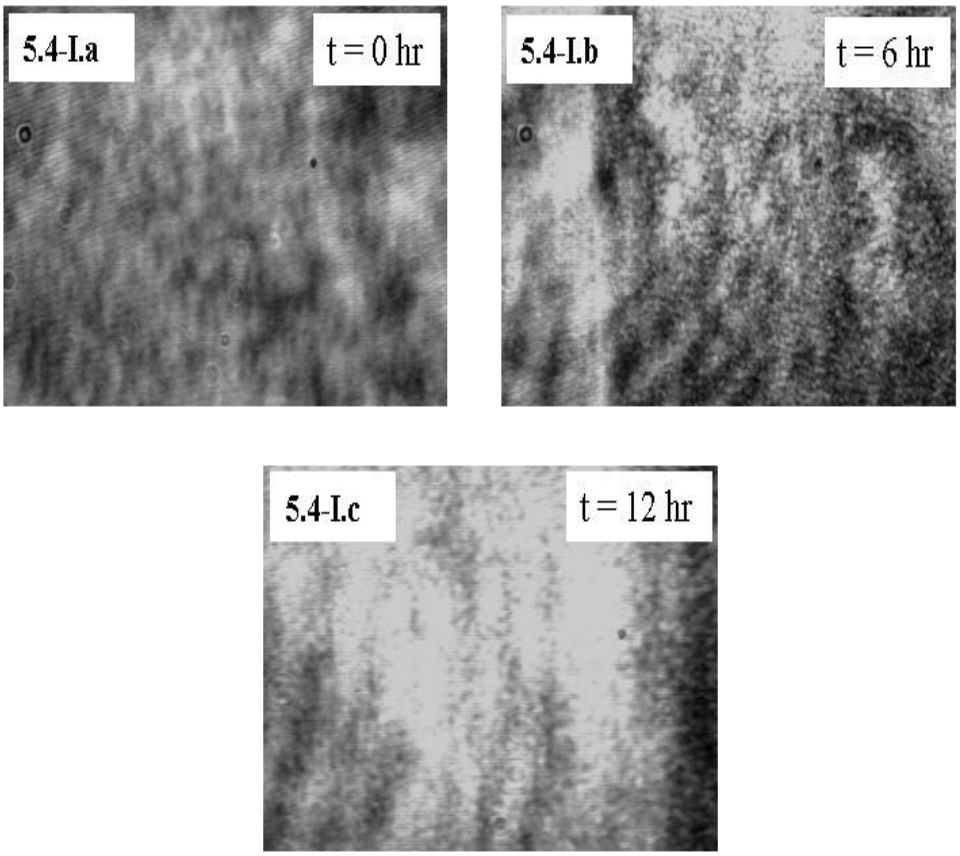

Figure 5.4-I Time dependent complexation of sodium borohydride reduced gold nanoparticles

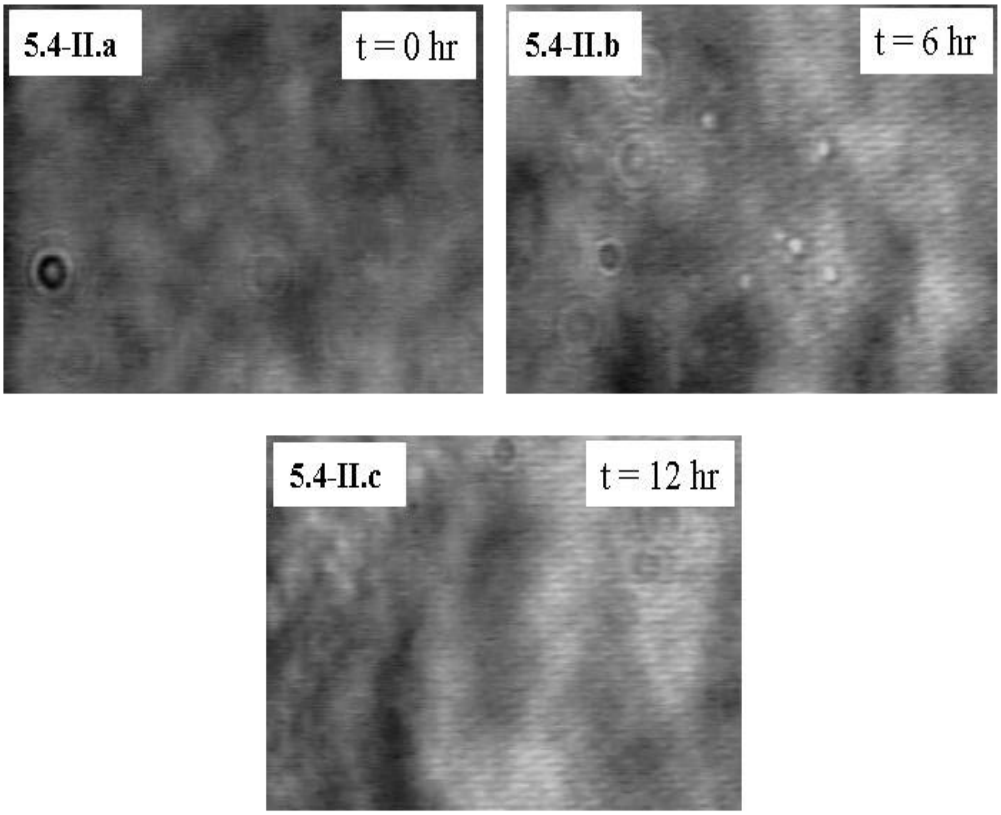

Figure 5.4-II Time dependent complexation of lemon grass reduced gold nanoparticles

Initially, the ODA monolayer was spread in drop wise fashion on the surface of colloidal $NaBH_4$ reduced gold nanoparticles. **A**fter 20 minutes of spreading, the barrier was positioned to a specific area where the surface pressure was around 10 mN/m (LC region from π-A isotherm). BAM images were recorded at subsequent time intervals and some of them are shown in Figure 5.4-I.a to Figure 5.4-I.c.

Similarly, the images were taken for lemon grass reduced gold nanoparticles after subsequent time interval and some of them are shown in 5.4-II.a to 5.4-II.c

BAM images clearly indicate that as the gold nanoparticle density at the air-water interface increases, the surface becomes more rigid and dense. The white domains also appear to be more continues than those observed at time t = 0. From the kinetics of the complexation process, it is evident that more spherical particles bind to ODA monolayer than the triangular nanoparticles in a given time due to their higher mobility.

References

1. Ariga, K.; Shin, J. S.; Kunitake, T. *J. Colloid Interface Sci.* **1995**, 170, 440-448.
2. Brinks, B. P. *Ad*V. *Colloid Interface Sci.* **1991,** 34, 343.
3. Morelis, R. M.; Girard-Egrot, A. P.; Coulet, P. R. *Langmuir* **1993**, 9, 3101-3106.
4. Stine, K. J.; Moore, B. G. In *Nano-Surface Chemistry*; Rosoff, M., Ed.; Langmuir Monolayer: Fundamental and Relevance to Nanotechnology; Marcel Dekker: New York**, 2002**; Chapter 3, p 59.
5. Muramatsu, K.; Takahashi, M.; Tajima, K.; Kobayashi, K. *J. Colloid Interface Sci.* **2001**, 242, 127.
6. Du, H.; Bai, Y. B.; Hui, Z.; Li, L. S.; Chen, Y. M.; Tang, X. Y.; Li, T. J. *Langmuir* **1997**, 13, 2538.
7. Vollhardt, D.; Retter, U. *Langmuir* **1998**, 14, 7250.
8. Angelova, A.; Vollhardt, D.; Ionov, R. *J. Phys. Chem.* **1996**, 100, 10710.
9. Vollhardt, D.; Retter, U.; Siegel, S. *Thin Solid Films* **1991**, 199, 189.
10. Vollhardt, D.; Gutberlet, T. *Colloids Surf. A: Physicochem. Eng Aspects* **1995**, 102, 257.
11. Lee, Y. L. *Langmuir* **1999**, *15*, 1796.
12. Ye, S.; Noda, H.; Nishida, T.; Morita, S.; Osawa, M. *Langmuir* **2004**, 20, 357.
13. Ganguly, P.; Parajape, D. V.; Rondelez, F. *Langmuir* **1997**, 13, 5433
14. Sastry M, Rao M, Ganesh K.N, *Acc. Chem. Res*. **2002**, 35, 847.
15. Swami, A; Kumar, A; Sastry, M; *Langmuir* **2003**, 19, 1168.
16. Mayya, K.M.; Jain, N.; Gole, A.; Langevin, D.; Sastry, M.; *J. of colloid and interface Science* 270, **2004**, 133.
17. Mayya, K.M.; Gole, A.; Jain, N.; Phadtare, S.; Langevin, D.; Sastry, M. *Langmuir* **2003**, 19, 9147.
18. G. Schmid, *Chem. Rev.* 92, 1709, **1992**.
19. M. Brust, D. Bethell, D. J. Schiffrin and C. J. Kiely, *Adv. Mater.* 7, 795, **1995**.
20. Z. L. Wang, *Adv. Mater.* 10, 13, **1998**.
21. Gole, S. R. Sainkar and M. Sastry, *Chem. Mater.* 12, 1234, **2000**.
22. E. Hao and T. Lian, *Chem. Mater.* 12, 3392**, 2000.**
23. A. Swami, A. Kumar, PR. Selvakannan, S. Mondal and M. Sastry, *J. Colloid and Int. Sci.* 260, 367, **2003**.

24. J.-Il Park, W. R. Lee, S. S. Bae, Y. J. Kim, K. H. Yoo, J. Cheon and S. Kim, *J. Phys. Chem. B* 109, 13119, **2005**.
25. K. Kuroishi, M. P. Chena, Y. Kitamoto and T. Seki, *Electrochimica Acta* 51, 867, **2005**.
26. M. Brust, N. Stuhr-Hansen, K. Nørgaard, J. B. Christensen, L. K. Nielsen and T. Bjørnholm, *Nano Lett.* 1, 189, **2001**.
27. D. K. Lee, Y. H. Kim, Y. S. Kang, and P. Stroeve, *J. Phys. Chem. B* 109, 14939 (**2005**).
28. Bala, T.; Joshi, B.; Iyer, N.; Sastry, M.; B.L.V. Prasad *J. Nanosci. Nanotechnol.* **2006**, Vol. 6, No. 12.
29. A. Swami, A. Kumar and M. Sastry, *Langmuir* 19, 1168 (**2003**)
30. P. Tartaj, M. del Puerto Morales, S. Veintemillas-Verdaguer, T. Gonzalez-Carreno and C. J. Serna, *J. Phys. D: Appl. Phys.,* 36, 182 (**2003**).
31. X. K. Li, W. J. Ji, J. Zhao, S. J. Wang and C. T. Au, *J. Catal.* 236, 181 (**2005**).
32. E. Heracleous, A. F. Lee, K. Wilson and A. A. Lemonidou, *J. Catal.* 231, 159 (**2005**)
33. A. N. Fatsikostas and X. E. Verykios, *J. Catal.* 225, 439 (**2004**).
34. A. I. Molina, J. M. Robles, P. B. Garcia, E. R. Castellan, E. Finoechio, G. Busca, P. M. Torres and A.J. Lopez, J. Catal. 225, 479 (**2004**).
35. See the special issue of *Sci. Am.* **2001**, 285.
36. B.L.V. Prasad, Savka I. Stoeva, C. M. Sorensen, K. J. Klabunde, *Chem. Mater.*, **2003**, 15, 935.
37. Patil, V.; Malvankar, R. B.; Sastry, M. Langmuir **1999**, 15, 8197.
38. Joshi, H.; Shirude, P. S.; Bansal, V.; Ganesh, K.N.; Sastry, M; J. Phys. Chem. B **2004**, 108, 11535.
39. Rai, A.; Singh, A.; Ahmad, A; Sastry, M. Langmuir, **2006**, 22, 737.

CHAPTER 6

CONCLUSIONS

This chapter covers the salient features of the work detailed in the thesis and the possible avenues for future work.

The developed BAM instrument coupled with Langmuir trough is an indigenous development for imaging Langmuir films at the air-water interface. While designing the instrument, a detailed study of commercially available instruments has been done taking into consideration the designing criteria. The developed instrument is compact, economical and does not include heavy and bulky parts. The instrument includes the pressure sensor for simultaneous measurement of surface pressure along with image acquisition. Real-time system software has been developed for controlling, imaging and storing the data. Following criteria have been used to make the instrument economical and user-friendly.

1. No unnecessary motorized adjustments are incorporated. Usually one-time adjustment is necessary for the experimentation.
2. Use of a small compact laser diode, instead of a laser, provides higher intensity/surface ratio with overall less laser power so as to avoid the potential danger of heating up the thin films.
3. Good quality Glan-Thompson polarizer is used. High quality polarizer ensures maximum image quality. The instrument has achieved required contrast and sensitivity.
4. User-friendly real-time system software has been developed using LabVIEW. It simultaneously plots the pressure area isotherm and captures and records the BAM images.
5. User-friendly hardware and software tools make the set-up and alignment of the instrument easy and quick.

The specifications of the developed instrument are as follows:

BAM specifications:

Optics:

Light source: High power visible laser diode (25 mW @ 650 nm).

Angle-of-incidence: 52-57° (for aqueous and non aqueous sub-phases) fine adjustment screw for angle-of-incidence adjustment.

Polarizing Optics: High quality Glan-Thompson polarizers.

Imaging system:

Detector: Computer controlled, high grade, CCD camera with 1/3 inch image sensor.

Field-of-view: 3.6 x 4.8 mm².

Resolution: < 10 µm.

Langmuir trough specifications:

Trough material: Teflon

Trough area: 20 x 10 cm^2

Pressure sensor specifications:

Model: PS4 from NIMA Technology, England

Surface tension measurement: Wilhelmy plate

Accuracy: 0.1mN/m for 10mm Wilhelmy plate

Dimension: 62 mm x 28 mm

Mounting: Mounted on specially designed and fabricated holder which has vertically movement to adjust the height of the pressure sensor from trough.

Software:

LabVIEW based user friendly real time system software with built in controls and image acquisition. Continuous real-time monitoring of Langmuir films is done. Image recording in done in AVI format and is stored on hard disk.

Future scope:

With the developed BAM instrument, only qualitative analysis of the Langmuir films is possible. By accurately measuring the reflectivity, the developed instrument can be used as a quantitative BAM. It will enable to calculation of the thickness of the Langmuir monolayer. Use of a high sensitivity camera can further improve the image quality. In case of Langmuir trough design, an addition of the Blodgett technique can be useful for lifting up of the monolayer on to the solid substrate.

Appendix A: CCD Camera Specifications

A.1 Specifications of the KCC310 CCD Camera

Power	DC +12 V or AC 24 V
Effective pixel	410,000 (N), 470,000 (P)
Image sensor	1/3 inch
Power consumption	150 mA or less
Horizontal Resolution	450 TV lines
Scan system	525 line 2:1 interface
Scanning frequency	(H) 15.734 KHz (N) (V) 59.94 Hz (N) (H) 15.625 KHz (P) (V) 50 Hz (P)
Sync system	Internal Sync.
Video output system	1.0 V p-p Composite signal (Sync. : 0.286 V p-p, Video : 0.714 V p-p)
S-VHS	Y Sig, C Sig, GND
Minimum illumination	0.1 Lux at F 1.4
S/N ratio	48 dB (AGC off, gamma = 1, Y signal)
White balance	Automatic White balance control
Shutter speed	Auto IRIS (1/50, 1/60 – 1/100,000), Manual (1/50,1/60,1/250,1/500,1/1,000, 1/2,000,1/4,000,1/10,000, Flickless)
Gain control	Automatic gain control (0~18dB), off
Back light compensation	Off, Pattern1, Pattern2
Output terminal	BNC and S-Video connector
Dimension	65(W) x 54(H) x 71(D), 223 g
Housing material	Aluminum

Figure A-I Specifications of KCC310 CCD camera

Appendix B: NI 6014 and NI 1411 Specifications

B.1 Cards and Hardware

Two types of cards were needed in this application.

1. A data acquisition card, in order to generate and to receive signals sent between the system and the computer.
2. A frame grabber card, also called Image Acquisition Board, is needed to carry out communication between the computer and the camera.

Both the cards used are developed by National Instruments (NI) and are installed in the computer using PCI slots.

B.2 Data Acquisition Card PCI-6014

A multi I/O data acquisition card is used as an interface between the computer and the computers surroundings. The card can generate signals at the request from the computer as well as receive data from external systems. The type of the input signals is physical signals, both analog and digital. National Instruments DAQ card PCI-6014 was used in this application. PCI-6014 card had several advantages. Firstly, the card had the desired number of input and output connections. Secondly, it was much cheaper than buying a specialized motor controller card.

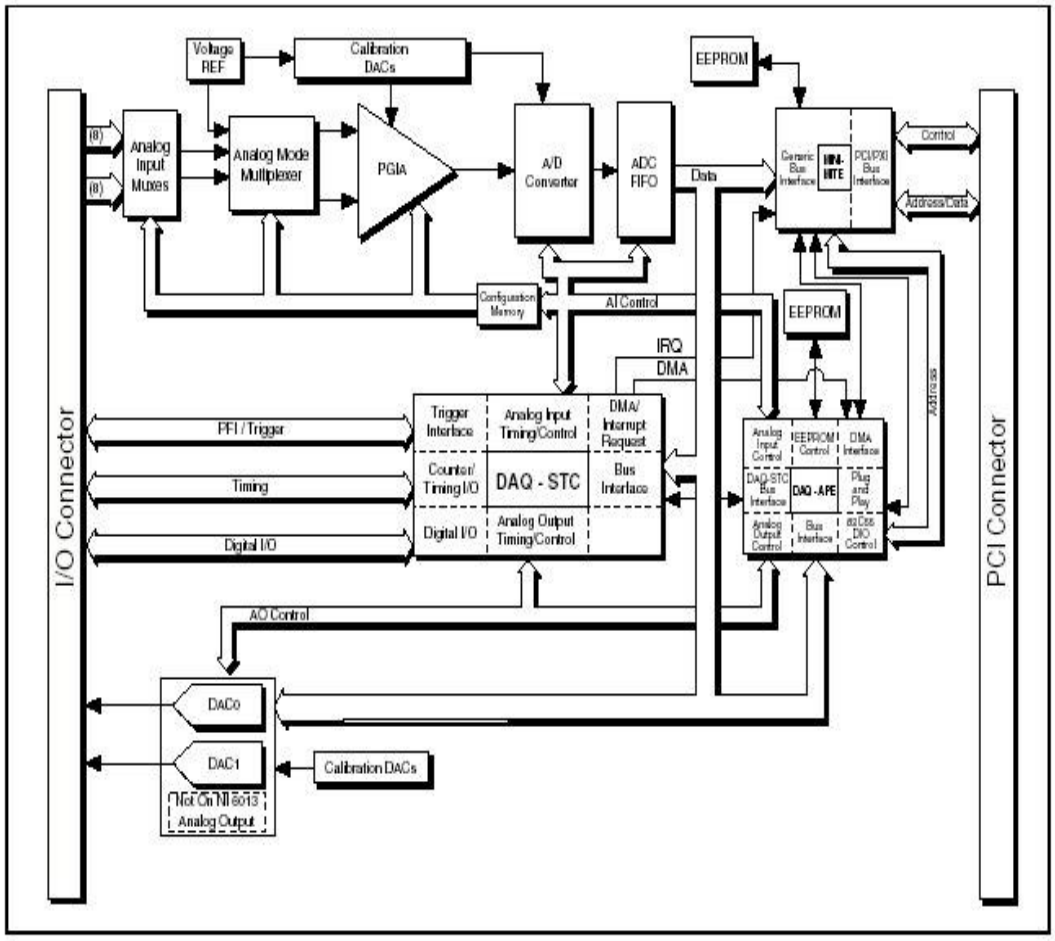

Figure B-I Block diagram of DAQ card PCI-6014

Connector details of the NO 6014:

Device with I/O Connector	**Number of Pins**	**Cable for connecting to 100-pin Accessories**	**Cable for Connecting to 68-pin Accessories**	**Cable for Connecting to 50-pin Accessories**
PCI-6014	68	N/A	SH6868 Shielded Cable, SH68-68R1-EP Shielded Cable, R6868 Ribbon Cable	SH6850 Shielded Cable, R6850 Ribbon Cable

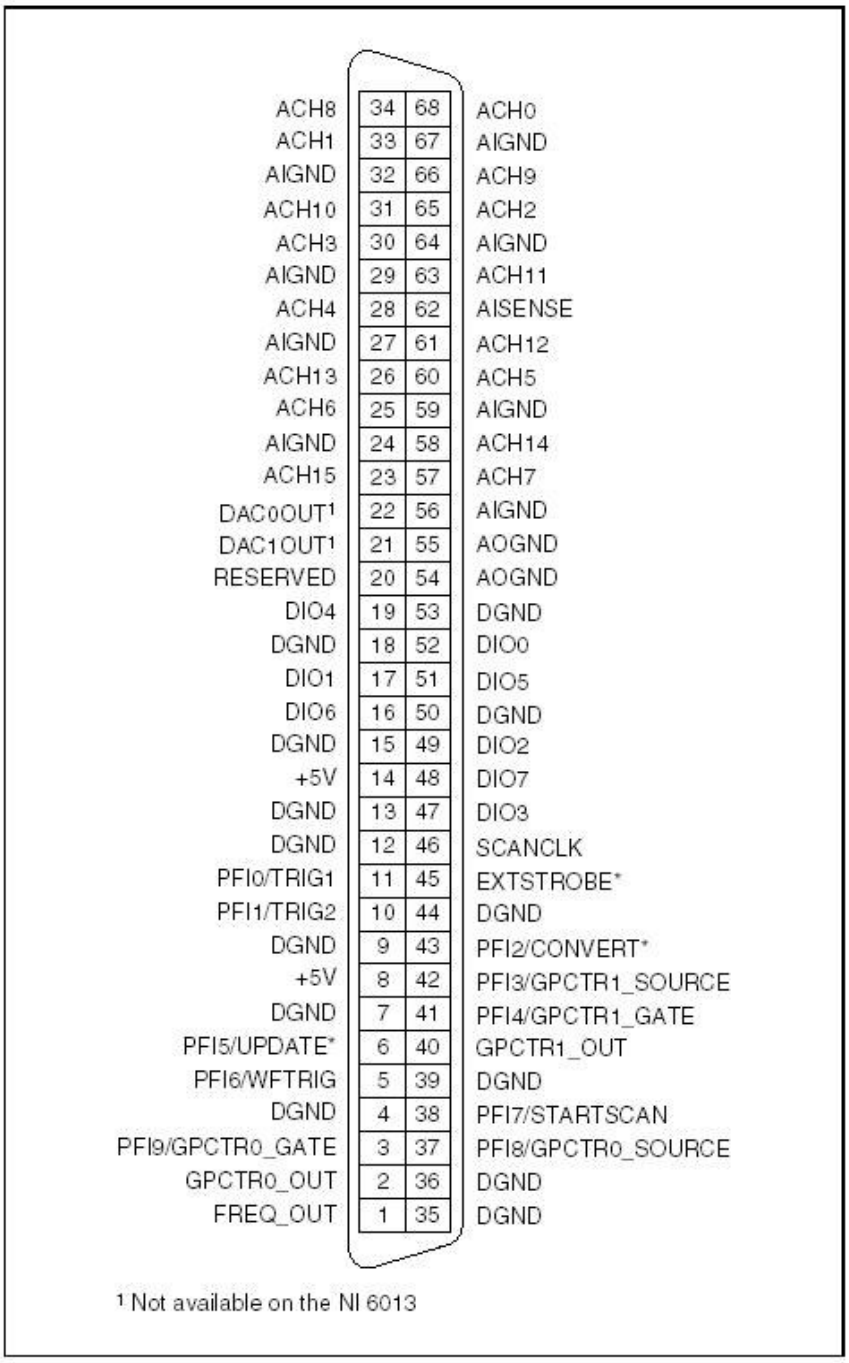

Figure B-II I/O Connector Pin Assignment for the NI 6013/6014

Signal Name	Reference	Direction	Description
AIGND	—	—	Analog Input Ground—These pins are the bias current return point for AI measurements. Refer to Figure 4-3 for recommended connections. All three ground references—AIGND, AOGND, and DGND—are connected on the device.
ACH<0..15>	AIGND	Input	Analog Input Channels 0 through 15—Each channel pair, ACH<*i*, *i*+8> (*i* = 0..7), can be configured as either one differential input or two single-ended inputs.
AISENSE	AIGND	Input	Analog Input Sense—This pin serves as the reference node for any of channels ACH<0..15> in NRSE configuration. AISENSE must be connected to AIGND directly or to an external ground reference for single-ended measurements. Invalid random readings result if AISENSE is left unconnected when using NRSE mode. Refer to Figure 4-3 for recommended connections.
DAC0OUT[1]	AOGND	Output	Analog Channel 0 Output—This pin supplies the voltage output of AO channel 0.
DAC1OUT[1]	AOGND	Output	Analog Channel 1 Output—This pin supplies the voltage output of AO channel 1.
AOGND	—	—	Analog Output Ground—The AO voltages are referenced to this node. All three ground references—AIGND, AOGND, and DGND—are connected on the device.
DGND	—	—	Digital Ground—This pin supplies the reference for the digital signals at the I/O connector as well as the +5 VDC supply. All three ground references—AIGND, AOGND, and DGND—are connected together on the device.
DIO<0..7>	DGND	Input Output	Digital I/O Signals—DIO6 and 7 can control the up/down signal of general-purpose counters 0 and 1, respectively.
+5V	DGND	Output	+5 VDC Source—These pins are fused for up to 1 A of +5 V supply. The fuse is self-resetting.
SCANCLK	DGND	Output	Scan Clock—This pin pulses once for each A/D conversion in scanning mode when enabled. The low-to-high edge indicates when the input signal can be removed from the input or switched to another signal.
EXTSTROBE*	DGND	Output	External Strobe—This output can be toggled under software control to latch signals or trigger events on external devices.

Signal Name	Reference	Direction	Description
PFI0/TRIG1	DGND	Input Output	PFI0/Trigger 1—As an input, this signal is a Programmable PFI. PFI signals are explained in the *Connecting Timing Signals* section. As an output, this signal is the TRIG1 (AI Start Trigger) signal. In posttriggered DAQ sequences, a low-to-high transition indicates the initiation of the acquisition sequence. In pretriggered applications, a low-to-high transition indicates the initiation of the pretrigger conversions.
PFI1/TRIG2	DGND	Input Output	PFI1/Trigger 2—As an input, this signal is a PFI. As an output, this signal is the TRIG2 (AI Stop Trigger) signal. In pretrigger applications, a low-to-high transition indicates the initiation of the posttrigger conversions. TRIG2 is not used in posttrigger applications.
PFI2/CONVERT*	DGND	Input Output	PFI2/Convert—As an input, this signal is a PFI. As an output, this signal is the CONVERT* (AI Convert) signal. A high-to-low edge on CONVERT* indicates that an A/D conversion is occurring.
PFI3/GPCTR1_SOURCE	DGND	Input Output	PFI3/Counter 1 Source—As an input, this signal is a PFI. As an output, this signal is the GPCTR1_SOURCE signal. This signal reflects the actual source connected to the general-purpose counter 1.
PFI4/GPCTR1_GATE	DGND	Input Output	PFI4/Counter 1 Gate—As an input, this signal is a PFI. As an output, this signal is the GPCTR1_GATE signal. This signal reflects the actual gate signal connected to the general-purpose counter 1.
GPCTR1_OUT	DGND	Output	Counter 1 Output—This output is from the general-purpose counter 1 output.
PFI5/UPDATE*	DGND	Input Output	PFI5/Update—As an input, this signal is a PFI. As an output, this signal is the UPDATE* (AO Update) signal. A high-to-low edge on UPDATE* indicates that the AO primary group is being updated for the NI 6014.
PFI6/WFTRIG	DGND	Input Output	PFI6/Waveform Trigger—As an input, this signal is a PFI. As an output, this signal is the WFTRIG (AO Start Trigger) signal. In timed AO sequences, a low-to-high transition indicates the initiation of the waveform generation.
PFI7/STARTSCAN	DGND	Input Output	PFI7/Start of Scan—As an input, this signal is a PFI. As an output, this signal is the STARTSCAN (AI Scan Start) signal. This pin pulses once at the start of each AI scan in the interval scan. A low-to-high transition indicates the start of the scan.

Signal Name	Reference	Direction	Description
PFI8/GPCTR0_SOURCE	DGND	Input Output	PFI8/Counter 0 Source—As an input, this signal is a PFI. As an output, this signal is the GPCTR0_SOURCE signal. This signal reflects the actual source connected to the general-purpose counter 0.
PFI9/GPCTR0_GATE	DGND	Input Output	PFI9/Counter 0 Gate—As an input, this signal is a PFI. As an output, this signal is the GPCTR0_GATE signal. This signal reflects the actual gate signal connected to the general-purpose counter 0.
GPCTR0_OUT	DGND	Output	Counter 0 Output—This output is from the general-purpose counter 0 output.
FREQ_OUT	DGND	Output	Frequency Output—This output is from the frequency generator output.
* Indicates that the signal is active low. [1] Not available on the NI 6013.			

Figure B-III Signal descriptions for I/O connector pins for DAQ 6014

B.3 Frame Grabber Card IMAQ-1411

A frame grabber card, also called Image Acquisition Board, handles the communication between the camera and the computer. The card converts analog video signals into digital form. The card is easily connected to the camera through a BNC cable.

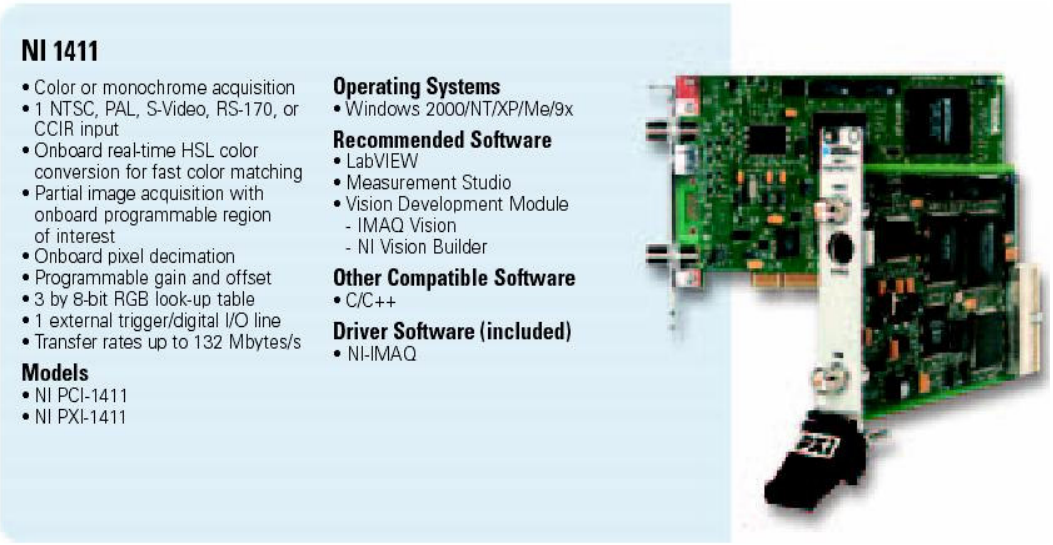

Figure B-IV NI 1411

Specifications

Typical for 25 °C unless otherwise noted.

Supported Formats

NTSC composite or S-video	30 frames/s
PAL composite or S-video	25 frames/s
S-Video NTSC	30 frames/s
S-Video PAL	25 frames/s

Video Inputs

Video 0	Single-ended BNC for CVBS
Video 1	Single-ended S-Video (Y/C)
Input impedance	All 75 Ω ±1%
Input range (black to white)	700 mV (calibrated) or 400 mV to 1.00 V (variable gain)

Accuracy

Luma gain	±2.5% of reading
Chroma gain	±2.5% of reading

Output Formats (Square Pixels)

RGB (Red, Green, Blue)	3 by 8 = 24-bit
HSL	3 by 8 = 24-bit
H, S, or L	8-bit
LUT	3 by 8 bit (RGB only)

Color Decoding

NTSC/PAL	Luma/Chroma COMB, Notch, or optional filters for Peaking

Gain and Offset

Brightness, contrast, saturation, and hue controls

External Synchronization and Trigger Signals

Trigger sense	TTL
Trigger polarity	Programmable (positive or negative)
Pulse width	20 ns minimum detectable
VIH (TTL)	2 V
VIL (TTL)	0.8 V

Pixel Clock (square pixel sampling rate)

Internally generated for square pixels mode

NTSC	12.27 MHz
PAL	14.75 MHz
Bus interface	Master, slave
Bus-master performance	100 Mbytes/s (sustained)

Power Requirements

+5 VDC (±5%)	1.25 A
±12 VDC (±5%)	<100 mA

Physical

Dimensions

PCI	10.7 by 17.5 cm (4.2 by 6.9 in.)
PXI	10 by 16 cm (3.9 by 6.3 in.)

Environment

Operating temperature	0 to 55 °C
Storage temperature	-20 to 70 °C
Relative humidity	5 to 90%, noncondensing

Figure B-V NI 1411 Specifications

Appendix C: Schematic of L298 Driver Circuitry

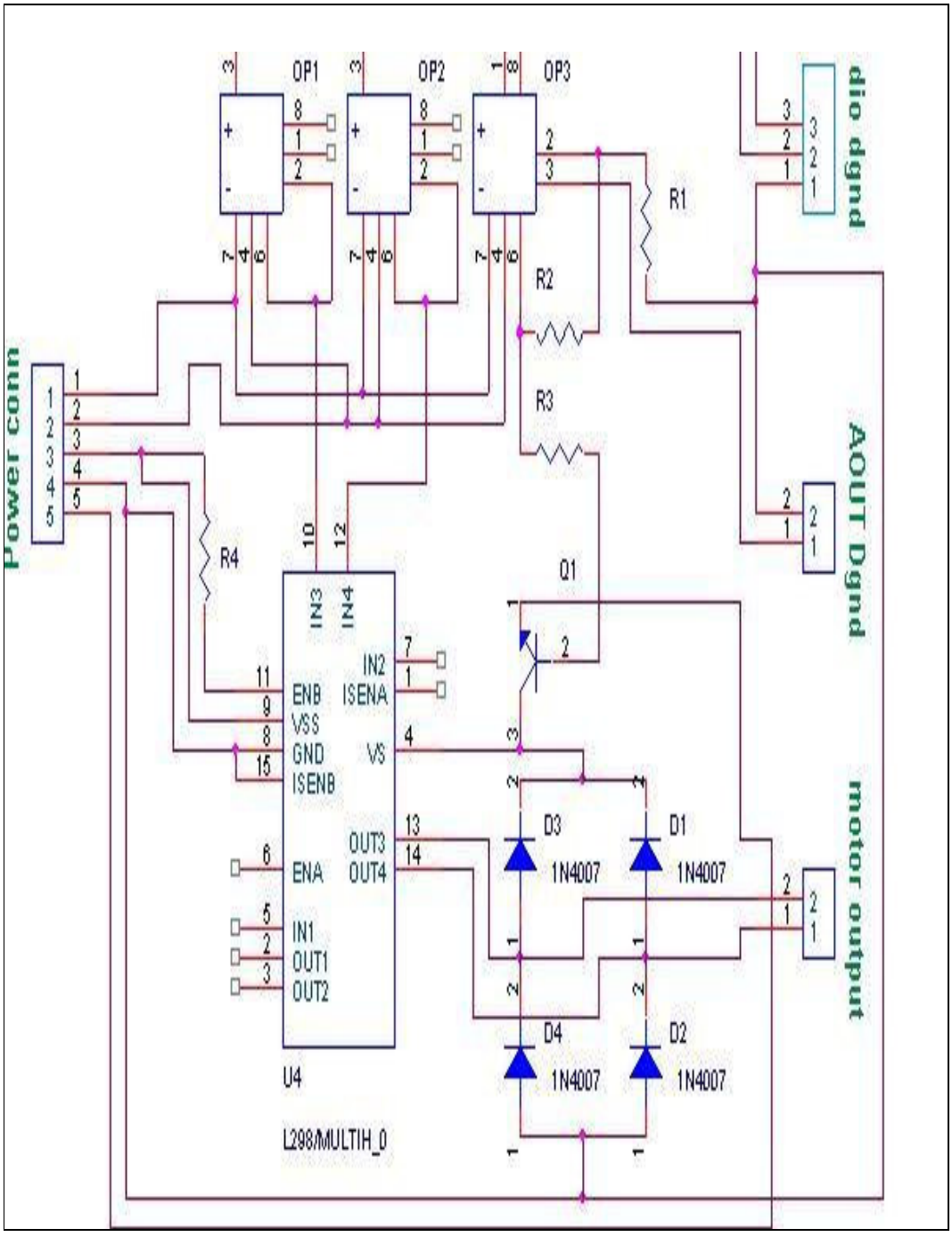

Figure C-I Schematic of L298 driver circuitry

Appendix D: LabVIEW Environment

The programming environment in LabVIEW consists of two separate windows, the front panel and the diagram.

D.1 Front Panel

The front panel is the interface for the written code. In the front panel, different types can be chosen e.g. Boolean, String, Numeric or Cluster. The functionality of each object such as representation or the data range with others can then be specified. The objects are dragged to the front panel from the Controls palette. This palette has several underlying menus (Figure D-I).

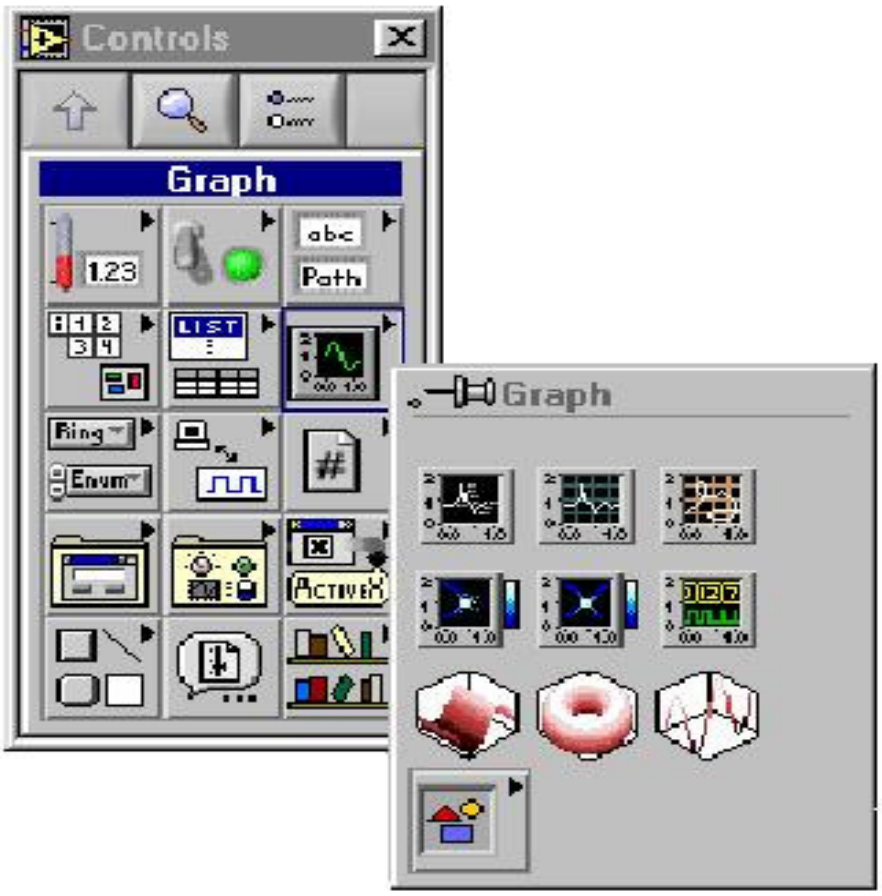

Figure D-I Controls palette in the front panel

On the front panel, all objects need to be defined as input variables (controls) or output variables (indicators). However, no wiring is done on the panel and the

placing of objects only affects the structure of the interface, it does not affect the execution of the code. The example in Figure D-II shows how the programming is done.

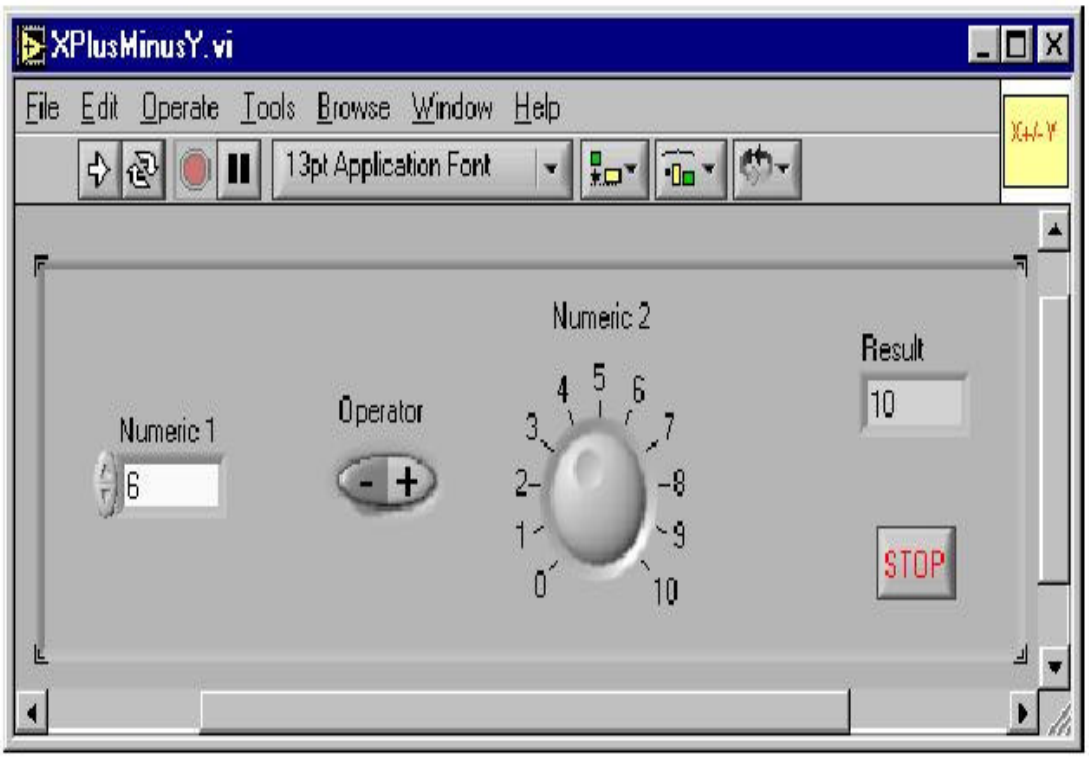

Figure D-II Front panel of the add or subtract example

Figure D-II shows the front panel of the plus or minus example. On the front panel, two different types of controls, a numerical (*Numerical 1*) and a knob (*Numerical 2*) are dragged onto the panel. They are either added or subtracted depending of the value of the boolean *Operator*. The sum is output in an indicator numerical (*Result*). The *Operator*, S*top, Numerical 1* and *Numerical 2* are inputs and thereby are all controllers. When the VI executes, the controllers can be altered and the result of the equation is displayed in the result value, which is an indicator. The execution stops when the boolean S*top* is pressed and the VI terminates.

D.2 Diagram

The diagram is where the actual programming takes place. The objects that were created on the front panel have their corresponding icons in the diagram. These icons can be wired with different VI's and other variables (Figure D-III).

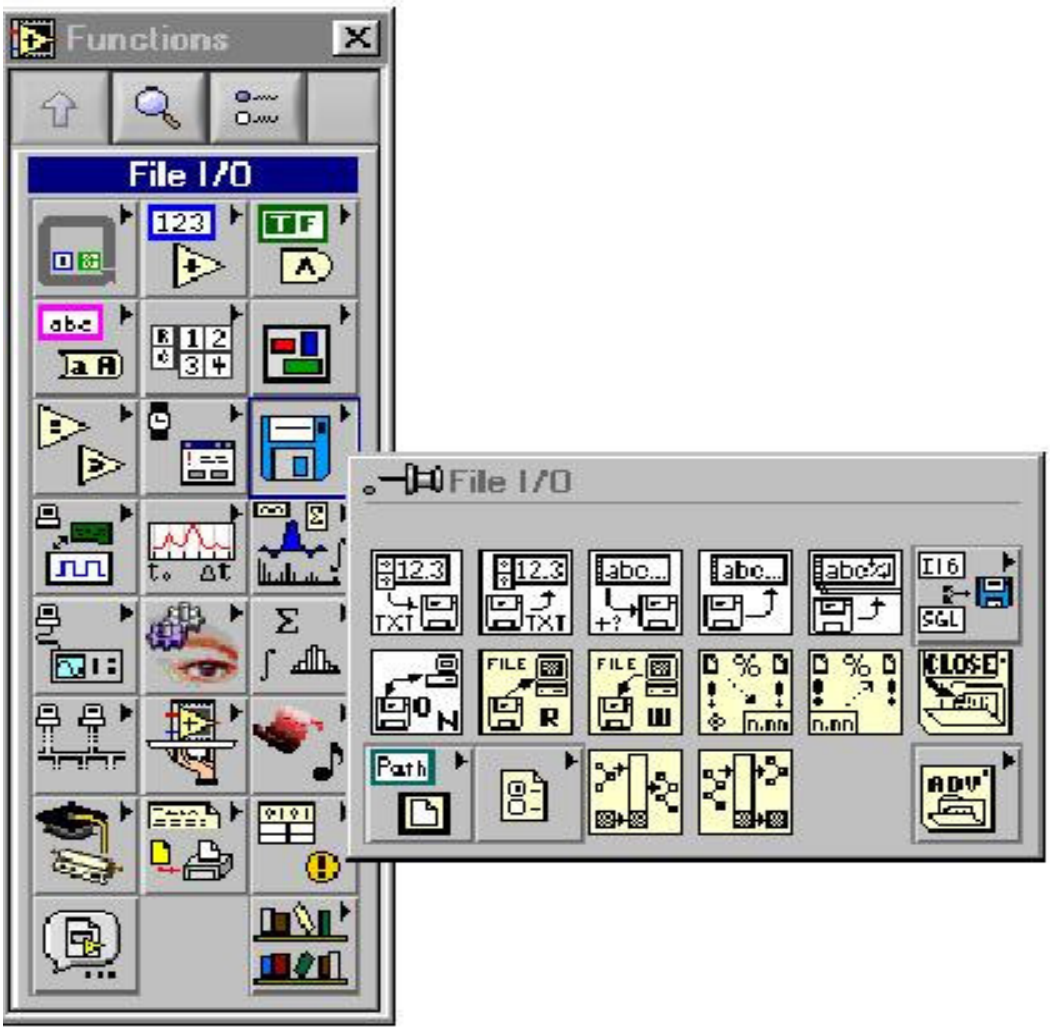

Figure D-III Functions palette in the diagram window

From this palette, all different tools that are needed when programming, such as, case structures, I/O handling, timers and mathematical functions, can be dragged into the VI. In addition, the palette upholds a clear structure of the available VI's. Due to the graphical programming method, with wiring objects in order to create functions, the code itself becomes well structured. Even if the diagrams can be big they are often easy to understand and the flow of the code is easy to follow. The "add

or subtract" example will give a picture as to how a diagram will appear. To be able to calculate the result more than once, a while loop is used (Figure D-IV).

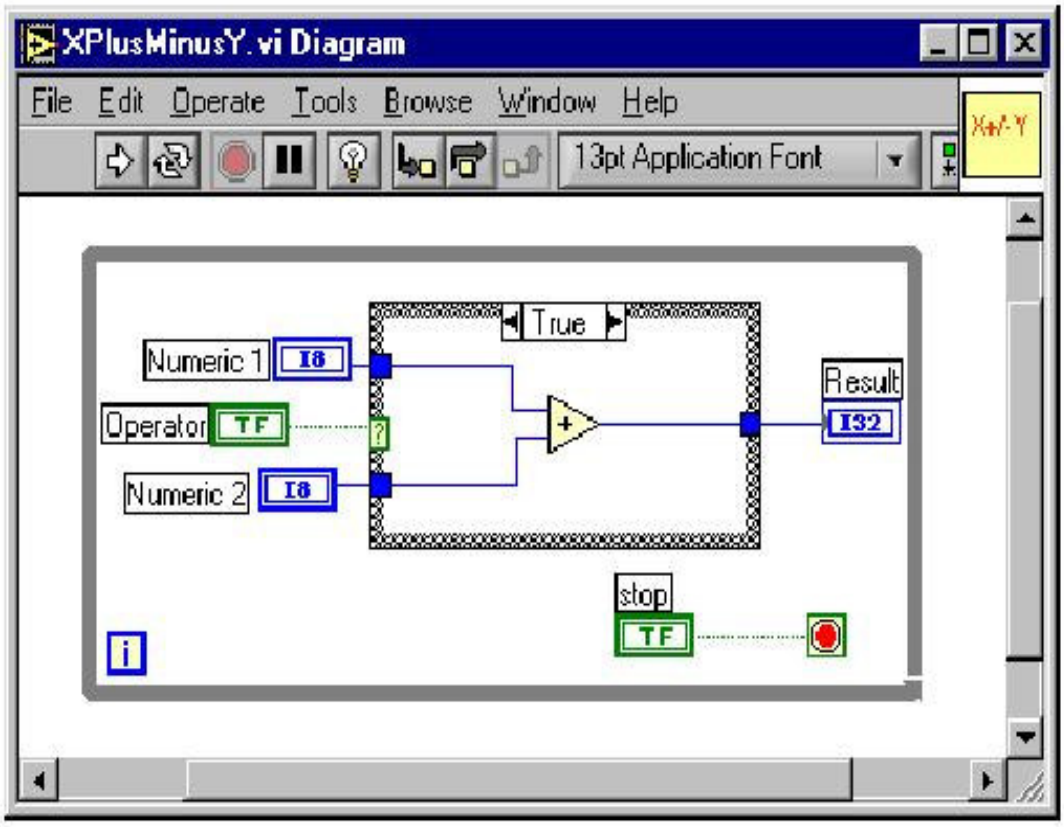

Figure D-IV Diagram of the add or subtract example

The loop will continue until the *Stop* button on the front panel is pushed. To know about the type of operation that is requested, a case structure is applied. If the O*perator* button is in mode "add", the "true" case is executed. In this case, the "add" block adds *Numeric 1* and *Numeric 2*. After this operation, the case clause terminates and the resulting value is output in *Result* on the front panel. If the S*top* button is true, the term of the case is investigated again and the corresponding case clause is executed again. If the S*top* button is false, the VI terminates.

Appendix E: Graphical User Interface

The graphical user interface (GUI) of the developed real-time system software is shown in Figure E-I, Figure E-II and Figure E-III.

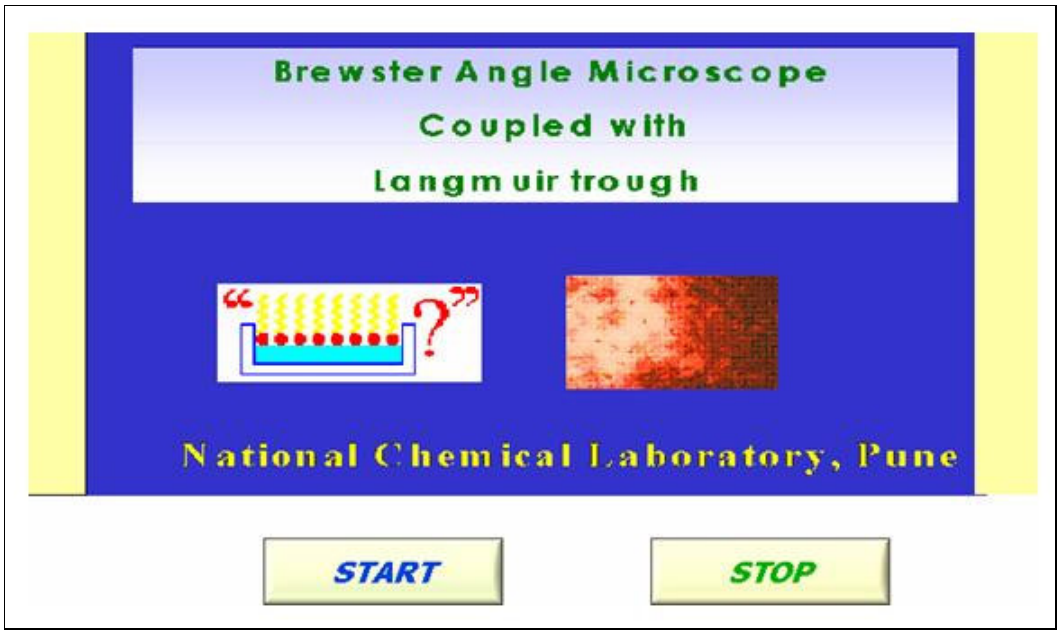

Figure E-I Main GUI window

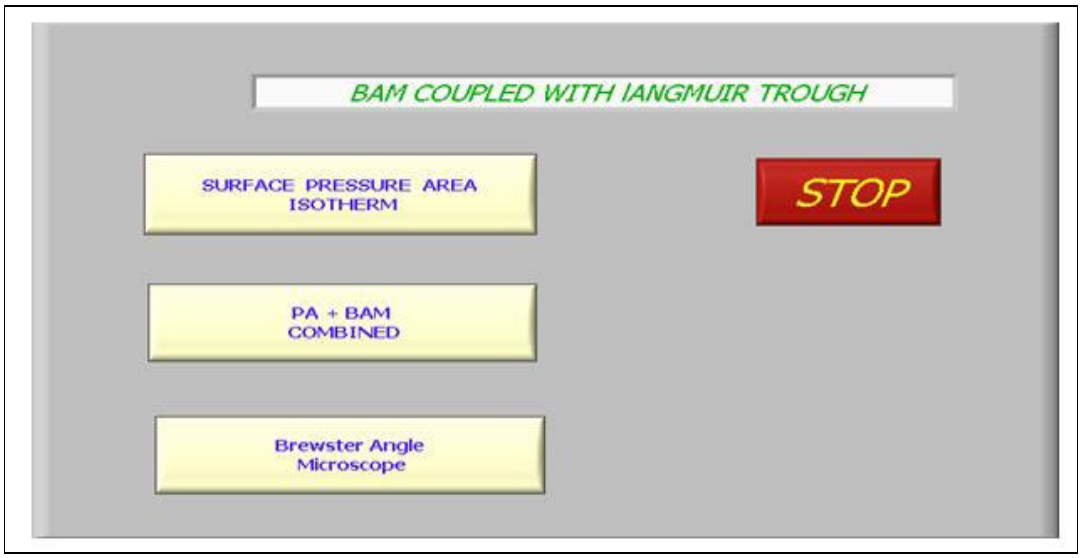

Figure E-II Choice between different applications

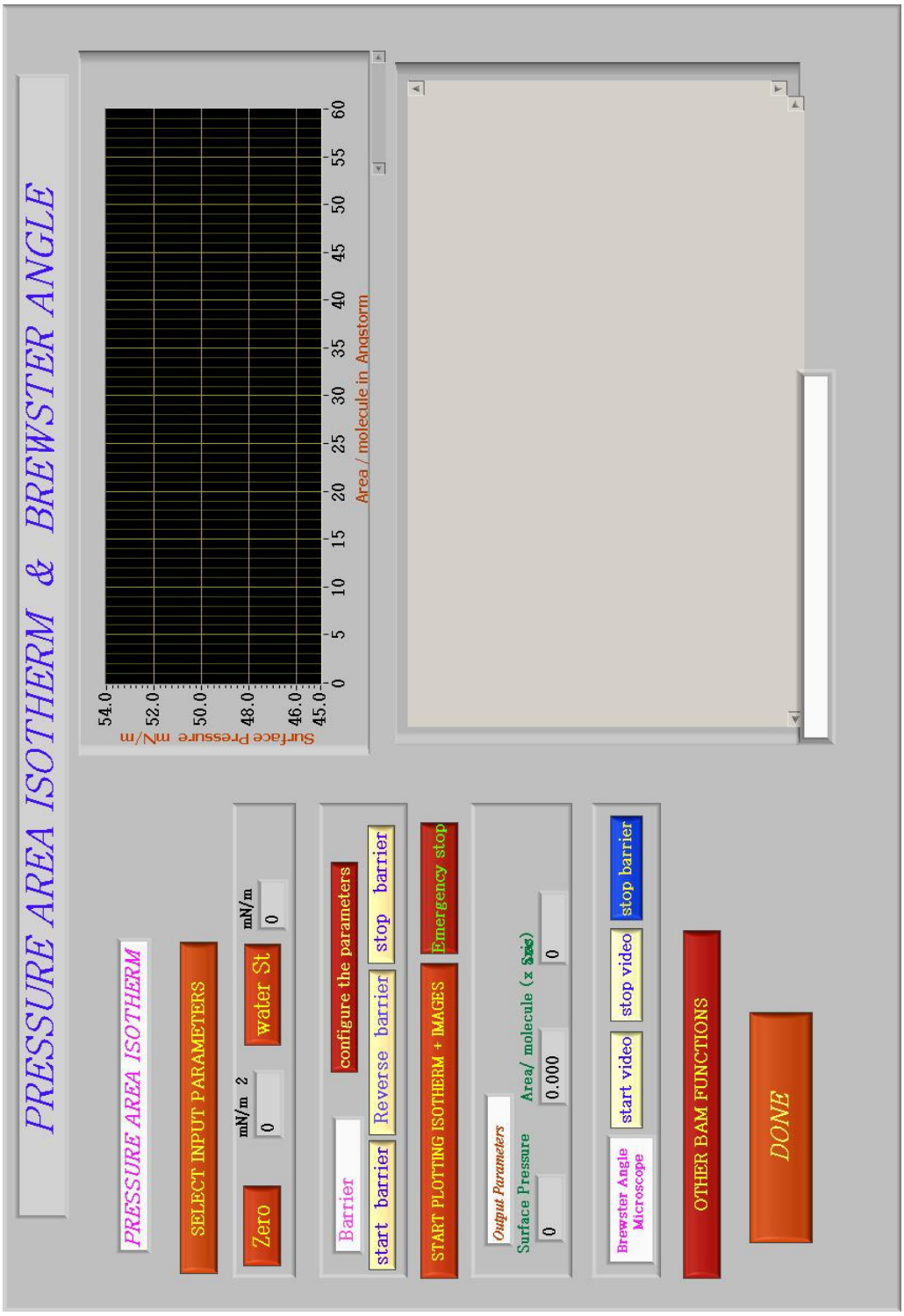

Figure E-III Combined application of BAM and Pressure Area Isotherm